Low-Temperature Fracture Behavior of Asphalt Concrete in Semi-Circular Bend Test

A DISSERTATION

SUBMITTED TO THE FACULTY OF THE GRADUATE SCHOOL

OF THE UNIVERSITY OF MINNESOTA

BY

EYOAB ZEGEYE TESHALE

IN PARTIAL FULFILLMENT OF THE REQUIREMENTS

FOR THE DEGREE OF

DOCTOR OF PHILOSOPHY

Mihai Marasteanu, Advisor

May, 2012

Acknowledgements

This Ph.D. thesis represents an important capstone toward the conclusion of a long journey that started in the classrooms of the Liceo Sperimentale “G.Marconi” in Asmara (Eritrea), passed through the University of Pisa and Polytechnic University of Turin, and continued here at the University of Minnesota. It is only fitting then, that I spend few words to acknowledge and thank the many people who have contributed to make this journey possible, and accompanied me through many setbacks and successes.

Firstly, I would like to express my sincere gratitude to Dr. Mihai Marasteanu for giving me the opportunity to join the University of Minnesota and for his continuous support and guidance. I would also like to express my deep respect to Dr. Andrew Drescher, Dr. Lev Khazanovich, and Dr. Henry K. Stolarski whose teachings, long discussions on my research, comments, and warm support have enormously benefitted my studies and boosted my confidence. This dissertation work owes too much to Dr. Jia-Liang Le whose expertise in the fracture behavior of quasi-brittle materials, and helpful guidance were crucial in preparing this manuscript. I am very thankful to Dr. Douglass Hawkins for his teachings and for taking the time to review this dissertation and serve in my examination committee. I cannot thank enough my dear friend Dr. Raul Velasquez who kindly reviewed this manuscript and provided me with valuable suggestions. The assistance rendered by Mugur Turos and Ki Hoon Moon is greatly appreciated. I am also very grateful to Timothy Clyne and Dr. Eshan Dave for sharing with me field performance data and laboratory test results. I acknowledge the funding and material provided by the Federal Highway Administration – National Pooled Fund Study TPF-5 (132).

Special thanks are due to Professor Ezio Santagata whose mentoring, kind words of encouragement and support have played an important role in my life.

My heartfelt gratitude goes to the many friends who have inspired me, accompanied me and at times put me back on track during this long journey. Among many, my friends and collegeagues from Asmara who have encouraged me to begin the PhD program: Temesghen Kahsay, and Carl Thodesen; my colleagues and friends in Minneapolis with whom I shared memorable times: Peter Bedard, Pietro Ferrero, Davide Gianuzzi, Bereket Yohannes, Dina Atta and Tewfik Hassen, Roberto Piccinin, Luke Johanneck, Steve Wilk, Fanuel Tsehaye, and all the members of the Voyagers F.C soccer team.

Words can hardly describe the massive depth of gratitude that I owe to the late Dr. Nino Zullo and his wife Nevenka Gregoric, to Enzo & Luisa La Conte, and to my dear friend Davide La Conte for the support, friendship and love bestowed upon me.

Pursuing an engineering degree far away from home is no easy task. But perhaps the most difficult challenge of all is living far from the warmth of a family. I am immensely indebted to Sennait Ghebrejohannes for her unconditioned love, partnership, support and for allowing me to be part of her beautiful family: Deglel Tecle, Irga Ghebrejohannes, and Sara & Yoseph.

Last but not least, my final thanks go to my family. I am forever indebted to my beloved brothers Selamab, Manaab, Tinbitaab, my nephew Thomas (Buruk) and to my most loved parents Zegeye Teshale and Genet Abraha whose love, unshakeable support, patience, and words of wisdom, hope and strength sustained me throughout this long journey and encouraged me to pursue my dreams.

To my parents Zegeye Teshale and Genet Abraha

"May the words from your mouth be strong as ink;

may the soil beneath your feet be always green,

may the wishes of your heart become true,

go my son and God be with you"

Blessings from my Great-Grandma

Abstract

Asphalt concrete mixtures behave as quasi-brittle materials at temperatures close to the glass transition of the component asphalt binder. A salient feature of structures that consists of quasi-brittle materials is that there exists an intricate size effect on the structural strength. The existence of such size effect is mainly attributed to the presence and the stable growth of a relatively large fracture process zone (FPZ) that develops ahead of the crack tip prior to failure (maximum load) of the structure. This inelastic region is characterized by non-linear material deformation and fracture energy dissipation that ultimately generate stress redistribution and govern the strain-softening of the material. Understanding this size effect is crucial for two purposes: a) extrapolation of small-scale laboratory testing results to full-scale design, and b) identification of material fracture properties. In this research work, laboratory experiments and numerical simulations were conducted to investigate the size effect of asphalt concrete tested in semi-circular bend (SCB) test at low temperature. Geometrically similar specimens of different sizes and with different notch lengths were tested. The experimental results were analyzed with the energetic-size effect theory, and were used to develop type I and II strength scaling laws, respectively, for the notchless and deep notched specimens. The validity of the scaling laws at large sizes was evaluated through finite element simulations of mode I crack growth in the SCB test. A cohesive zone model (CZM) was successfully calibrated by experimental data, and implemented to predict the nominal strength in large SCB specimens. The strengths predicted from the numerical models

were in good agreement with the scaling laws' strength prediction. Based on the analyses of the strength scaling laws derived, important conclusions on the fracture behavior of asphalt concrete at low temperature, as well as size of FPZ were drawn.

Building on the above findings, the study was extended to investigate the ability of the standard SCB test protocol to characterize and differentiate relatively small aggregate size mixtures with respect to their resistance to low temperature cracking. Laboratory compacted and field cored test samples from the Minnesota Test Track (MnROAD) were tested using the SCB and other traditional and newly developed fracture test methods. The investigation included monitoring and analyzing field performance observations of the test cells from MnROAD. Statistical analysis was used to identify the factors which affect the results and to rank the mixtures according to their resistance to cracking. The SCB test method resulted to be better equipped to differentiate materials than traditional test methods, and in good agreement with the prediction of other fracture test methods. The findings reinforce earlier research showing that SCB is a simple reliable laboratory test method that can be effectively used to select paving materials and to improve the existing mix design procedure.

In the final part of this thesis work, research was conducted to develop a unified laboratory test methodology for evaluating linear viscoelastic properties and fracture parameters from a single SCB test configuration. The proposed methodology consists of an initial creep test, followed by a standard SCB fracture test. Finite element analyses were performed to investigate the stress state in the SCB, and to establish an optimal load

range producing appreciable displacement measurements for the estimation of viscoelastic properties. Expressions that relate displacement, from particular regions of the SCB specimen, to the creep compliance function were derived. The validity of the proposed SCB creep method was tested both by numerical simulations and experimental testing. Good agreement was found between the creep function obtained from SCB and those obtained from three-point bending beam and the Indirect Tensile creep test (IDT).

Table of Contents

List of Tables

List of Figures

Chapter 1. Introduction

Low temperature cracking is one of the main distresses that affect asphalt pavements in cold regions. At very low temperatures, the top asphalt layer shrinks but it is constrained by friction which occurs at the interface with the underlying layers. As a result, thermal induced tensile stresses are produced in the pavement. The tensile stresses gradually increase with decrease in temperature, until the tensile strength of the asphalt concrete is reached (Jung, et al., 1994). At this critical low temperature, cracks are initiated and propagated transversely throughout the pavement. With time, the cracks widen, and, unless promptly repaired, they provide easy access for water and moisture to penetrate the entire pavement structure and accelerate pavement failure. As a result, the durability of the pavement, as well as the comfort and safety of the users are severely damaged. This inevitably leads to increased maintenance requirements that may drain state budgets.

In order to find a solution for thermal cracking in asphalt pavements, one has first to investigate the complex fracture mechanics that govern crack initiation and propagation in asphalt concrete. If this is achieved, appropriate fracture parameters can be identified and used for the design and selection of asphalt concrete paving mixtures with higher resistance to cracking.

Currently, the Superpave Performance Grade (PG) specification attempts to limit thermal cracking mainly by selecting asphalt binders that have good low temperature properties. The low temperature behavior of asphalt binders are determined using two laboratory instruments developed during the Strategic Highway Research Program

(SHRP): the Bending Beam Rheometer (BBR) and the Direct Tension Test (DTT). However, this approach fails to take into consideration the response of the aggregate phase which represents 90-95 percent of the total weight of typical asphalt concrete mixtures.

A laboratory testing method developed during SHRP for the low temperature characterization of asphalt concrete is the Indirect Tensile (IDT) creep and strength tests performed according to AASHTO T322-07 (2007). The results are used to determine the critical cracking temperature in the thermal cracking (TC) model implemented in the AASHTO Mechanistic-Empirical Pavement Design Guide (MEPDG). The IDT creep results are used to compute thermal stress curves and IDT strength are used to generate strength master curves. The critical cracking temperature is determined at the intersection of these two curves. However, the IDT creep and strength parameters provide limited information on the fracture mechanism of the material, do not address crack propagation, and cannot fully reflect the coupling of thermal and traffic loading.

Recent research has indicated that fracture mechanics-based approaches are necessary in order to properly address the initiation and propagation of cracks in materials. This is also true for as asphalt concrete as demonstrated by several studies in which fracture mechanics based tests and analyses method were found to be better suited to evaluate the material's resistance to thermal cracking (Mobasher, et al., 1997; Molenaar, et al., 2000; Marasteanu, et al., 2002; Li, et al., 2004; Wagoner, et al., 2005; Wagoner, et al., 2005). Among the test methods available, the Semi-Circular Bend (SCB)

test has received considerable attention due to its simplicity: the notched SCB specimen can be easily prepared from standard laboratory compacted or field cored asphalt concrete cylinders. Depending on the orientation of the initial notch, the SCB fracture test can be used to study both mode I and II fractures (Chong, et al., 1988). A standard SCB specimen used for asphalt concrete characterization has a diameter of 150 mm and the thickness of 30 mm. A vertical notch, with a length of 15 mm and width of 1 mm, is fabricated at the center axel of the disk. However, the relatively small size of the SCB specimens raises the question of the suitability of this method and geometry for proper fracture characterization.

The fracture behavior of quasi-brittle materials, such asphalt concrete at very low temperatures, is governed by the size of the fracture process zone (FPZ) that develops ahead of the crack tip during fracture testing. Depending on the FPZ's relative size to the structure, two types of fracture behavior can be distinguished: brittle and quasi-brittle. In the first case, because the size of the FPZ is negligible, linear elastic fracture mechanics (LEFM) based tests and analysis methods can be used to determine size and shape independent fracture parameters. The second type of fracture is observed when the size of FPZ relative to the structure is large and cannot be neglected. In this case, LEFM cannot be applied to laboratory scale structures and alternative methods that use very large structures and/or non-linear fracture methods are required. Both options may result in expensive and complex experimental efforts. Thus, a good understanding of the size effect and the softening behavior that occur in the FPZ are crucial in determining the

fracture behavior of asphalt pavements, and in identifying the proper fracture analysis method.

Analyzing the size effect on the nominal strength of the structure is one way of understanding the fracture behavior in quasi–brittle materials. However, the traditional power law size effects of type $\sigma_N \propto D^{-p}$,where D represents a characteristic dimension of the structure and p can take the values of 0, $1/2$, and n/m (i.e.,Weibull modulus), respectively, for strength theory, LEFM, and Weibull's statistical theory, can describe quasi-brittle materials only at either very large or very small sizes. The main reason for this is the absence of a characteristic length, which defines quasi-brittle materials with large FPZ and noticeable heterogeneity. The size effect exhibited in laboratory scale specimens is explained by the deterministic energetic theory of quasi-brittle size effect derived by Bažant.

The main objective of this dissertation is to investigate the type of fracture of asphalt concrete SCB specimens tested at low temperature. This includes experimental investigation and modeling of size effect. The results are further analyzed through the well established size effect theories of quasi-brittle, and used to estimate the size of the FPZ and determine size-independent fracture parameters.

Further, this dissertation proposes a unified laboratory test methodology for evaluating linear viscoelastic properties and fracture parameters from the SCB test configuration. The proposed methodology consists of an initial creep test, followed by a standard SCB fracture test. Finite element simulations are used to derive expressions that

relate displacement measurements from particular regions of the SCB specimen to the viscoelastic creep compliance function.

This dissertation includes an extensive literature review which includes: current low temperature characterization of asphalt concrete, Linear Elastic Fracture Mechanics analysis (LEFM), Equivalent LEFM analyses, Cohesive Crack Model, application of SCB fracture test for asphalt concrete, and size effect theories.

Chapter 2. Literature review

In order to achieve the goals of the thesis, a comprehensive literature review of previous and current research efforts in the area of low temperature characterization of asphalt concrete was performed. This chapter includes the findings of the literature search as follow: asphalt concrete characterization approaches, fracture mechanics theories and size effect applied to quasi-brittle materials, application of fracture mechanics-based testing and analysis methods to evaluate the low temperature fracture properties of asphalt concrete.

2.1. Asphalt Concrete characterization

Asphalt concrete is a composite material consisting of three phases: aggregate, asphalt binder, and air voids. By volume, aggregates, asphalt binder and air voids typically account for 75, 20, and 5% of the asphalt concrete, respectively. The proportions of the components play a significant role in defining the mechanical properties of the asphalt concrete. In principle, the behavior of the aggregates and asphalt binder can be idealized, as linear elastic and viscoelastic, respectively. The resulting composite material has a rather complicated behavior that is time, rate, and temperature dependent (Monsmith, et al., 1962). Given the small strains that the material exhibits at low temperatures, it is fairly accurate to consider asphalt concrete as a linear viscoelastic material (Lytton, et al., 1993; Buttlar, et al., 1994), and a constitutive relationship

between stresses σ_{ij} and strains ε_{ij} can be expressed in the form of convolution integrals by means of the Boltzman's superposition principle (Christensen, 1982; Findley, et al., 1989):

$$\varepsilon_{ij} = \int_0^t D_{ijkl}(t-\xi)\frac{\partial \sigma_{kl}(\xi)}{\partial \xi}\, d\xi \qquad [2.1.a]$$

$$\sigma_{ij} = \int_0^t E_{ijkl}(t-\xi)\frac{\partial \varepsilon_{kl}(\xi)}{\partial \xi}\, d\xi \qquad [2.1.b]$$

where $D(t)$ and $E(t)$ represent the *creep compliance* and *relaxation modulus*, respectively, and can be determined from relatively simple laboratory experiments. Creep compliance represents the material's creep strain caused by a unit stress; likewise relaxation modulus represents the stress output due to unit strain. Equation 2.1.a can be used to determine the strain history of a material when the stress history and creep compliance $D(t)$ are known. Equation 2.1.b is used to determine the stresses knowing the strain history and the relaxation modulus $E(t)$.

Due to its simplicity, creep test is most commonly used to characterize asphalt concrete. Nevertheless, $D(t)$ and $E(t)$ are related through the following relation:

$$t = \int_0^t E(t-\xi)D(t)\, d\xi \qquad [2.2]$$

Several numerical methods (Hopkins, et al., 1957; Secor, et al., 1964) are available to solve equation 2.2, since for many materials an analytical solution for this integral is not available.

For the purpose of this research, the creep compliance function is used to describe the linear viscoelastic behavior of asphalt concrete at low temperature. It should be mentioned that other viscoelastic functions can be used to describe the mechanical response of this material. For example, for dynamic loading, high loading rates and short times, Findley et al., (1989) recommend the use of *complex modulus* E^* derived from oscillatory tests. However, once the creep compliance is determined, the other functions can be computed using inter-conversion methods.

The effect of temperature on the constitutive equations of viscoelastic materials can be taken into account by applying the *time-temperature superposition principle* (Leaderman, 1955). According to this principle, the creep compliance and relaxation modulus in equations 2.1.a and 2.1.b are assumed to be functions of temperature, T, and time, t. For a certain class of material, referred to as *thermo-rheologically simple* materials, the effects of temperature and time on the material properties can be combined through the *reduced time* ζ concept (Schwarzl, et al., 1952):

$$\zeta(T,t) = \frac{t}{a_T(T)} \qquad [2.3]$$

where a_T is known as the temperature shift factor and it can be related to temperature through an empirical equation proposed by Williams et. al., (1955):

$$log(a_T) = \frac{-k_1(T-T_0)}{k_2+T-T_0} \qquad [2.4]$$

where k_1 and k_2 are material constants and T_0 is the reference temperature.

The viscoelastic material properties determined from different test temperatures and expressed in terms of *reduced time* ζ can be shifted to the reference temperature T_0. The resulting single smooth curve is known as *master curve*.

2.1.1. Indirect Tensile test

The Indirect Tensile (IDT) creep and strength test procedure is used to evaluate the low temperature fracture properties of asphalt concrete (Roque, et al., 1992; Buttlar, et al., 1994; Zhang, et al., 1997). The test method was first developed in Brazil and Japan in 1940 to determine the tensile strength of elastic brittle materials such as rocks. It was later expanded to Portland concrete by Hondros (1959) who provided analytical solutions for the elastic stress and strain fields of a diametrically compressed cylindrical specimen. Thereafter, the IDT has been used to determine the modulus and the Poisson's ratio of elastic-brittle materials.

In the IDT test configuration, a cylindrical specimen is loaded vertically along its length, as shown in Figure 1, and displacements are measured on both faces of the specimen. The compressive loading induces almost uniform transverse tensile stresses over a significant central portion across the plane of loading, and horizontal tensile stresses along the central horizontal axis (Hondros, 1959).

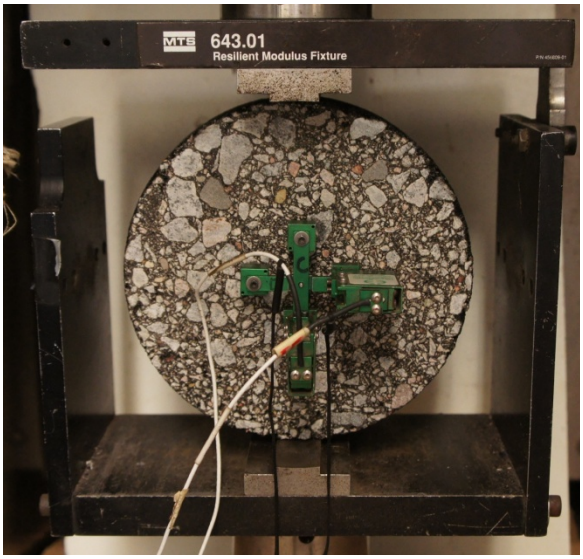

Figure 1. IDT test setup

Roque et al., (1992) observed that the IDT test is also particularly suitable to determine creep compliance and strength of asphalt concrete, because it simulates a state of stress similar to the state of stress induced by moving traffic load in asphalt pavement layers. Based on Frocht solution (Frocht, 1948) and applying the *elastic-viscoelastic correspondence principle*, Roque et al., (1992) proposed a method for determining the low temperature creep compliance $D(t)$ of asphalt concrete from an IDT creep test. The method is incorporated in the AASHTO standard (AASHTO T 322-07, 2007) and accordingly the creep compliance is determined by:

$$D(t) = \frac{\varepsilon_x}{\sigma_x - \upsilon\sigma_y} = \frac{\frac{\Delta U(t)}{GL} C_{Bx} \cdot C_{\varepsilon x}}{\frac{2P}{\pi \cdot b \cdot d}(C_{Sx} + 3\upsilon C_{Sy})} \qquad [2.5]$$

where υ is Poisson ratio, b and d are thickness and diameter of the specimen, respectively, P is the applied force, GL is the gage length, and ΔU is the measured

horizontal deformation. The C parameters are correction coefficients described in the AASHTO standard. After rearranging, the final expression for $D(t)$ is given by:

$$D(t) = \frac{\Delta U_m \cdot d_{avg} \cdot t_{avg}}{P_{avg} \cdot GL} C_{CMPL} \qquad [2.6]$$

where

ΔU_m – trimmed mean of the horizontal deformations,

t_{avg}, d_{avg} – average specimen thickness and diameter, respectively,

P_{avg} – average force,

C_{CMPL} – creep compliance parameter computed as

$$C_{CMPL} = 0.6354 \left(\frac{\Delta U}{\Delta V}\right)^{-1} - 0.332$$

where

ΔU –measured horizontal deformations,

ΔV –measured vertical deformations,

The standard recommends testing three replicates, for each test temperature. The *trimmed mean* approach consists in removing the extreme displacement values and taking the average value of the remaining values. The testing time for the IDT creep test is 1000 sec. At the completion of the creep test, the specimen is brought to failure by increasing the compressive load. The maximum load P_{max} is used to compute the tensile strength of the asphalt concrete by equation [2.7]:

$$T = \frac{2\,P_{max}}{\pi\,b\,d} \qquad [2.7]$$

IDT test results are also used to determine the critical cracking temperature in the thermal cracking (TC) model implemented in the AASHTO Mechanistic-Empirical Pavement Design Guide (MEPDG).

2.1.2. Bending Beam tests

The Euler-Bernoulli beam theory and the elastic-viscoelastic correspondence principle can be applied to calculate both flexural strength and creep compliance from a three-point bending beam test. The test consists of a rectangular beam resting on two roller supports and subjected to a concentrated load applied in the middle of the beam (see Figure 2).

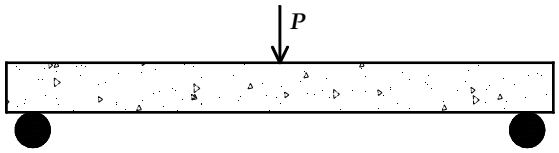

Figure 2. Schematic of 3-point bending test

The Euler-Bernoulli beam theory is based on the assumption that the material is linear and isotropic and that the normal deflection of the beam is very small compared to the length of the beam. The second assumption implies that cross sections remain planar and perpendicular to the beam axis during deformation (Gere, et al., 1990). According to this theory, the maximum deflection δ_{max} at the mid-span of the beam is given by:

$$\delta_{max} = \frac{PL^3}{48EI} \qquad [2.8]$$

where *L* is the length of the span, *P* applied load, and *I* moment of inertia. The equation can be modified using the elastic-viscoelastic correspondence principle and applied to determine the creep compliance *D(t)* of asphalt concrete, given a creep displacement history.

$$D(t) = \frac{48\, I\, \delta(t)}{PL^3} \qquad [2.9]$$

There is a modest literature on using the three-point bending test in low-temperature characterization of asphalt concrete. The lack of interest is mainly due to the restrictions posed by the prismatic geometry of the test specimen. It is much easier to prepare cylindrical test specimens through laboratory compaction or field coring. In this regard, the most popular asphalt concrete compaction method is the Superpave Gyratory Compactor (SGC), which produces cylindrical specimens. Nevertheless, Zofka et al., (2010) compared creep compliances of asphalt concrete obtained from the IDT to those from three-point bending test, and found relatively good agreement. The authors used the Bending Beam Rheometer (BBR) device that was developed during the Strategic Highway Research Program (SHRP) for testing asphalt binders at low temperature (Bahia, et al., 1992).

2.2. Fracture Mechanics

Fracture mechanics based testing and analysis methods provide material parameters that describe the ability of structures containing cracks to resist crack initiation and propagation. These methods are becoming increasingly applied to characterize asphalt concrete's resistance to cracking. The basic concepts of these theories are summarized below.

2.2.1. Linear Elastic Fracture Mechanics

The Linear Elastic Fracture Mechanics (LEFM) theory is based on the assumption that the considered material is isotropic, homogeneous, and linear elastic in all its parts, except for an extremely small region near the crack tip (Anderson, 1995). If the size of this inelastic zone is relatively large compared to the size of the crack and the dimensions of the body, LEFM is no longer valid.

The first attempts to compute stress concentrations, near the crack tip, were made by Inglis (1913). The researcher addressed sharp crack as a limit case of an elliptical hole, for which he formulated the exact solution of stress concentration. Based on Inglis's work, Griffith (1920) concluded that the strength criterion cannot be applied because the stress at the tip of a sharp crack approaches infinity regardless of the load magnitude. He further noted that the formation of crack requires a certain energy per unit area of the crack surface and formulated the energy release rate approach. The energetic approach, further developed to its current version by Irwin (1956), states the following: the energy

release rate G (energy available for crack extension) is defined as the change in elastic strain energy U per unit area of crack growth:

$$G = \left[\frac{\partial U}{\partial a}\right]_P = -\left[\frac{\partial U}{\partial a}\right]_u \qquad [2.10]$$

where a represents the crack length. P and u indicate, respectively, fixed load and fixed displacement conditions.

A practical method of determining the fracture energy is based on measurement of compliance of a specimen with different crack lengths. The compliance C of a specimen is given by the displacement u per unit load:

$$C = \frac{u}{P} \qquad [2.11]$$

The relationship between compliance and fracture energy is then given by the following expression:

$$G = \frac{P}{2}\frac{\partial u}{\partial A} = \frac{P^2}{2}\frac{\partial C}{\partial A} \qquad [2.12]$$

where ∂A represents the crack surface extension. Fracture occurs when the energy available for crack growth exceeds the resistance of the material. The critical energy release rate G_c is used as a measure of the fracture toughness of the material. But experimental determination of this parameter needs accurate measurements of crack extensions, which are difficult to obtain.

In the sixties, Irwin developed the stress intensity approach which is effectively equivalent to the energetic approach, but relatively easier to derive for practical problems (1961). If the LEFM assumptions are valid, the stress intensity approach states that the stress concentration near a crack tip has the same distribution regardless of size, shape and boundary conditions of the structure. The only factor that varies is the intensity of the stress concentration. Considering a mode I type of fracture, in which the crack lies in a plane normal to the direction of largest tensile loading, the stress state around the crack tip is characterized using the stress intensity factor K_I proportional to load P, and function of crack size a and the geometry of the structure. The stress value at any point near the crack tip is given by:

$$\sigma_{ij}(r,\theta) = \frac{K_I}{\sqrt{2\pi r}}\, Y_{ij}(r,\theta) \qquad [2.13]$$

where, σ_{ij} are the stresses acting at a small distance r from the crack tip, and angle θ from the crack plane, and $Y_{ij}(r,\theta)$ dimensionless functions of polar coordinates. The $Y_{ij}(r,\theta)$functions are independent of size and load, but they depend on the geometry of the structure and the loading configuration.

The critical value of K_I for which failure occurs, referred to as fracture toughness K_{IC}, describes the local stress state that leads to the propagation of a crack. Therefore, K_{IC} represents the highest value of stress intensity factor that the material can bear without fracture. Equation [2.13] highlights an important concept of fracture

mechanics: flaws are responsible for lowering the global strength of the material by amplifying the stress locally.

The two LEFM fracture toughness parameters are equivalent and related through the Irwin's relationship (Irwin, 1957) as follow:

$$G_{IC} = \frac{K_{IC}^2}{E'} \qquad [2.14]$$

where E' is equal to Young's Modulus E for plane stress, and to $E/(1-\nu^2)$ for plane strain conditions.

2.2.2. Applicability of LEFM

The stress intensity equation in [2.13] can be redefined in such a manner that the size D is made explicit (Bažant, et al., 1998):

$$K_I = \frac{P}{b\sqrt{D}}\,\hat{k}(\alpha) = \sigma_N\sqrt{D}\,k(\alpha) \qquad [2.14]$$

Equation [2.14] represents the general form of the K_I expression, based on load P and the nominal stress σ_N. The term D is a characteristic dimension of the structure, $\alpha = {}^{a}/_{D}$ represents the ratio of crack length to the characteristic dimension, and $\hat{k}(\alpha)$ and $k(\alpha)$ are dimensionless functions. The crack growth condition $K_I = K_{IC}$ is attained when σ_N reaches the nominal strength corresponding to the peak load:

$$\sigma_N = \frac{K_{IC}}{\sqrt{D}\;k(\alpha)} \qquad [2.15]$$

Equation [2.15] describes an inverse square root relationship $\sigma_N \propto D^{-1/2}$ between size and strength of geometrically similar structures that meet the LEFM conditions. This power law relationship is described by an inclined straight line of slope -1/2 in a $\log(\sigma_N)$ vs. $\log D$ plot, and it is a powerful tool for testing the applicability of LEFM.

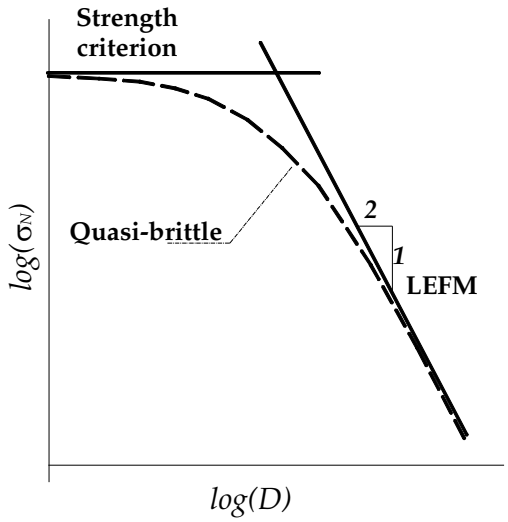

Figure 3. Size effect: nominal strength vs. size in log-log plot

For LEFM to be applied, experimental nominal strength results obtained from geometrically similar structures would have to lie on the line of slope -1/2 (see Figure 3). Only in this case the fracture parameters determined using the LEFM equations are material constants and thus independent of size or shape. However, quasi-brittle materials, in particular concrete, have been shown to exhibit a rather different behavior than that described by the LEFM or strength criterion (horizontal line in Figure 3) power

laws (Leicester, 1969; Kesler, et al., 1972; Walsh, 1972; Walsh, 1976). For notched fracture specimens, the behavior of quasi-brittle materials appears to obey the strength criterion law on small scale, and on large scale the LEFM. The bridging between the strength theory and LEFM must be described by a size effect law that contains material characteristic length. The reasons for this deviation from LEFM are discussed in the following pages.

2.2.3. Types of fracture behavior in Quasi-Brittle materials

The fracture behavior of quasi-brittle materials is governed by the size of the inelastic zone that develops ahead of the crack tip. This zone tends to reduce the stresses (softening) at the crack tip and dissipate the fracture energy through tortuous crack path, aggregate interlocking, micro-cracking, permanent deformation, and viscoelastic relaxation (Mobasher, et al., 1997). The inelastic zone is also referred to as fracture process zone (FPZ).

Depending on the FPZ's relative size to the structure (see Figure 4), two types of fracture behavior can be distinguished: brittle and quasi-brittle. In the brittle type of fracture, the size of the FPZ is relatively small and the fracture process is assumed to occur entirely at the crack tip. In this case the LEFM analysis can be applied, and the structure fails by unstable (self-propagating) growth of the crack when the stress intensity factor reaches its critical value K_{IC}. This type of failure can be observed in brittle materials, such as glass, and can be modeled using only the K_{IC} parameter.

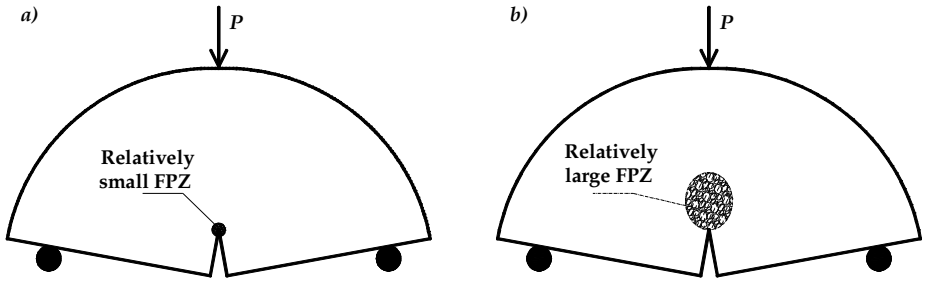

Figure 4. Size of FPZ: a) relatively small FPZ, and b) relatively large FPZ

In the second type of fracture, the size of the FPZ is relatively large and it cannot be neglected. Thus, LEFM is inapplicable. In this type of failure, a crack can extend in a stable manner under increasing load until the FPZ is fully developed. This phenomenon can be described by relating the crack growth resistance R to the effective crack extension as shown in Figure 5. According to this model, the R-curve plateau is reached when the FPZ is fully developed and has a size equal to the effective length of FPZ c_f. Therefore, the toughening of the material during stable growth can be significant and needs to be taken into account by relatively complicated fracture analysis methods.

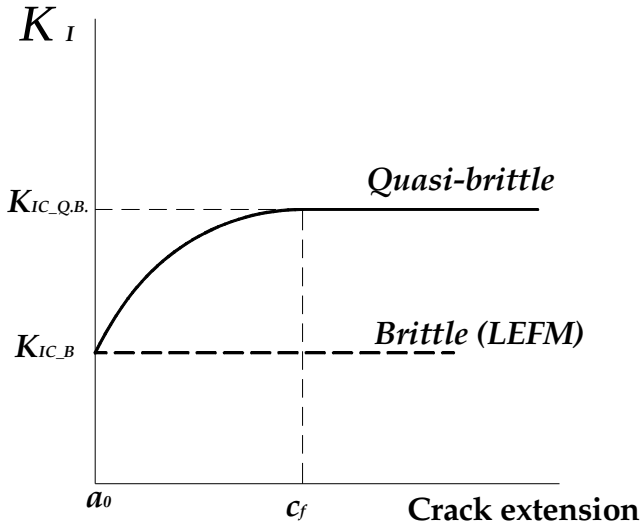

Figure 5. Failure mechanism of brittle and quasi-brittle materials

This implies that a good understanding of the softening behavior that occur in the FPZ and the size of the FPZ are crucial in determining the fracture behavior of the structure and identifying the proper fracture analysis. An estimate of the size of the FPZ in quasi-brittle materials can be derived using a method similar to Irwin's (i.e., estimate of inelastic zone for ductile materials) (Irwin, 1958). But unlike plastic materials, in which stress is assumed to be constant throughout the inelastic zone, the FPZ in quasi-brittle fracture is characterized by a progressive softening. Accordingly, the size of FPZ c_f is found to be proportional to the square of the ratio between the fracture toughness K_{IC} and the strength of the material f_t' as:

$$c_f = \eta \left(\frac{K_{IC}}{f_t'}\right)^2 \qquad [2.16]$$

where the second term in the equation has the dimension of length and it represents the ration of two material constants, thus it is referred to as the *characteristic length* or *material length* l_{ch}:

$$l_{ch} = \left(\frac{K_{IC}}{f_t'}\right)^2 = \frac{E' G_f}{{f_t'}^2} \qquad [2.17]$$

η is a dimensionless constant that can take large value. Bažant et al (1998) indicated that for concrete, η vary between 2 and 5 and the values for l_{ch} varie between 0.15 m and 0.40 m. Therefore, the size of FPZ for concrete can take values ranging from 0.3 m to 2 m. Although only few studies on the size of FPZ of asphalt concrete mixtures have been carried out, it appears that the FPZ size is smaller than that expected in Portland concrete materials, but still relatively large to be neglected. Li et al. (2010) used Acoustic Emission (AE) technique to estimate the size of FPZ in asphalt concrete mixtures tested at low temperature in semi-circular bending test. The authors concluded that the length of the FPZ ranged between 20-30 mm. These sizes of FPZ suggest that, in order to properly apply LEFM testing and analysis method to quasi-brittle materials, large specimens need to be used for experimental testing. This might become impractical and costly. As an alternative, non-linear fracture testing and analysis methods to obtain fracture parameters from small-scale laboratory specimens can be used.

2.2.4. Size Effect in Quasi-Brittle materials

Analyzing the size effect on the nominal strength of the structure is one way of understanding the fracture behavior in quasi–brittle materials. The size effect observed in these type of materials cannot be described by traditional power scaling of type $\sigma_N \propto D^{-p}$ where can p can take the values of 0, $1/2$, and n/m (i.e., Weibull modulus), respectively, for strength theory, LEFM, and Weibull's statistical theory. The main reason is that the indicated power laws do not contain a characteristic length, essential in describing quasi-brittle materials with large FPZ and noticeable heterogeneity. The size effect in quasi brittle materials is of deterministic type and can be described through an energetic approach. Two types of size effects have been distinguished:

a. Type I size effect: the structure attains its peak load when a macro-crack initiates from one representative volume element (RVE), which often happens to structures with a smooth boundary, such as flexural failure of beam under bending and tensile fracture of bar under uniaxial tension. For small and medium size structures, the Type I size effect can be derived based on the Taylor series expansion of the energy release function at zero crack length. At large size limit, the size effect is governed by the Weibull statistics. The statistical size effect can be amalgamated with the energetic size effect to form the complete Type I size effect (Bažant, 2005). Recent studies also showed that the Type I size effect can be alternatively derived from a finite weakest link model where the structure is statistically represented by a finite chain of RVEs and the probability distribution

of RVE strength is derived from fracture mechanics of nano-cracks propagating by small, activation-energy controlled, random jumps through a nano-structure (Bažant, et al., 2009; Le, et al., 2011) .The type I size effect can be expressed as:

$$\sigma_N = \sigma^{\infty}\left[\left(\frac{D_b}{D}\right)^{r\,n/m} + \frac{r\,D_b}{D}\right]^{1/r} \qquad [2.18]$$

where σ_N is the nominal strength given by P/bD or P/D^2 , respectively, for scaling in two or three dimensions; P = maximum applied load; D = characteristic size; b = thickness of the structure; m = Weibull modulus; n = scaling dimension; and σ^{∞}, r, and D_b are positive material constants. D_b is an index parameter related to the effective length of the boundary layer. In the case of a three-point bending test performed on a beam of span S and rectangular cross section of depth D, the relationship between D_b and the length of the FPZ c_f is given by (Bažant, 1999):

$$D_b = \left(\frac{3\,S}{2D}\right) c_f \qquad [2.19]$$

It can be noticed that, for geometrically similar beams the ratio S/D is constant, thus also D_b is constant.

b. Type II size effect: the maximum load of the structure is reached once a single large crack is formed. The Type II size effect is typically applied to quasi-brittle structures containing a large notch or a large stress-free (fatigued) crack formed prior to maximum load. This size effect can be derived by using the asymptotic

approximation of the energy release function for the propagating crack or the J-integral:

$$\sigma_N = B f_t' \left(1 + \frac{D}{D_0}\right)^{-1/2} \qquad [2.20]$$

where D_0 represents a constant called transitional size; B is a dimensionless constant structure-geometry dependent; f_t' is the tensile strength. The ratio $D/D0_0$ is commonly referred to as the brittleness number, β. Large values of β indicates that the structure behaves in a more brittle manner.

A graphical representation of the two size effect laws is given in (Bažant, et al., 2009) and is presented in a log-log plot as in Figure 6.

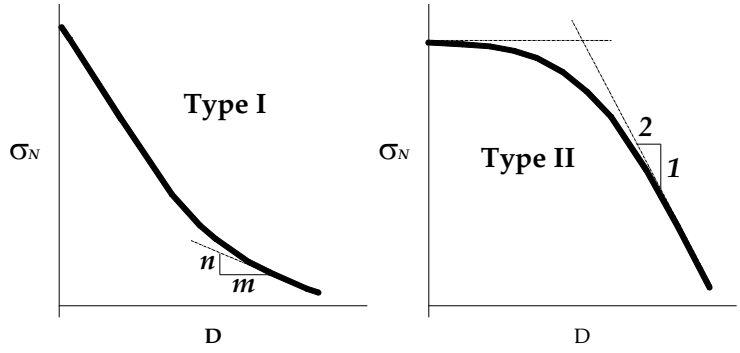

Figure 6. Asymptotic analysis of Type I and Type II size effect

The large-size asymptote of Type I size effect follows a power law, which is consistent with classical Weibull size effect. The large-size asymptote of Type II size effect follows a power law with an exponent equal to -1/2, which is consistent with

LEFM. Type I and Type II size effects represent two different failure mechanisms. The large-size asymptote of Type I size effect is purely statistical because the fracture can occur anywhere in the structure. In contrast, for Type II size effect, which usually applies to structures with pre-existing crack, the fracture must occur at the crack tip. Therefore, the size effect must be governed by energy release at the crack tip, and not by the statistics of material strength.

The small-size asymptotes for Type I and Type II size effects are also different although both can be derived using the equivalent linear elastic fracture mechanics method. The key difference between them is that, for Type I size effect, the initial energy release rate is zero (i.e. zero crack length) whereas for Type II size effect, there is a finite energy release rate (i.e. finite crack length).

2.2.5. Equivalent LEFM approaches

Most of the alternative methods to the LEFM analysis rely in determining the non-linear relationship between the increase in fracture toughness and the crack extension (see Figure 5). These methods assume that the fracture condition $K_I = K_{IC}$ is obtained at an equivalent elastic crack length $a_e = a_0 + \Delta a_c$. Thus, knowledge of the critical effective crack extension Δa_c is required.

Several methods have been proposed for the determination of Δa_c from experimental testing of quasi-brittle materials. These methods make use of the fact that in LEFM displacements are proportional to the load, and the resulting compliance is related

to the crack length (see equation [2.12]). The *Compliance Calibration Method* (Swartz, et al., 1979) and *Nallathambi-Karihaloo Method* (1986a; 1986b), to name a few salient approaches that can be found in literature.

Another variant of LEFM, proposed by Jenq and Shah (1985), assumes that fracture occurs when the Crack Tip Opening Displacement (CTOD) reaches its critical value δ_{CTOD}. In LEFM, there are few cases for which closed form of the functions describing the crack opening profiles are given. In this cases, given the initial crack length a_0 , the specimen dimension, and the material parameter K_{IC}, the equivalent crack length a_e and the nominal strength σ_N can be solved from the system of equations describing the condition for fracture $K_I = K_{IC}$ and the critical crack opening $CTOD = \delta_{CTOD}$. However, for most of the cases, the effective crack extension Δa_c and the peak load need to be measured from experiments. The crack extension is then measured by optical inspection or through the *compliance approach* proposed by Jenq and Shah (1985). The latter approach is based on compliance measurements obtained from successive loading unloading cycles and used to determine the effective crack length. The *compliance approach* is also used to construct the compliance-crack length relationship, which in turn can be used to determine the energy release rate G_I at every incremental crack length through expression [2.12]. The fracture toughness K_I at every incremental crack length is then calculated through the Irwin's relationship to construct R-curve of the material (Figure 5). This approach was successfully applied to asphalt concrete mixtures by Mobasher et, al (1997). However, it can be observed that the measurement of

crack extension is both complex and difficult to implement in small environmental chambers.

2.2.6. Cohesive Zone Model

Cohesive Zone Model (CZM) is a fracture analysis method that takes into account the non-linear behaviors that occur at the front of a preexisting crack. The concept was first proposed by Barenblatt (1962) and Dugdale (1960) and applied to materials with ductile behavior (e.g., metals). The theory was later extended by Hillerborg et al.,(1976) to be applied to quasi-brittle materials, particularly concrete, that do not necessarily have a preexisting macro-crack, from which the name *fictitious crack model* was derived.

The concept of *cohesive crack model* is explained in Hillerborg (1985) through the analysis of a concrete specimen subjected to pure tension in a strain controlled test. The test identifies the following three sequence-phases:

a. Prior to reaching the peak load, the material response is characterized by a linear stress-elongation curve. While in this region, the stresses keep increasing and the strains are uniformly distributed along the whole volume of the specimen.

b. At the peak load, a single cohesive crack normal to the axis of the bar starts developing at the weakest point of the specimen.

c. After the peak load is reached, all the deformation localizes into the crack and a finite opening ω is developed along the crack while still transferring stress. At this stage, a *strain softening* phenomenon, decrease of stress under increasing strain,

takes place in the narrow region ahead of the crack tip. Whilst, the remaining part of the specimen unloads and its strains decrease elastically. Experimental studies have shown that the permanent deformations that can occur on the region of the specimen far from the *fictitious crack* are generally small and negligible.

The *fictitious crack model* assumes that the stress transferred through the cohesive crack is related to the crack opening ω by:

$$\sigma = f(\omega) \qquad [2.21]$$

where $f(\omega)$ represents the softening curve of the material as shown in Figure 7. Considering that the model assumes that the crack starts opening at peak load, the following is true about the softening curve function:

$$f(0) = f_t' \qquad [2.22]$$

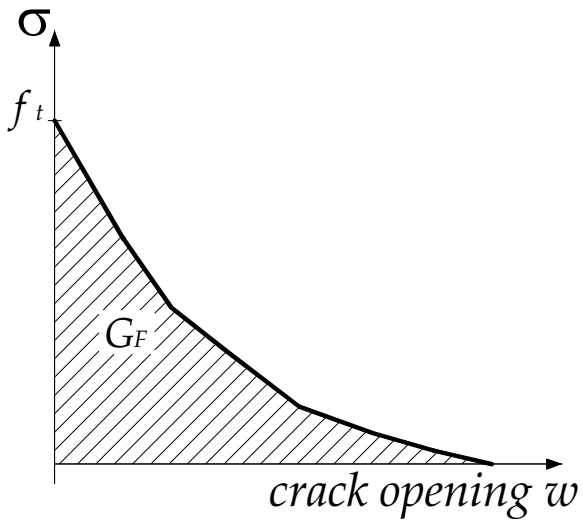

Figure 7. Softening curve of a cohesive model

The energy dissipated in creating a unit surface area, cohesive fracture energy G_F, is then computed using the area below the *stress – crack opening* curve using equation [2.23] :

$$G_F = \int_0^\infty \sigma \, d\omega \qquad [2.23]$$

Therefore, in order to characterize a material's fracture properties through the cohesive model, the following need to be determined from experiment: shape of the softening, fracture energy G_F, and tensile strength f_t'.

The softening curves for quasi-brittle materials are usually smooth and non-linear, similar to the curve in Figure 7. However, these curves can be approximated quite well by simple analytical functions. The linear softening illustrated in Figure 8 is the simplest approximation that can be used.

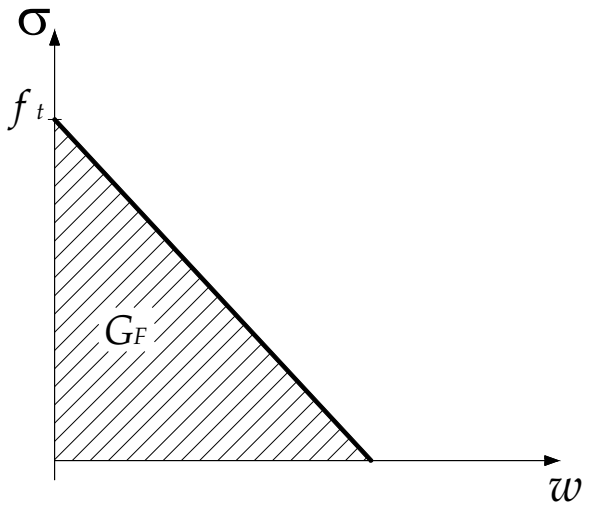

Figure 8. Linear approximation of the softening curve

Ideally, the cohesive zone model parameters are determined from a uni-axial tensile test. However, due to difficulties associated with gripping the ends of the specimens and uncertainty on the location where crack or cracks will develop, other indirect methods are often used to determine the cohesive parameters. The tensile strength f_t', can be computed from the IDT, also known as the Brazilian Test, and the cohesive fracture energy can be computed through the *work-of-fracture method* (Hillerborg, 1985) from a notched bending beam as described in the RILEM TC-50 FMC (1985) specification. The total fracture energy consumed in the process of breaking the notched specimen into two pieces can be evaluated from the area under the load-load line displacement curve. Consequently, an approximate fracture energy can be obtained by averaging the total fracture energy over the fracture surface, as shown in equation [2.24]:

$$G_F = \frac{1}{b(W-a)} \int P \, d\delta \qquad [2.24]$$

where a is the initial notch length, W is the specimen width in the crack growth crack direction, and b is the specimen thickness. The *work-of–fracture method* was successfully used to compute the fracture energy from SCB by Li et al. (2009). The backdrop is that both IDT tensile strength f_t' and G_F computed from small specimens are size-dependent and thus not true material parameters.

2.2.6. Determining fracture properties from the Energetic Size Effect law

Bažant's energetic size effect law in equation [2.20] can also be expressed in terms of LEFM fracture parameters and functions (Bažant, et al., 1998; Bažant, 2005) as:

$$\sigma_N = \sqrt{\frac{EG_f}{g'(\alpha_0)c_f + g(\alpha_0)D}} = Bf_t' \left(1 + \frac{D}{D_0}\right)^{-1/2} \qquad [2.25]$$

where $g(\alpha_0)$ and $g'(\alpha_0)$ represent the LEFM energy release function and its first derivative at the initial crack length. Bažant (1998) showed that for large sizes (large D) the size effect predicted by the equivalent LEFM analysis methods converges to the size effect in [2.25]. In addition, the terms D_0 and Bf_t' can be expressed as:

$$D_0 = c_f \frac{g'(\alpha_0)}{g(\alpha_0)} \qquad [2.26]$$

$$Bf_t' = \sqrt{\frac{EG_f}{c_f\, g'(\alpha_0)}} \qquad [2.27]$$

Therefore, by determining D_0 and Bf_t' from experiments, size independent LEFM fracture parameters for large sizes can be obtained through:

$$G_f = \frac{\left(Bf_t'\right)^2 D_0 \, k_0^2}{E'} \qquad [2.28]$$

$$K_{IC} = Bf_t' \sqrt{D_0} \, k_0 \qquad [2.29]$$

2.2.6. Fracture Mechanics applied to Asphalt Concrete

Since the 1970s, a growing number of researchers have applied fracture mechanics-based testing and analysis methods for characterizing the low temperature fracture properties of asphalt concrete. Because it was generally assumed that at low temperatures the LEFM conditions are valid for asphalt concrete, the Mode I fracture toughness parameter K_{IC} has been frequently used in the literature. Nevertheless, the fracture energy G_F parameter, which has been shown to better describe the non-linear behavior of quasi-brittle materials, is increasingly being used. Below, a brief description of some fracture mechanic-based test methods used to investigate the low temperature performance of asphalt concrete mixtures is presented.

One of the earliest applications of LEFM analysis for asphalt concrete (Labuz, et al., 1994) used a simple three-point bending configuration to determine multiple measurement of fracture toughness K_{IC} through a computer controlled unload-reload procedure. The experimental tests revealed the complexity of measuring the load-point displacement due to the non-linear deformations and crushing that occur at the roller to specimen contact. This problem was solved by using a differential displacement

measurement: the deflection of the notch relative to a point located on the test frame. The test results indicated that the energy required to initiate fracture increased as the test temperature decreased. Similarly, specimens with lower air void content exhibited higher fracture toughness K_{IC}, than specimens with higher air void content.

In the research work conduct by Roque et al (1999), the possibility of using the IDT test configuration to determine the fracture properties of asphalt concrete was investigated. The test specimen consisted of a typical IDT cylinder with an 8-mm diameter hole drilled at its center. The aim of the test was to determine suitable crack growth rate parameters that characterize the fatigue cracking of asphalt concrete under traffic loading at intermediate temperatures. Zhang et al., (2001) later argued that in the modified IDT fracture test the crack growth process is mainly governed by an unrestrained permanent deformation that occur near the crack tip. Whereas, in field asphalt pavements, in which permanent deformation is constrained from developing to the same degree as in the IDT geometry, the crack growth mechanism is controlled by other factors.

Another type of fracture test that has been widely used for characterizing the fracture properties of asphalt concrete is the Semi-Circular Bending (SCB) test. Molenaar et al. (2000) investigated the fracture properties of seven standard asphalt concrete mixtures through the SCB test and analysis method. Three different specimen sizes, four test temperatures (-10˚C, 0˚C, 15˚C, and 25˚C) and three loading rates (0.005 mm/s, 0.05 mm/s, and 0.5 mm/s) were used for the purpose of the investigation. The sizes of the

initial notch were 10 mm and 0.35 mm, respectively in length and width. The fracture toughness parameter was determined according to the ASTM E399-90 standard. The test results indicated that at high temperatures the LEFM conditions may be violated by the excessive plastic deformation, but overall the SCB test proved to be well suited for asphalt concrete characterization. For specimens with diameter larger than 220 mm, a size independent fracture toughness parameter was obtained using a loading rate of 0.05 mm/s. In contrast, for specimens with diameter larger than 150 mm the optimal loading rate was of 0.005 mm/s. In addition, the fracture toughness parameter computed from the SCB test had higher discriminative ability compared to the IDT tensile strength.

More recently Li et al.(2004) used the SCB test to investigate the low temperature fracture properties of three Superpave asphalt concrete mixtures. The test results were used to determine the fracture toughness and fracture energy of the mixtures. The researchers found that both fracture parameters were significantly affected by temperature and type of asphalt binder.

Wagoner et al.,(2005(a)) proposed the Disk-Shaped Compact Tension (DCT) test for the determination of fracture energy of asphalt concrete tested at low temperatures. They found good agreement between the fracture energy results obtained from the DCT and those obtained from the SCB and three-point bending test of notched beams.

2.3. Semi-Circular Bend Beam test for Asphalt Concrete

The Semi-Circular Bend (SCB) test was first used by Chong et al. (1984) for fracture testing of rock materials. The test is based on a semi-circular specimen with a single edge notch subjected to a three-point loading. The test specimens can be easily prepared from gyratory compacted cylinders or field cores. The test set up is shown in Figure 9. Depending on the orientation of the notch, the SCB test can be used to determine both mode I and II stress intensity factors. A compressive load is applied vertically at the top of the specimen in such a manner as to produce constant crack mouth opening displacement (CMOD) rate. The CMOD is measured at the bottom of the specimen using an Epsilon clip gauge. The load line displacement (LLD) is measured using a vertically mounted Epsilon extensometer attached to the specimen in one end, and to a specially made external frame to the other end (see Figure 9).

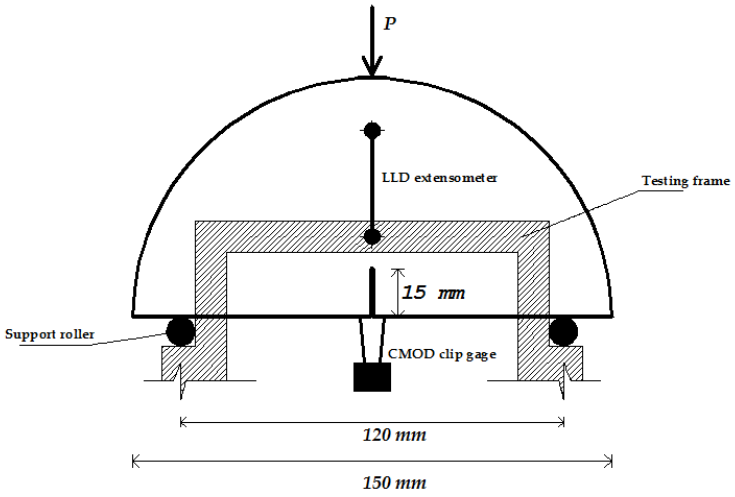

Figure 9. Schematic of Semi-Circular Bend (SCB) test

Due to the complex geometry of SCB specimens, it is difficult to obtain analytical solutions for the stress intensity factors. For this reason, Chong *et al*. (1984), provided numerical solution for a very limited range of notch lengths and specimen sizes. Later, Lim *et al*. (1993) expanded the numerical solutions to a wider range of SCB geometries and tabulated the normalized stress intensity factors. For SCB specimen with a vertical notch, the mode I stress intensity factor is given by (Lim, et al., 1993):

$$K_I = \sigma_0 \sqrt{\pi\, a}\; k(\alpha) \qquad [2.30]$$

where

$$\sigma_0 = \frac{P}{D\, b}$$

D = diameter of the specimen

b = thickness of the specimen

P = load applied

a= notch length

α = ratio of notch length to radius

$k(\alpha)$ = normalized stress intensity factor function of α

The Mode I fracture toughness K_{IC} is determined using equation [2.28] in which P refers to the peak load.

Li et al. (2009) used the load – LLD curve obtained from the SCB fracture test to calculate the fracture energy. According to this approach, the fracture energy G_F is computed by dividing the fracture work (i.e., area under the load-LLD curve) by the fracture ligament area.

Chapter 3. Investigation of Size Effect in Asphalt Concrete

The size effect on the nominal strength of an asphalt concrete mixture tested in SCB test at low temperature was investigated. In this chapter, the experimental work including the selection of material, preparation of samples, design of experiments, and testing procedure, is discussed in detail. Following, the test results are analyzed through the energetic size effect theories to determine strength scaling laws associated with the tested material. Finally, the validity of the experimentally determined scaling laws for larger structures is verified through numerical simulation using the Cohesive Zone Model approach.

3.1. Material

The first step of the experimental work consisted in identifying the size of the SCB specimens that can be produced and tested in laboratory. Based on limitations imposed by specimen preparation, test set up, and size of the environmental chamber used for low temperature conditioning, the lower and upper limits for the specimen diameter were found to be 75 mm and 300 mm, respectively.

The second step consisted in identifying the largest aggregate size that can be used to prepare the smallest asphalt concrete specimen. The concept of minimum specimen dimensions is strictly correlated to the representative volume element (RVE) of the tested material. The RVE can be described as the smallest volume of the material that

contains all the information required to describe the mechanical properties of the global structure; therefore, it must be sufficiently large to include the largest aggregate size. A rule of thumb recommends that specimen dimensions should be at least four times the RVE. The smallest SCB specimen tested has a diameter of 75 mm and a fracture ligament length of approximately 37 mm. An accurate fracture test would necessitate an RVE four times smaller than the fracture ligament dimension, which is approximately 9 mm.

Based on the above considerations, an asphalt concrete mixture with a nominal maximum aggregate size (NMAS) of 4.75 mm was selected. The mixture contains a blend of ISPAT taconite tailings, MINTAC taconite tailings, and locally produced sand, and was used in test cell 6 at MnROAD (Clyne, et al., 2010). The performance grade (PG) of the asphalt binder was PG 64-34 and the asphalt content was 7.4%.

3.2. Sample preparation

The specimens were prepared from loose mix, sampled at MnROAD during construction of cell 6, at Iowa State University using a Linear Kneading Compactor (LKC). A total of 10 slabs of standard dimensions (381 x 210 x 75 mm) were prepared at 7% air void content. Coring of cylindrical specimens from the slabs was performed at University of Minnesota, as illustrated in Figure 10. The coring machine consisted of a motor driven head and a water cooling system. The largest size samples were obtained from six different slabs. The remaining slabs were used to cut cylinders for the three small size samples.

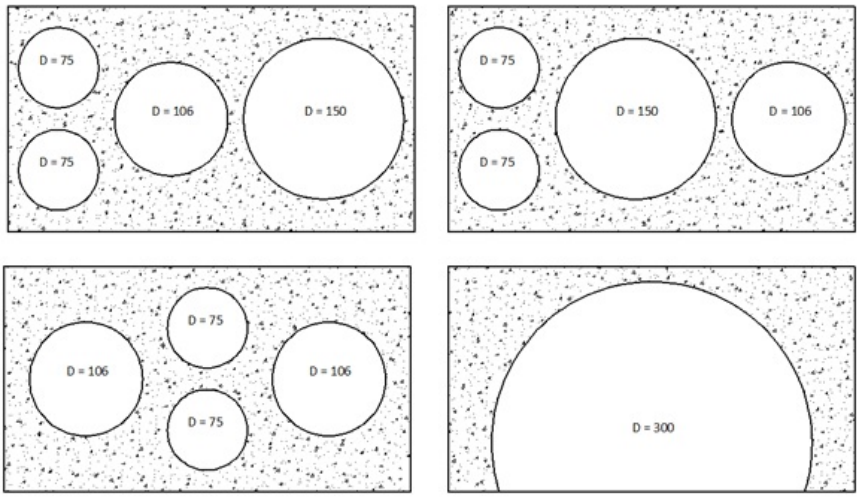

Figure 10. Coring of cylindrical specimens from slabs

To account for slab to slab variability, and to reduce the effect of non-uniform density that occurs along the compaction line, the small size samples were cored from different slabs and different regions of the slab, as shown in Figure 10. The large size samples were all obtained from the central region of the slabs, thus do not take into account of the density variation within the slabs.

The cored specimens were cut into two cylindrical slices of target thickness of 31 mm. SCB specimens were then obtained by cutting in two the cylindrical slices. The final diameter of the SCB specimen was determined by the interior diameter size of the coring bits. Therefore, the following SCB diameter sizes were obtained: 76.4 mm, 101 mm, 147 mm and 296 mm. This is equivalent to a 1: 1.32: 1.92: and 3.87 size ratio among the specimens. The final SCB slices are shown in Figure 11.

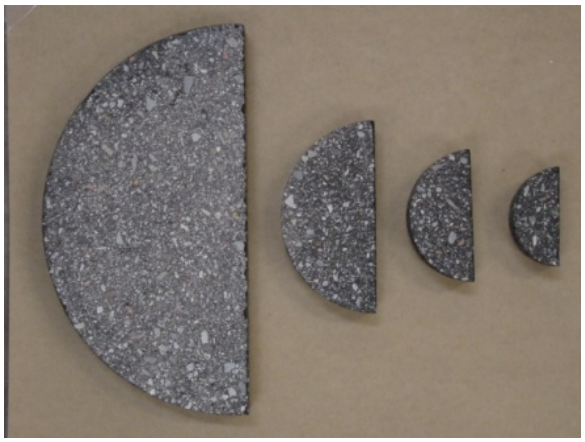

Figure 11. SCB specimens of different size

Each size was then divided into three subsets of different notch length. The first subset of specimens was designed to be tested without notch. Specimens of the other two subsets were notched in the middle of the span, using a water-cooled masonry saw with a 1 mm wide blade. Notch length to specimen radius (a/r) ratios of 5% and 20% were used, respectively, in the second and third subset.

Table 1. Experimental design

SCB Specimen	D [m]	No. of replicates			Loading rate [mm/s]	T [°C]
		a/r = 0*	a/r=0.05*	a/r = 0.2***		
Small	76.4	6	6	6	0.0003	-24
Medium	101	4	4	4	0.0034	-24
Standard	147	3	3	3	0.0005	-24
Large	296	3	3	3	0.001	-24

(*) notchless

(**) shallow notch

(***) deep notch

Table 1 presents the initial experimental design. Due to testing problems, the number of tested specimens ended up being higher.

3.3. Experimental setup

A typical SCB fracture test scheme is shown in Figure 12. The specimen is simply supported by two rollers with span, S, equal to 0.8 times the diameter of the specimen, and loaded in a three-point bending configuration. All tests were conducted at -24°C, equivalent to the low service temperature limit of the PG 64-34 binder plus 10°C. Prior to testing, all samples were conditioned for 2 hours in a controlled chamber at the test temperature using liquid nitrogen.

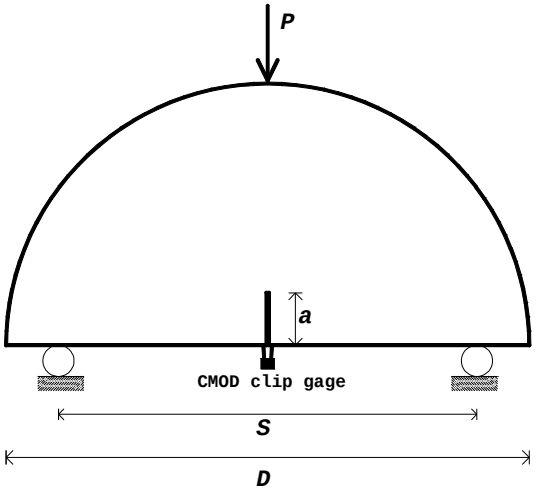

Figure 12. Typical scheme of a notched SCB test

The fracture tests were performed under constant crack-mouth opening displacement (CMOD) rates in a closed-loop servo-hydraulic testing machine. For the notched specimens, in which crack initiates at the tip of the notch, an Epsilon clip gauge

with 10 mm gage length was used. For the notchless specimens, in which cracks can initiate randomly at any location near the mid-span, a clip gauge and two long-armed knife edges, glued to the specimens, were used as shown in Figure 13. In this way, it was possible to perform CMOD controlled fracture tests on notchless SCB specimens, as long as the crack started in a region within the ends of the knife edges.

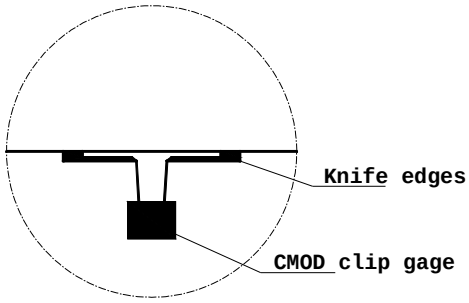

Figure 13. Installation of CMOD clip gage on a notchless specimen

In the current SCB fracture procedure, a CMOD rate of 0.0005 mm/s is used to test 150 mm diameter SCB specimens. The low loading rate was selected to reflect the rate of temperature change that occurs in real field conditions. In the present work, the same loading rate was applied for the 147 mm diameter SCB specimen. The CMOD rates for the other sizes were selected so that all specimens reached the peak load at approximately similar times. This ensures that the FPZ is loaded at the same rate, which eliminates the rate effect on the fracture process (Bažant, et al., 1998; Bažant, 2005). Limited preliminary experiments indicated that an average peak time of 3 min can be achieved using 0.0003 mm/sec, 0.00034 mm/sec, 0.0005 mm/sec, and 0.001 mm/sec, respectively for the 76.4 mm, 101 mm, 147 mm and 296 mm SCB specimens. The

following measurements were recorded: displacement of the loading piston, load, CMOD, and time.

3.4. Experimental test results

A total of 60 SCB specimens were tested to failure. Details of the tested specimens, as well as the time and load to failure recorded are reported in Table 2 to

Table 5. The shaded cells represent specimens that satisfactorily passed the quality control described in the following pages. The nominal strength σ_N values were calculated by dividing the peak load P by the diameter D and thickness b of the specimens. The apparent fracture toughness K_{IC} values were computed using equation [2.28] and normalized stress intensity factors proposed in Lim et al., (1993).

Table 2. SCB results from small specimens

Specimen ID	D	r	b	a_0	Peak Time	Peak Load	σ_N	K_{IC}
	[mm]	[mm]	[mm]	[mm]	[min]	[kN]	[MPa]	[MPa *√m]
SCB-75-0-2	76.4	36.3	31	0.0	6.1	5.73	2.42	N/A
SCB-75-0-3	76.4	37.3	31	0.0	6.1	1.09	0.46	N/A
SCB-75-0-4	76.4	37.9	31	0.0	9.5	6.19	2.61	N/A
SCB-75-0-5	76.4	36.4	31	0.0	4.9	5.25	2.22	N/A
SCB-75-0-6	76.4	36.2	31	0.0	12.9	4.12	1.74	N/A
SCB-75-5-1	76.4	37.3	31	2.0	2.7	4.03	1.70	0.65
SCB-75-5-2	76.4	35.7	31	1.8	3.2	3.72	1.57	0.57
SCB-75-5-3	76.4	36.3	31	1.8	1.6	3.50	1.48	0.53
SCB-75-5-4	76.4	36.3	31	1.8	1.8	3.90	1.65	0.60
SCB-75-5-5	76.4	35.6	31	1.8	10.1	4.18	1.76	0.64
SCB-75-5-6	76.4	37.4	31	2.0	3.1	4.24	1.79	0.68
SCB-75-20-1	76.4	37.4	31	7.5	3.8	2.46	1.04	0.76
SCB-75-20-2	76.4	38.1	31	7.8	3.4	1.60	0.68	0.51
SCB-75-20-3	76.4	37.5	31	7.6	7.1	2.01	0.85	0.63
SCB-75-20-4	76.4	37.3	31	7.6	3.8	1.85	0.78	0.58
SCB-75-20-5	76.4	35.1	31	7.1	3.7	2.26	0.95	0.68
SCB-75-20-6	76.4	36	31	7.3	7.0	2.05	0.87	0.63
SCB-75-20-7	76.4	38.2	31	7.6	0.5	2.56	1.08	0.80
SCB-75-20-8	76.4	38.1	31	7.6	5.8	2.26	0.95	0.71
SCB-75-20-9	76.4	38.1	31	7.5	2.7	2.42	1.02	0.75

Table 3. SCB results from medium specimens

Specimen ID	D	r	b	a_0	Peak Time	Peak Load	σ_N	K_{IC}
	[mm]	[mm]	[mm]	[mm]	[min]	[kN]	[MPa]	[MPa *⊠m]
SCB-101-0-1	101.1	48.8	31	0.0	2.3	6.12	1.95	N/A
SCB-101-0-2	101.1	50.3	31	0.0	3.3	6.81	2.17	N/A
SCB-101-0-3	101.1	49.3	31	0.0	4.5	5.73	1.83	N/A
SCB-101-0-4	101.1	49.1	31	0.0	2.9	4.46	1.42	N/A
SCB-101-5-1	101.1	49.9	31	2.5	2.45	4.28	1.37	0.58
SCB-101-5-2	101.1	49.5	31	2.7	2.05	4.55	1.45	0.64
SCB-101-5-3	101.1	49.4	31	2.6	2.12	3.98	1.27	0.55
SCB-101-5-4	101.1	48.7	31	2.5	1.6	4.62	1.47	0.63
SCB-101-20-1	101.1	48.8	31	9.7	5.4	2.33	0.74	0.62
SCB-101-20-2	101.1	48.6	31	9.9	6.9	2.11	0.67	0.57
SCB-101-20-3	101.1	49.3	31	9.9	13.1	1.97	0.63	0.53
SCB-101-20-4	101.1	48.8	31	9.7	2.88	2.98	0.95	0.80
SCB-101-20-5	101.1	48.7	31	9.7	3.1	3.53	1.13	0.94
SCB-101-20-6	101.1	48.7	31	9.7	3.2	2.81	0.90	0.75

Table 4. SCB results from standard specimens

Specimen ID	D	r	b	a_0	Peak Time	Peak Load	σ_N	K_{IC}
	[mm]	[mm]	[mm]	[mm]	[min]	[kN]	[MPa]	[MPa *⊠m]
SCB-150-0-1	147	72.1	31	0.0	2.3	9.38	2.06	N/A
SCB-150-0-2	147	72.2	31	0.0	7.6	7.02	1.54	N/A
SCB-150-0-3	147	71.8	31	0.0	6.4	10.76	2.36	N/A
SCB-150-5-1	147	71.8	31	3.9	1.8	4.32	0.95	0.50
SCB-150-5-2	147	71.5	31	3.5	2.1	5.11	1.12	0.57
SCB-150-5-3	147	71.6	31	3.6	1.5	6.51	1.43	0.73
SCB-150-20-1	147	72.7	31	14.3	4.8	3.82	0.84	0.85
SCB-150-20-2	147	72.7	31	14.4	3.8	4.41	0.97	0.99
SCB-150-20-3	147	72.0	31	14.7	4.7	4.41	0.97	1.00
SCB-150-20-4	147	72.0	31	14.7	4.7	3.09	0.68	0.70
SCB-150-20-5	147	72.5	31	14.7	3.1	3.44	0.75	0.78
SCB-150-20-6	147	72.0	31	14.7	4.0	3.28	0.72	0.74

Table 5. SCB results from large specimens

Specimen ID	D	r	b	a_0	Peak Time	Peak Load	σ_N	K_{IC}
	[mm]	[mm]	[mm]	[mm]	[min]	[kN]	[MPa]	[MPa *⊠m]
SCB-300-0-1	296	153.8	31	0.0	1.8	19.97	2.18	N/A
SCB-300-0-3	296	153.8	31	0.0	4.6	26.06	2.84	N/A
SCB-300-5-1	296	153.8	31	6.96	2.43	11.9	1.30	0.92
SCB-300-5-2	296	153.4	31	8.4	1.9	11.20	1.22	0.95
SCB-300-5-3	296	153.8	31	8.4	2.3	11.90	1.30	1.01
SCB-300-20-1	296	153.8	31	30	2.98	8.81	0.96	1.41
SCB-300-20-2	296	152.7	31	30.0	3.9	7.47	0.81	1.20
SCB-300-20-3	296	153.8	31	30.0	4.1	8.77	0.96	1.41

3.4.1. Inspection of experimental data

The SCB fracture tests were successfully performed on all specimens, except for the notchless specimen of diameter 296 mm. For these specimens, failure occurred at the support, far from the central region. Thus, the results were discarded.

For all notched specimens, cracking initiated at the notch tip and almost always the crack propagated in a straight, Mode I, failure path, as illustrated in Figure 14. In the picture, the surface of the specimen was colored in order to highlight the fracture path.

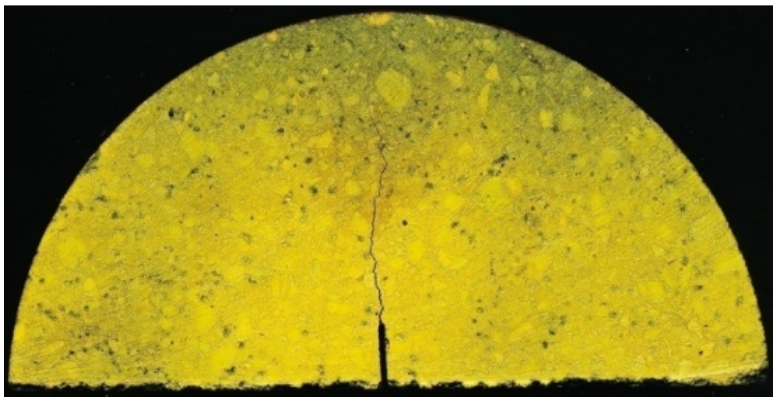

Figure 14. Failure path in SCB fracture test

At the end of each SCB test, plots of load vs. CMOD, CMOD vs. time, piston displacement vs. time, and load vs. piston displacement, were generated and visually inspected for any testing errors, see Figure 15.

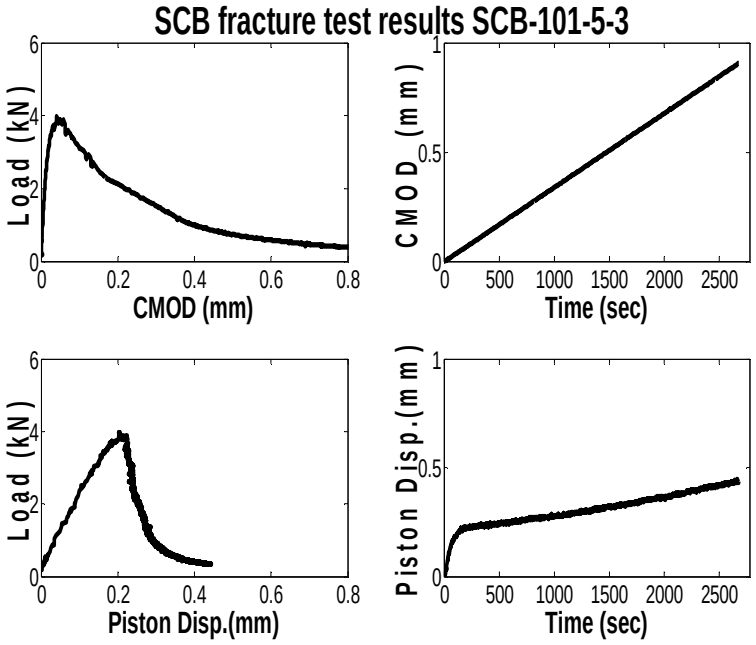

Figure 15. Plots from SCB test of specimen 101-5-3

In addition, both back and front surfaces of the specimen were scanned to allow visual inspection of the crack path.

In a second stage of data processing, the test results generated from similar specimens and test conditions were grouped and analyzed (see Figure 16). In particular, it was checked that the initial slopes of the load-CMOD curves were similar and represented similar material behavior.

Finally, the times to peak load were checked. Only the test results which satisfactorily passed all the indicated inspections were considered valid and used in the following analysis.

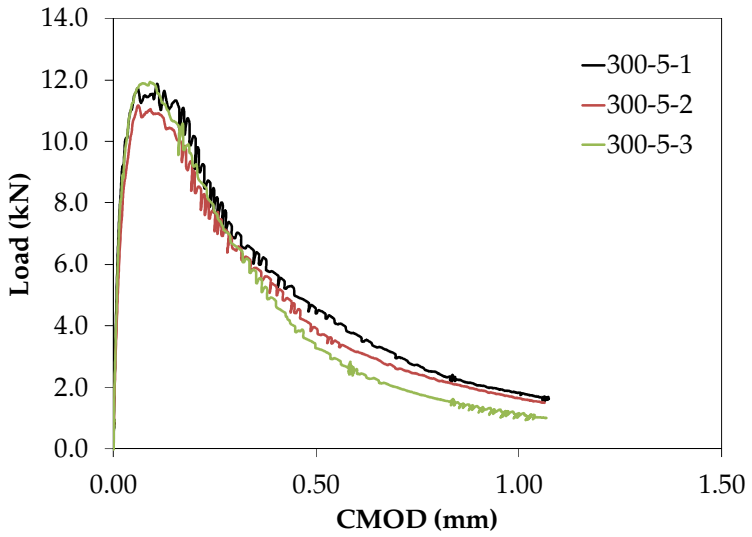

Figure 16. Load-CMOD for SCB D = 296 mm with notch a/r = 0.05

3.4.2. Analysis of test plots

Plots representing average nominal stress versus average relative CMOD are presented in Figure 17 to Figure 19. The nominal stress is computed as P/bD. The relative CMOD refers to the CMOD measurements normalized by the radius of the specimen.

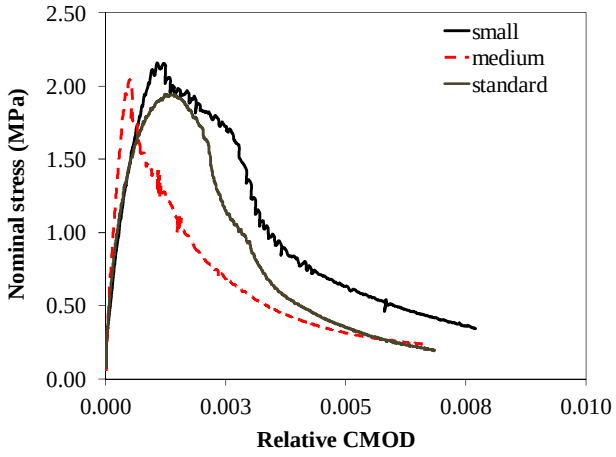

Figure 17. Nominal stress versus relative CMOD for notchless specimens

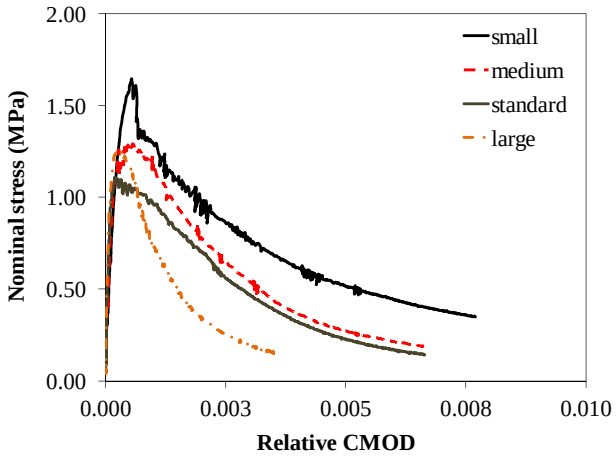

Figure 18. Nominal stress versus relative CMOD for specimens with a/r = 0.05

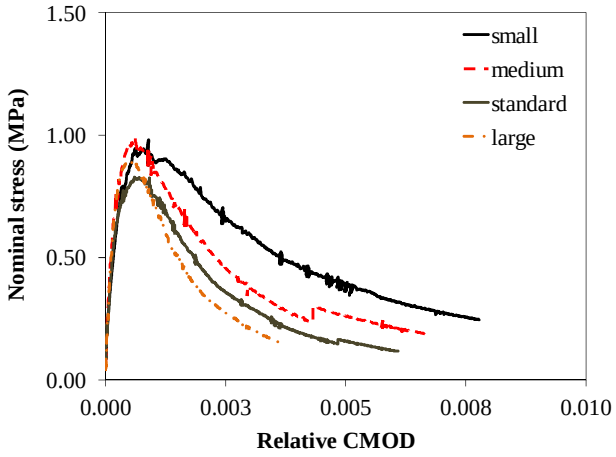

Figure 19. Nominal stress versus relative CMOD for specimens with a/r = 0.2

In all plots, it can be observed a gradual reduction of the post peak softening curves accompanied by steeper and steeper slopes as the size of specimen increases. This indicates that the range of specimen sizes considered captures accurately the transition from ductile behavior, for small-size specimens, to brittle behavior, for large-size specimens. The peak loads of the large specimens, however, were higher than expected and almost similar to those obtained from standard specimens (147 mm).

The peak loads obtained from the SCB tests were used to compute the nominal strength σ_N. The average nominal strength results are reported in Table 6.

Table 6. Average nominal strength results

a/r = 0		a/r = 0.05		a/r = 0.2	
Diameter (mm)	**σ_N (MPa)**	**Diameter (mm)**	**σ_N (MPa)**	**Diameter (mm)**	**σ_N (MPa)**
76.4	2.41	76.4	1.69	76.4	1.00
101	2.06	101	1.37	101	0.99
147	1.99	147	1.17	147	0.78
296		296	1.22	296	0.91

The nominal strength values for 296 mm diameter specimens were considerably larger than expected. In Figure 17 to Figure 19, the largest specimens had relatively short and steep strain-softening curves that suggest a relatively brittle behavior compared to the other sizes. Thus, it would be expected that the nominal strength of large specimens fall within the LEFM region. Instead, the large specimens provided nominal strength values similar to those provided by the standard SCB specimens. It is hypothesized that the specimen fabrication process affected the largest specimens' results. Only one specimen could be cored from each slab (see Figure 10) from the same location within the slab. For all other specimen sizes, the location varied within each slab and the specimens were more representative of the air voids distribution within the slabs.

The following considerations and size effect investigations include only the results for specimens with diameters 76.4 mm, 101 mm, and 147 mm.

3.5. Statistical analysis of experimental results

Statistical analyses were performed to evaluate the significance of the specimen size and notch length on the nominal strength and on the fracture toughness of the tested specimens. The MacAnova statistical software package was utilized to perform the analyses through a two way analysis of variance (ANOVA).

For the investigation on nominal strength the experiment factors considered were: specimen size (three levels: 76 mm, 101 mm, and 147 mm) and notch length (three levels: 0, 0.05, 0.2). While for the investigation on fracture toughness only the results

obtained from notched specimens (three levels of size 76 mm, 101 mm, and 147 mm and two levels of notch length 0.05 and 0.2) were considered.

The significance of the differences was tested at 0.05% level of error. In running the statistical tests, particular attention was paid to some aspect of the ANOVA models. The methods of analysis of experimental results by comparing the average responses of different treatment groups using ANOVA or contrasts are based on the assumption that the errors in the data are independent normals with constant variance. If these model assumptions do not hold, the inference may be misleading. Therefore, the ANOVA models used in this study were checked through graphical and numerical tools (provided in MacAnova) such as normal probability plots and residual plots, and met satisfactorily the validity requirements.

In addition, the occurrence of unbalanced data (not all factor-level combinations have the same amount of replication) necessitated an ANOVA model adjusted to type III sum of squares.

3.5.1. Effect of notch length and specimen size on strength

A summary of the ANOVA results for all test parameters is shown in

Table 7. The significant treatment effects are indicated in the table. According to the analysis of variance, the main effects of size and notch length on the nominal strength are highly significant. Whilst, the interaction factor between size and notch length is statistically not significant.

Table 7. ANOVA: Effect of size and notch on strength

```
anova("strength=size*notch",pvals:T,fstat:T,marg:T)
Model used is strength=size*notch
WARNING: SS are Type III sums of squares
```

	DF	SS	MS	F	P-value
CONSTANT	1	55.704	55.704	1376.29954	< 1e-08
size	2	0.65956	0.32978	8.14807	0.0032996
notch	2	6.0376	3.0188	74.58759	< 1e-08
size.notch	4	0.12281	0.030703	0.75860	0.56632
ERROR1	17	0.68805	0.040474		

The effect of notch length on the nominal strength is illustrated in Figure 20. It can be observed that the strength decreases with increasing notch length. In particular, the small and standard size specimens show similar rate of strength decrease.

The highest nominal strength values are observed for the small specimens, and the values gradually decrease as the size of the specimen increases.

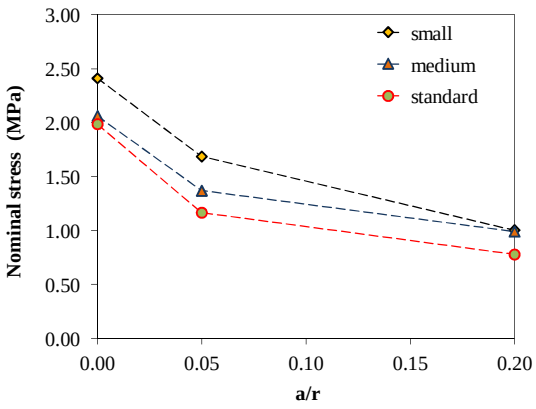

Figure 20. Nominal strength as a function of notch length

3.5.2. Effect of notch length and specimen size on fracture toughness

The effect of size and notch length on the fracture toughness parameter were also investigated using the results obtained from the notched specimens of diameter 76 mm,

101 mm and 147 mm. The ANOVA table reported in Table 8 indicates that only the effect of the notch length is statistically significant.

Table 8. ANOVA: Effect of size and notch on fracture toughness

```
anova("kic=size*notch",marg:T,pvals:T,fstat:T)
Model used is kic=size*notch
WARNING: SS are Type III sums of squares
```

	DF	SS	MS	F	P-value
CONSTANT	1	9.1524	9.1524	1029.54812	< 1e-08
size	2	0.0026023	0.0013011	0.14636	0.86525
notch	1	0.15308	0.15308	17.21981	0.0011419
size.notch	2	0.016875	0.0084375	0.94913	0.41234
ERROR1	13	0.11557	0.0088897		

3.6. Analysis of results through the Size Effect theories

A size effect investigation was performed in order to identify the type of size effect involved. In Figure 21 the mean nominal strength versus size is plotted for the notchless, shallow notch, and deep notch specimens, respectively.

The results obtained from the notchless specimens indicate a trend consistent with the Type I size effect. It is clear that the RVE size is not negligible compared to the structure size.

The size effect of the deep notch specimens indicated a Type II size effect. This can be attributed to the relatively small fracture ligament of these specimens. Assuming the size of the FPZ remains constant (regardless the size of specimen), its size gains relevance as the fracture ligament length decreases. Small fracture ligaments do not allow full development of the FPZ, and thus the material deviates from the LEFM behavior as the specimen size decreases.

For shallow notch specimens, the small-asymptote of size effect curve is similar to the case of notchless specimens, whereas the large-asymptote of size effect curve is close to the size effect of deep notch specimens. Such a phenomenon agrees well with the universal size effect equation recently proposed by Bažant and Yu (2009).

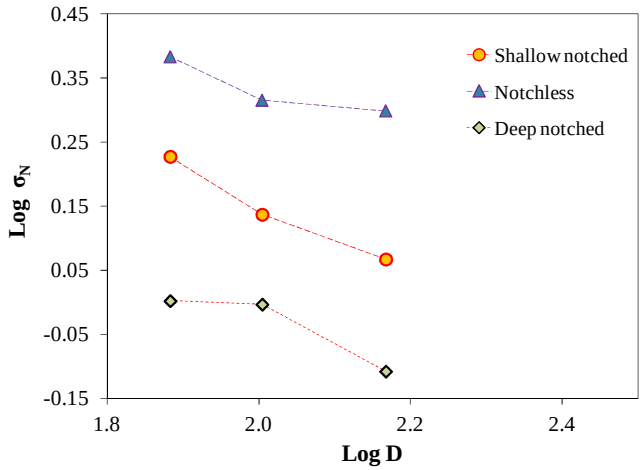

Figure 21. Nominal strength data for shallow notch SCB specimens

3.6.1. Size effect of notcheless specimens: type I size effect

The test results obtained from the notchless specimens were used in the Type I size effect law, shown in equation [2.18], to identify the material parameters σ^{∞}, D_b, and r. Weibull modulus $m=26$ was used based on an ongoing size effect research study conducted on the same asphalt concrete mixture tested in a three-point bending test configuration. A non-linear optimization method based on the Levenberg-Marquardt

algorithm was used to fit the test data. The fitting procedure consisted of several iterative optimization steps in which the value of D_b was varied between 4 and 6 times the NMAS.

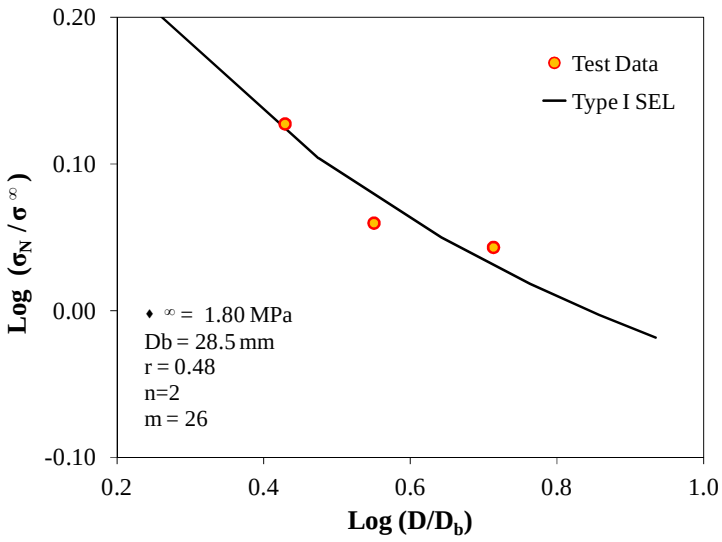

Figure 22. Size effect of notchless SCB specimens

The optimum material parameters found were σ^{∞} = 1.80 MPa, r =0.46, and D_b = 28.5 mm. Figure 22 shows comparison of the Type I size effect law and the data obtained from notchelss specimens.

3.6.2. Size effect of deep-notched specimens: type II size effect

The nominal strength results of the deep-notch specimens were fitted using the size effect law in equation [2.20]. In order to determine the material parameters Bf_t' and D_0, equation [2.20] was rearranged in a linear function of the following form:

$$Y = AX + C \qquad [3.1]$$

where $X = D$ and $Y = 1/\sigma_N^2$. The intercept and slope (A and C) of the linear equation were determined by means of linear regression analysis. Consequently, the parameters were computed as $Bf_t' = 1/\sqrt{C}$ and $D_0 = C/A$. Figure 23 illustrates the fitted Type II size effect law and the data obtained from deep notched specimens.

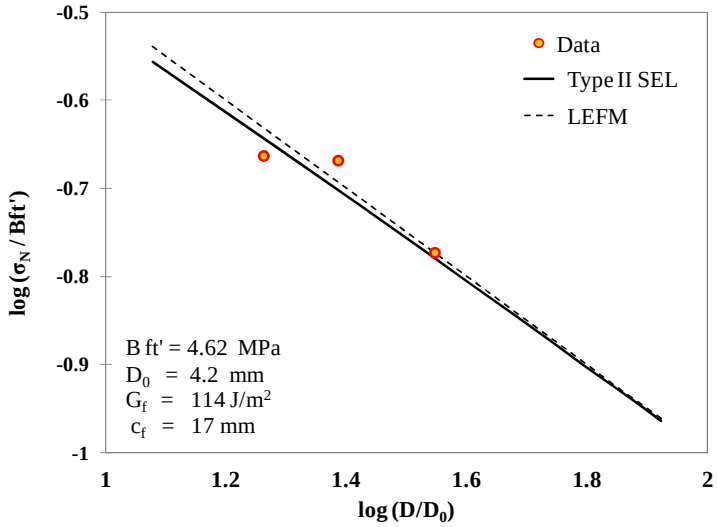

Figure 23. Size effect of deep-notched SCB specimens

3.7. Numerical modeling

One plausible limitation of the size effect investigation discussed in the paragraphs above is the small range of specimen sizes from which the size effect laws were developed. In order to assess the validity of the scaling laws at larger sizes, a finite element model (FEM) was developed to simulate the mode I crack growth in the SCB fracture test. In particular, the cohesive zone model (CZM) was used to model the damage occurring in the cohesive zone ahead of a crack tip. The experimental SCB load

versus CMOD curves were used to calibrate the numerical models and to determine the CZM parameters. The calibrated models were then used to simulate SCB fracture tests in notchless and deep-notched specimens of diameter 296 mm. The strength values predicted from the numerical models were compared to the type I and type II size effect laws described in chapter 6.

3.7.1. Cohesive Zone Model

The concept of CZM is widely discussed in the literature review section. In this section, the cohesive element modeling approach is used to simulate the mode I crack growth in SCB test configuration. Initially, the finite element numerical simulation was used to replicate the experimental load versus CMOD curves in order to determine the CZM parameters f_t' and G_F that best fits the results. Then, the calibrated CZM models were used to predict the responses of larger SCB structures.

The dimensions of the SCB specimens used in the numerical simulations were the same as those used for experimental testing. The specimens were simply supported with a span of 0.8 D and were loaded from the top.

The bulk in the SCB models was meshed using 2D plane stress four-node quadrilateral elements CPS4R. The material in this region was assumed to be isotropic, homogeneous and linear elastic and defined using Young Modulus E and the Poisson's ratio υ.

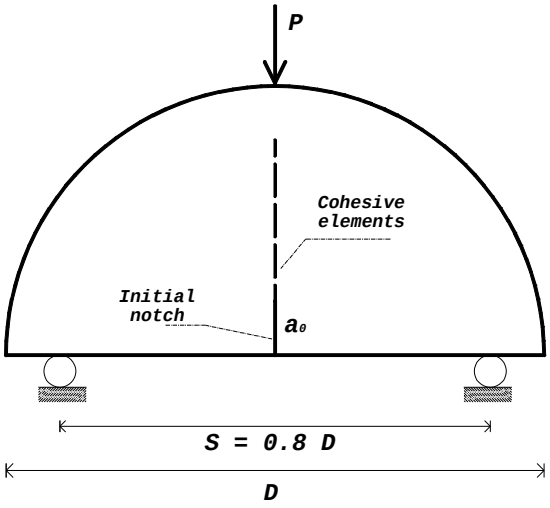

Figure 24. Geometry of SCB specimen for FE analysis

The initial un-cracked ligament in front of the crack tip was modeled using the cohesive elements COH2D4 available in ABAQUS. The width of the ligament was 1 mm and it was meshed using elements with length of 1 mm. Figure 24 shows the geometry of the SCB model used for the finite element analyses. The stress fields in the cohesive elements during various stages of the crack propagation are shown in Figure 25. It can be observed that crack initiates at the crack tip when the peak traction or strength of the cohesive interface is reached, and then propagates throughout the length of the FPZ by successive softening of the cohesive elements.

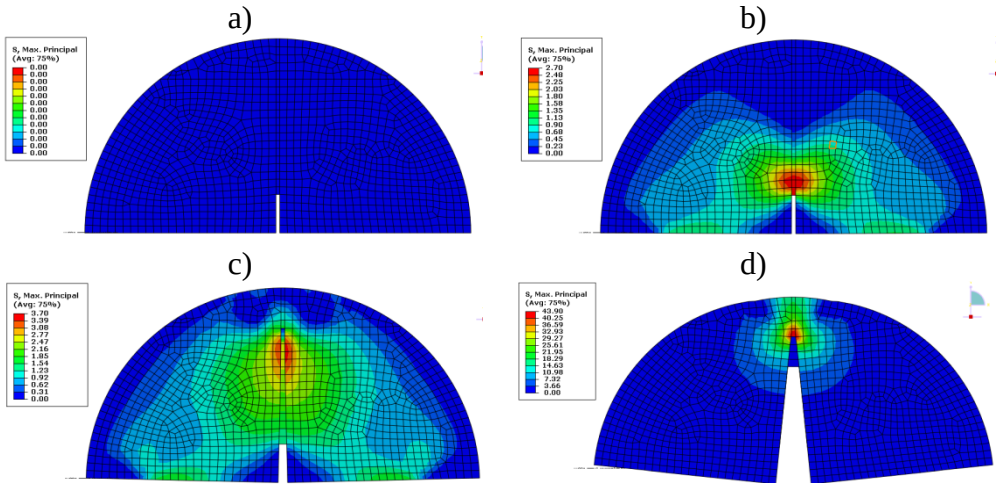

Figure 25. Maximum principal stresses at different stages of crack propagation

The calibration of the numerical models was conducted by varying the model parameters, peak traction f_t' and cohesive fracture energy G_F, in order to replicate the load versus CMOD curves obtained from the laboratory experiments. The fitting strategy consisted in finding a unique cohesive strength f_t' (for each geometry configuration) that best describes the load-CMOD curves of the three specimen sizes. The fracture energy varied slightly among the different test configurations. The elastic modulus for the initial part of the load vs. CMOD curves fluctuated between 18 GPa and 20 GPa. The scatter is mainly attributed to the heterogeneity of the asphalt concrete mixture and to the non-uniform compaction of slabs.

The simulation results are shown in Figure 26 to Figure 31. In these plots, the solid lines represent the experimental curves averaged over the test replicates, and the marked lines represent the curve obtained from finite element simulations. The curves

were compared by visual inspection and the parameter values that best fit the test data are reported in Table 9.

It can be noticed that the slope in the initial parts of the load vs. CMOD curves of the experimental results are less linear than the simulations ones. This suggests that the accuracy of the model might be improved by taking into account the viscoelastic behaviors of asphalt concrete.

An important observation is that the fracture energy of standard specimens (diameter 147 mm), reported in Table 9, was found to be very close to the fracture energy value computed using the size effect approach. This is another indication that standard SCB specimen of asphalt concrete mixtures with relatively small NMAS can be employed for LEFM based test and analysis methods.

Table 9. Material parameters for numerical simulation

SCB geometry		Modulus	Peak traction	Fracture energy	Pmax [kN]	
D [mm]	*a/r*	*E [GPa]*	*ft' [MPa]*	G_f *[J/m^2]*	FEA	Experiments
76	0.00	18	5.40	220	5.05	5.71
101	0.00	18	5.40	160	6.23	6.46
147	0.00	18	5.40	280	9.53	9.05
296	0.00	18	5.40	280	15.42	-
76.4	0.20	18	2.72	95	2.54	2.32
101.6	0.20	22	2.72	85	2.85	3.08
147	0.20	18	2.72	125	3.63	3.48
296	0.20	18	2.72	125	5.64	-

Table 9 also indicates that the energy required to extend a crack by unit area in was significantly higher for notchless specimens than that for the deep notched ones.

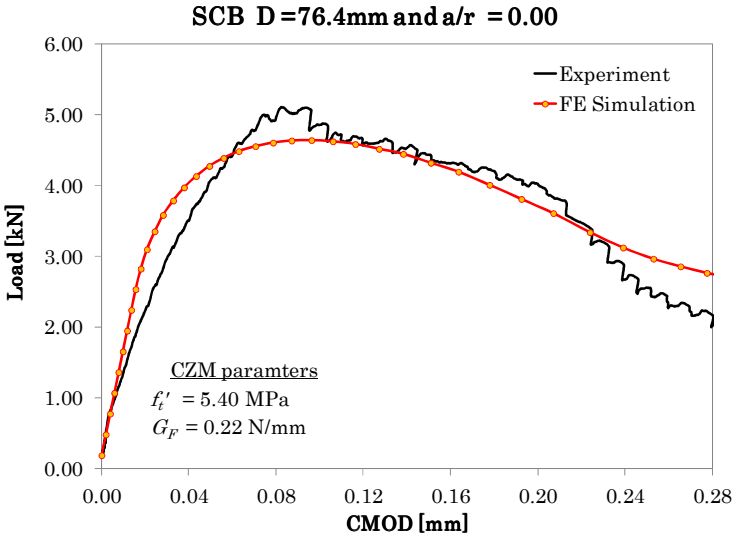

Figure 26. Simulation of SCB with D = 76 mm and a/r =0

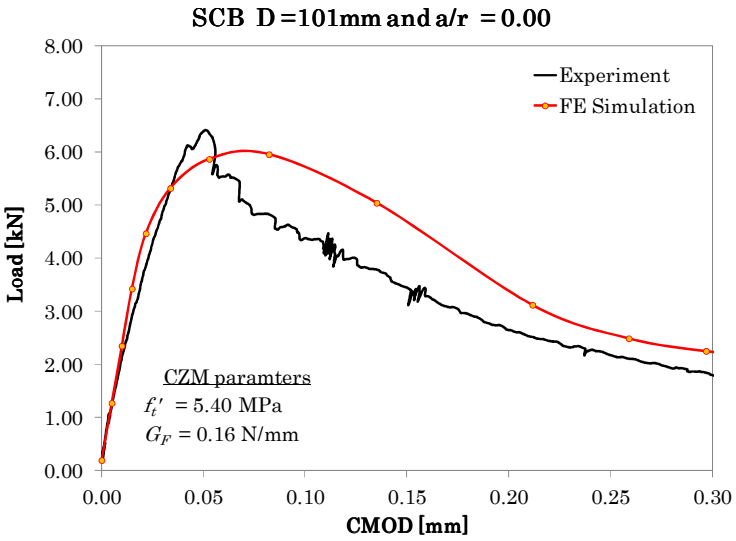

Figure 27. Simulation of SCB with D = 101 mm and a/r =0

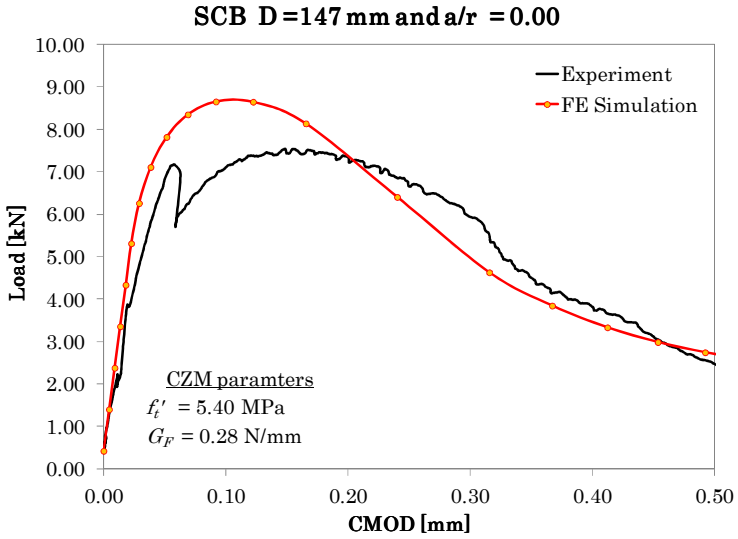

Figure 28. Simulation of SCB with D = 147 mm and a/r =0

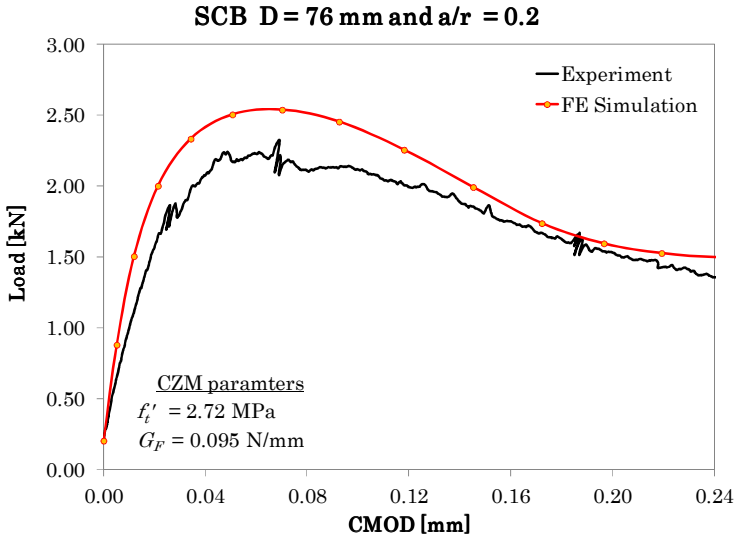

Figure 29. Simulation of SCB with D = 76 mm and a/r =0.2

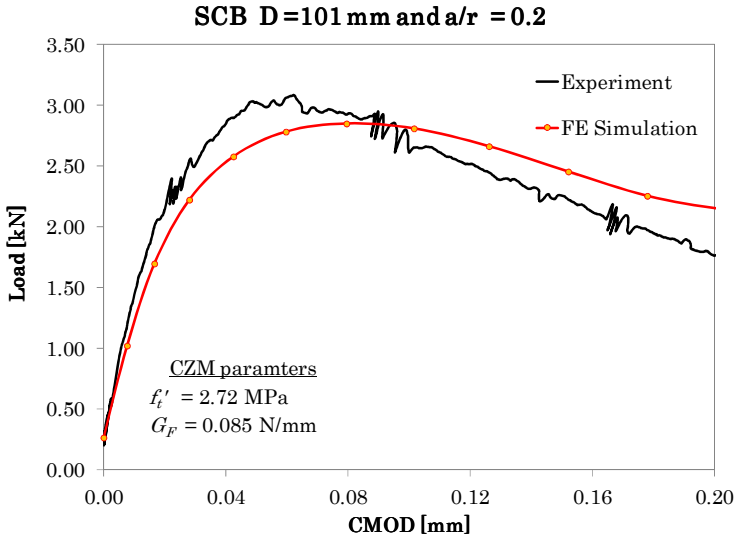

Figure 30. Simulation of SCB with D = 101 mm and a/r =0.2

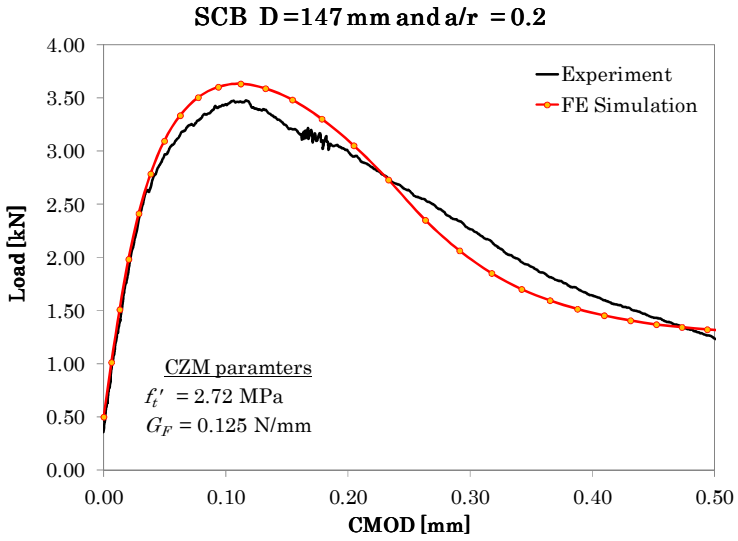

Figure 31. Simulation of SCB with D = 147 mm and a/r =0.2

3.7.2. Prediction of nominal strength for large size specimens

The calibrated models were used to simulate SCB fracture test in notchless and deep-notched specimens with diameter of 296 mm. The simulated load versus CMOD plots for notchless and deep notched specimens are shown, respectively in Figure 32 and Figure 33. The simulations produced peak loads of 15.42 kN and 5.64 kN, respectively, for the notchless and deep-notched specimens. These values were then used to compute the predicted nominal strength values.

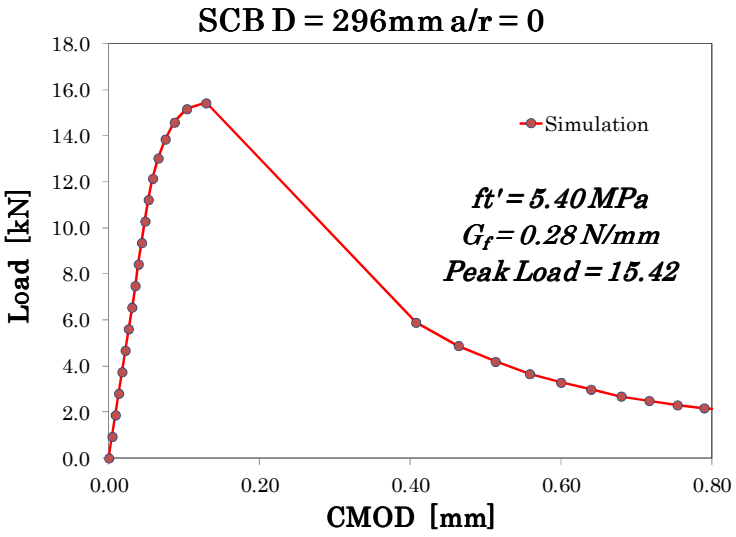

Figure 32. Simulation of SCB test with deep-notched specimen of D = 296 mm

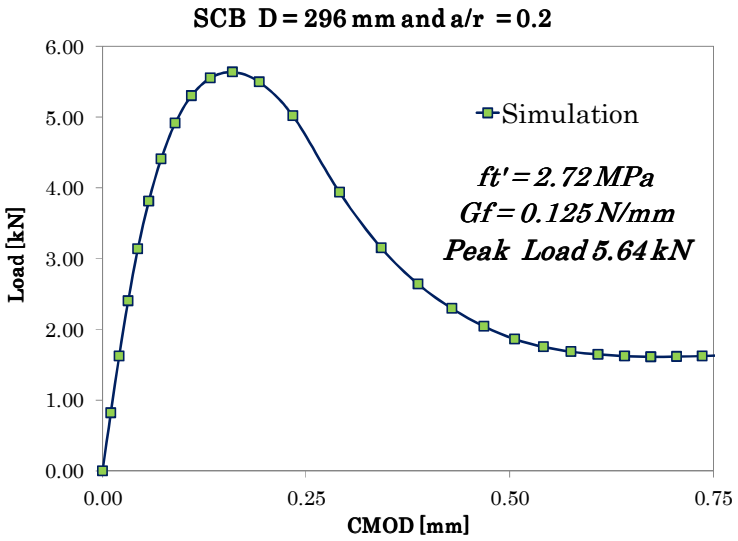

Figure 33. Simulation of SCB test with deep-notched specimen of D = 296 mm

The predicted nominal strength values were plotted against the type I and type II size effect models, respectively, in Figure 34 and Figure 35. It can be observed that the numerically predicted strength values fall fairly close to the size effect prediction laws derived from experimental results.

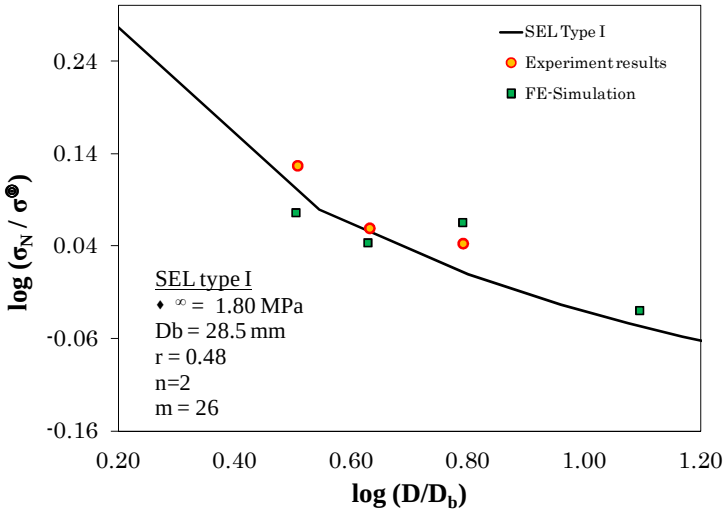

Figure 34. Predicted strength versus size effect law of type I

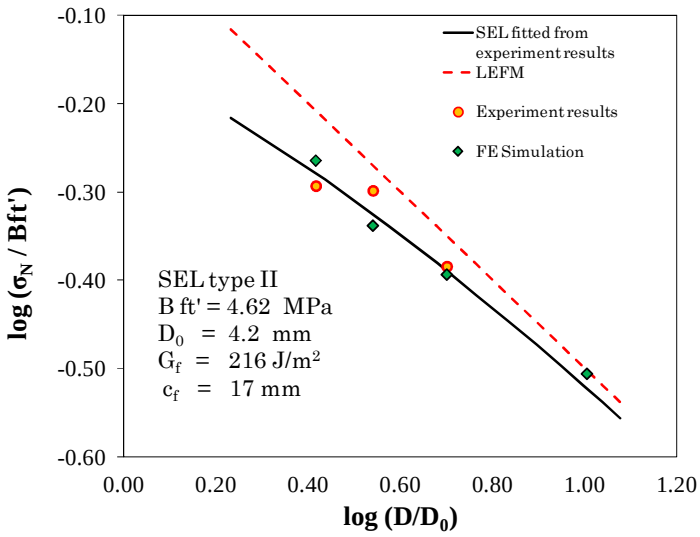

Figure 35. Predicted strength versus size effect law of type II

3.8. Deviation from LEFM

The type II size effect law obtained from the test results of deep-notched specimens indicated that the tested asphalt concrete mixture was fairly brittle. Figure 36 compares the size effect on the strength predicted by type II scaling law, derived from experimental results, and the one predicted by the LEFM theories. It can be observed that the deviation from the straight line asymptote for LEFM is minimal and reduces to less than 2% for SCB specimen with diameter larger than 80 mm. For the tested material, a diameter of 80 mm is equivalent to approximately 16 times the NMAS. This finding suggests that asphalt concrete mixtures, with relatively small NMAS, tested in standard low temperature SCB test configuration, can be accurately characterized by LEFM parameters.

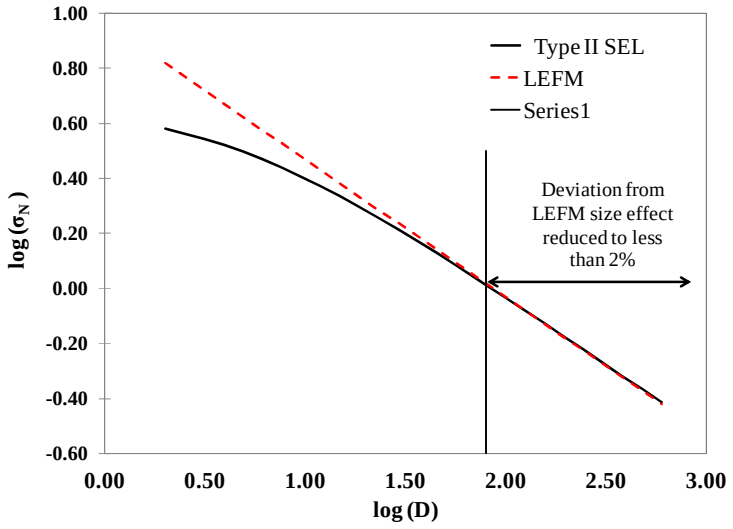

Figure 36. Deviation from LEFM

3.9. Determination of the size of the effective FPZ

One important application of the strength scaling laws in equation [2.18] and [2.20] is that they can be used to determine non-linear fracture parameters of the tested asphalt concrete mixture (Bažant, 2005). The effective size of the fracture process zone can be determined both from the size effect law of the notchless specimens and the deep-notched specimens.

In the case of the size effect of type I, equation [2.19] relates the material parameter D_b to the effective size of FPZ. Thus, using D_b = 28.5 and S/D =0.8, the length of FPZ c_f is found to be 23.75 mm.

In the case of the type II strength scaling law, the test results obtained from the deep notch specimens were employed to evaluate the size of the effective fracture process zone, c_f. Constants *A* and C in equation [3.1] can be related c_f (Bažant, et al., 1998).

$$c_f = \frac{k(\alpha_0)}{k'(\alpha_0)} \frac{C}{A} \qquad [3.2]$$

The computed length of the effective FPZ was 17 mm.

In the study conducted by Li et al., (2010) using AE technique, the length of the FPZ was approximately 30 mm. However, in this previous research, asphalt concrete mixtures with NMAS of about 12 mm were tested, approximately three times the NMAS used in the present work.

3.10. Determination of size-independent fracture parameters

The test results obtained from the deep notch specimens were also employed to evaluate size independent LEFM fracture parameters for large sizes. The slope A in equation [3.1] was used to compute the fracture energy G_f (Bažant, et al., 1998):

$$G_f = \frac{k_0^2}{E'} \frac{1}{\sqrt{A}} \qquad [3.3]$$

where $k(\alpha_0)$ represents the dimensionless stress intensity factor for semi-circular notched specimen, given by Lim *et al.*, (1993):

$$k_0 = k(\alpha_0) = 4.782 - 1.219\,\alpha_0 + 0.063\,exp\,(7.045\,\alpha_0) \qquad [3.4]$$

The fracture toughness K_{IC} can be simply computed by applying Irwin's relationship:

$$K_{IC} = k_0 \frac{1}{\sqrt{A}} \qquad [3.5]$$

The Young modulus *E* at test temperature -24°C was determined as the slope of the initial linear part of the load vs. CMOD curve. Its value varied between 18 and 21 GPa reflecting a relatively poor control quality associated with having to work with loose asphalt concrete mixture not prepared in laboratory and a non-uniform compaction. The size independent LEFM fracture parameters, computed using the energetic size effect law, were $114\,J/m^2$ and 1.43 MPa $\sqrt{m}$, respectively, for fracture energy G_f and fracture toughness K_{IC}. It is important noting that the fracture energy computed from the area below the load versus load line displacement (LLD) curve is expected to be larger than that obtained in this work. This difference can be attributed to the fact that the fracture

energy calculated by the present size effect analyses represents only the initial fracture energy, whereas the fracture energy calculated from the load-deflection curve represents the total fracture energy G_F. Typically, G_F is about 2.5 times G_f for concrete (see Figure 37).

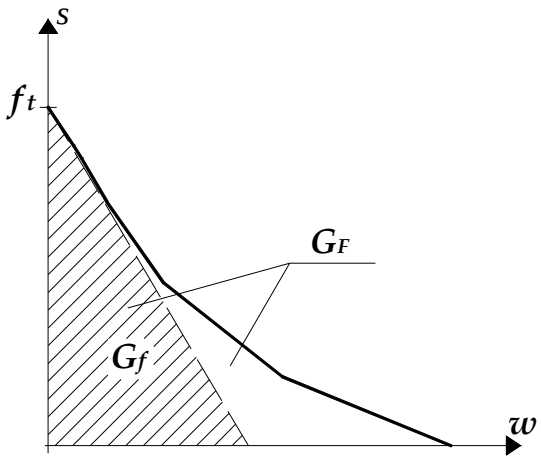

Figure 37. Initial fracture energy G_f and total fracture energy G_F

Similar behavior was observed in recent study by Wagoner *et al.*, (2007), in which the authors applied the size effect law on data obtained from the Disk-Shaped Compact Tension (DCT) fracture tests and compare it to the fracture energy computed from the load versus CMOD plots.

The fracture parameters defined through the size effect approach correspond to cases of infinitely large specimens at failure (Bažant, et al., 1998). Thus, they are to be considered as size and shape independent LEFM parameters for large sizes.

3.10. Summary of findings

In the first part of this study, laboratory experiments and numerical simulations were conducted in order to evaluate the fracture behavior of asphalt concrete tested in the SCB at low temperatures. For this study taconite asphalt concrete with a nominal maximum aggregate size (NMAS) of 4.75 mm and PG 64-34 was selected. The study included notchless, shallow-notched, and deep-notched SCB specimens of different sizes tested at -24°C, equivalent to the low service temperature limit of the PG 64-34 binder plus 10°C. The following observations were made during the experiments:

a. The size effect described by the small, medium and standard specimens can be divided into the following: the data obtained from notchless specimens revealed the Type I size effect; the results from the shallow notch specimens indicated a size effect whose small-size asymptote is close to the Type I size effect and large-size asymptote is close to Type II size effect; and the data from the deep notch specimens demonstrated the Type II size effect.

b. The nominal strength is highest for the smallest specimens, and then gradually decreases as the size of the specimen increases. Deviations from this trend were observed for the largest specimens.

c. The nominal strength considerably decreases with increase in relative length of notch. The rates of decrease observed were similar for the medium and standard size specimens.

d. In testing asphalt concrete specimens of diameter 296 mm, several difficulties were encountered. In addition, the notchless specimens failed always at the support, far from the middle region where the CMOD gauge was installed. The results from these specimens were not considered in size effect investigation.

e. The strain softening curves, observed in load versus CMOD plots, reasonably capture the transition from the relatively ductile behavior of the small specimens to the relatively brittle behavior of the large specimens.

The experimental results for SCB tests conducted on specimens with diameters of 76 mm, 101 mm, and 147 mm were analyzed through the energetic-size effect theory, and were used to develop strength scaling laws, respectively, for the notchless and deep notched SCB specimens.

In order to evaluate the validity of the scaling laws at large sizes, a numerical model was developed to simulate the mode I crack growth in the SCB fracture test. In particular, the cohesive zone model (CZM) was used to model the damage occurring in the cohesive zone ahead of a crack tip. The experimental SCB load versus CMOD curves were used to calibrate the numerical models and to determine the CZM parameters. The calibrated models were then used to simulate SCB fracture tests in notchless and deep-notched specimens of diameter 296 mm. The strength values predicted from the numerical models were in good agreement with the scaling laws' strength prediction.

Based on the analyses of both experimental and numerical results some general conclusions on the fracture behaviors of asphalt concrete mixtures tested in SCB at very low temperature can be drawn:

- The fracture behavior of asphalt concrete mixtures tested in the SCB test configuration at temperatures close to the glass transition of the component asphalt binder can be described very well by the energetic size effect theory of quasi-brittle materials.
- The size effect exhibited in testing deep-notched SCB specimens of asphalt concrete indicate that the material fails in a fairly brittle manner. By comparing the type II strength scaling law and the straight line asymptote for LEFM, it can be noticed that the deviation from LEFM is minimal and can be reduces to less than 2% for SCB specimens sizes larger than 80 mm, equivalent to approximately 16 times the NMAS of the tested asphalt concrete mixture.
- The above findings suggests that for asphalt concrete mixtures, with relatively small size of aggreagtes, tested in the standard SCB test configuration at very low temperature, the concept of LEFM is applicable.
- Another important application of the energetic size effect theory of quasi brittle materials is that it can be used to determine the length of the effective fracture process zone (FPZ) of the investigated material. For the taconite asphalt concrete considered in this study, the lengths of the effective FPZ

computed from the type I and type II size effect laws are 23.75 mm and 17 mm respectively. The FPZ length values are approximately 3 to 5 times the NMAS. It is worth mentioning that Li *et al.,* (2010) computed the size of FPZ in asphalt concretes using AE technique, and found that the length of the FPZ was approximately 30 mm. However, in this previous research, asphalt concrete mixtures with NMAS of about 12 mm.

- An application of the type II size effect law to determine non-linear fracture parameters of the asphalt concrete was demonstrated. As a result, size independent fracture parameters for the tested material were determined. These size and shape-independent parameters are defined as LEFM parameters for infinitely large specimens.
- The fracture parameters obtained by numerical fitting of the experimental data of the standard SCB specimen (diameter 147 mm) were in good agreement with the fracture parameters computed through the size effect approach. This indicates that asphalt concrete mixtures with relatively small NMAS can be adequately used for LEFM based test and analysis methods.

Chapter 4. Application of SCB test in differentiating mixtures

In the previous chapter, it was observed that asphalt concrete mixtures with fairly small size of aggregates, tested in semi-circular bend (SCB) test at very low temperatures exhibit a brittle failure and have relatively small fracture process zone (FPZ). This implies that the standard SCB test procedure can be comfortably applied to characterize and differentiate asphalt concrete mixtures with respect to their resistance to cracking.

In this chapter, an example of application of the SCB test protocol is provided. The low temperature fracture properties of Polyphosphoric acid (PPA) modified mixtures are evaluated and compared to those of polymer modified mixtures. The main objective was to determine whether PPA can partially or completely substitute traditional polymer modifiers, without adversely affecting the mixture's resistance to thermal cracking. Laboratory compacted and field cored test samples from MnROAD were tested using traditional methods as well as newly developed fracture testing protocols: Indirect Tensile Test (IDT), Semi-Circular Bending (SCB), and Disk-Shaped Compact Tension (DCT). The effects of temperature, air-void content and long-term aging on the low temperature fracture properties were analyzed and field performance observations of the test cells from MnROAD were discussed. Based on the analysis, PPA modified mixture's fracture resistance is less than the SBS modified mixture. However, when PPA is used to substitute part of the SBS, a mixture with comparable fracture resistance to the SBS-only modified mixture is produced.

4.1. Background on use of modified asphalt binders

The increasing traffic loads to which asphalt pavements are subjected have further accelerated the need to explore new paving materials and new technologies that improve the performance of pavements. A common method used to improve the performance of asphalt binders consists in increasing the high temperature limit of the Performance Grade (PG), thus expanding the temperature range without affecting the low temperature limit. For this reason, special polymer additives have been used to produce modified asphalt binders with improved resistance to rutting and unaltered resistance to thermal cracking. Recent investigations showed that asphalt binders modified by PPA, alone or in combination with traditional polymers, can yield similar gains in PG limit for lower cost of modification (Clyne, et al., 2009). However, due to premature failures observed in some asphalt pavements containing PPA modified binders, its application has been restricted by some highway agencies (Arnold, et al., 2009).

In the present research work, the effect of PPA modification on the low temperature fracture properties of asphalt mixtures is investigated. Traditional and new fracture tests were used to determine fracture properties for a set of laboratory prepared specimens and field samples cored from MnROAD.

4.1.1. Acid modifiers in asphalt mixtures

One of the earliest documented use of PPA as an asphalt binder modifier consisted in altering the viscosity-penetration relationship of asphalt (H. Alexander,

1973). Unlike air blown oxidation process, which stiffened the binder at high temperatures but severely damaged its low temperature properties, adding PPA increases the resistance to rutting while still meeting the low temperature requirements.

In the past decades, several researchers (Dickinson, 1974; Giavarini, et al., 2000; Bishara, et al., 2001; Ho, et al., 2001; Maldonado, et al., 2006; Arnold, et al., 2009) have documented the mechanisms of PPA modification. The strength of the effect may vary from binder to binder, but it is generally observed that the PG higher service temperature limit increases almost linearly with the amount of added PPA (Maldonado, et al., 2006; Arnold, et al., 2009).

Giavarini et al., (2000) and Arnold et al., (2009) performed in-depth rheological and physiochemical analysis, including binder fractionation, to investigate whether the chemical composition of the binder affects the outcome of PPA modification. Both studies reported an increase in asphaltene and decrease in resin fraction with increasing PPA concentrations. Stiffening is more likely to occur in binders that exhibit high asphaltene to resin ratio caused by adding PPA.

Kodrat et al., (2007) investigated the low temperature fracture properties of PPA modified binders and compared them to those of plain and polymer modified (SBS, Elvaloy) binders of similar grades. Tests were performed on a large number of binder types using the Extended Bending Beam Rheometer (EBBR), the Compact Tension (CT), and the Double Edge-Notched Tension (DENT). Their result confirmed that addition of PPA increases the PG span without affecting the lower temperature limit. The effects of

PPA on the fracture properties in the brittle state and on the reversible aging process were found to be insignificant. However, PPA modified binders subjected to DENT test at ambient temperature had significantly reduced strain tolerance, thus increasing the probability of fatigue cracking in service.

The combined effects of PPA and other additives such as hydrated lime, SBS, Elvaloy etc., on some properties of asphalt mixtures were also extensively discussed by Fee et al., (2010). The researchers investigated the moisture susceptibility of mixtures composed of limestone aggregates and PPA-modified asphalt binder. Hydrated lime used in combination with PPA did not affect the PG grade gain and it improved significantly the mixture performance. However, they noted that if used in great amounts, it may react with the PPA and reduce or neutralize the expected gain in PG high temperature limit. Furthermore, when PPA is used in conjunction with Elvaloy or SBS, the improvement in mixture performance is higher than when using PPA alone.

The considerably lower cost of PPA compared to polymer modifiers has made PPA modification a popular choice for pavement applications. In addition, using PPA in combination with other polymers can reduce the cost of modification (Clyne, et al., 2009), and improve the mixing and compaction characteristic of the mix (Arnold, et al., 2009).

4.2. Material and sample preparation

Four Superpave asphalt mixtures were used in this investigation (see Table 10). The mixtures were used in cells 33, 34, 35, and 77 of MnROAD and they varied in the type and amount of binder modification utilized: PPA (Cell 33), SBS (Cell 34), PPA+SBS (Cell 35), and PPA+Elvaloy (Cell 77). These modifications were used to upgrade a base binder of about PG 49-34 to a binder with PG 58-34. Accordingly, 0.75 PPA, 1% SBS + 0.3 PPA, 2% SBS, and 1.1% Elvaloy + 0.3 PPA, were used respectively for cells 33, 34, 35 and 77. The amount of modifiers used varied to obtain the same gain in high temperature PG limit.

Table 10. Description of asphalt mixtures used

MnROAD Test Cell	Construction date	Binder Grade	Asphalt modifiers	Innovalt W Liquid Antistrip
33	September 2007	PG 58-34	0.75% PPA	0.5%
34	September 2007	PG 58-34	1.0% SBS + 0.3%PPA	0.5%
35	September 2007	PG 58-34	2.0% SBS	None
77	September 2007	PG 58-34	1.1% Elvaloy + 0.3% PPA	0.5%

The effects of the modifications on the rheological properties of the base binder are summarized in Figure 38 (Clyne, et al., 2009). It can be observed that the 4 different type and amount of modification, yielded similar gains in high temperature PG without deteriorating the low temperature limit.

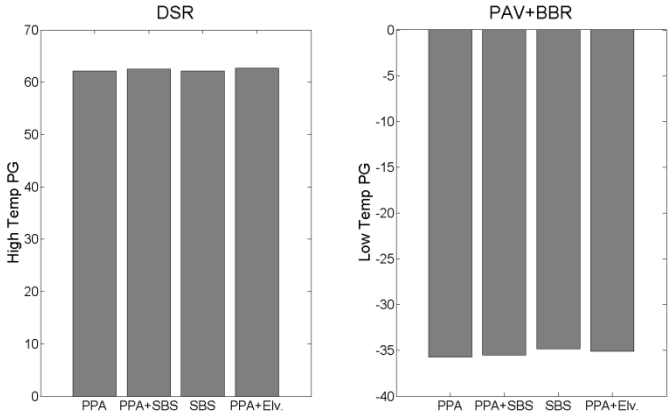

Figure 38. PG grade of modified binders

The mixtures have a maximum aggregate of 12.5 mm, limited (< 10%) limestone, and 1% hydrated lime. In addition, three of the mixtures also contained a liquid phosphate ester antistrip, as indicated in Table 10. The decision whether to add or not liquid antistrip was based on Hamburg wheel track testing on laboratory mixtures performed during the mix design stage.

The test samples for this study were prepared from loose mix compacted in laboratory using the Superpave Gyratory Compactor (SGC). The mixtures were compacted at the University of Minnesota (UMN) with two target air void contents: 4% and 7%. The latter is assumed to be more representative of typical asphalt pavements immediately after construction.

In addition, field cores taken from MnROAD cells 33, 34, 35, and 77 were also investigated. The cores were taken in June 2010, approximately 2 ½ years after their constructions. Eleven cylindrical field cores for each mixture, sampled from between wheel paths, were delivered to UMN. The thickness of the cores ranged from 100 mm to

150 mm (4" to 6"). The cells from which the samples were collected had two identical 50 mm (2”) lifts, but only the top layers were made of the mixtures of interest to this research study. Therefore, the bottom layers were cut and discarded. In addition, the upper 5 mm (0.20") was also cut and discarded in order to produce a smoother surface. The air void contents of the field cores, determined according AASHTO T166, are presented in Table 11.

Table 11. Air void contents for field cores.

Cell	Mean	CV
33	5.3	1%
34	5.9	2%
35	6.4	2%
77	5.1	13%

4.2. Experimental variables

The cylindrical SGC compacted and field cores were cut into IDT, SCB, and DCT test specimens. Three replicates were used for each factor to level combination.

The IDT, SCB, and DCT laboratory specimens obtained from the 4% and 7% SGC cylinders were tested at two temperatures: binder PG low temperature limit (PGLT), and PGLT + 10°C, respectively.

An additional set of the 7% void content SGC cylinders was long term aged by placing the SGC cylinders in oven for 5 days at 85°C, according to AASHTO R30-02 protocol. The long term aged and field samples were tested only at PGLT.

4.2. Test methods

The IDT and SCB tests were performed at the UMN, and the DCT tests were performed at University of Illinois Urbana Champaign (UIUC).

The IDT test was used to determine the creep compliance and strength of the mixtures according to AASHTO specification T322 (2007).

The SCB test was used to determine the fracture toughness (K_{IC}) and fracture energy (G_F) of the mixtures. The test procedure, as well the computation of the SCB fracture parameters are reported elsewhere ((Li, et al., 2004; Li, et al., 2009). The SCB specimen consisted of 150 mm wide and 25 mm thick semi-circular slice. A vertical notch with 15 mm length and 2mm width was cut in the middle of the span between the supports. The tests were performed in a MTS servo-hydraulic testing system equipped with an environmental chamber. The loading was controlled by the crack mouth opening displacement (CMOD) and varied in order to maintain a constant CMOD rate of 0.0005 mm/s for the entire duration of the test. This slow loading rate was selected to reflect the rate of temperature change that occurs in real field conditions.

The DCT test was performed to determine the fracture energy of the mixtures according to the ASTM standard D7313-07 (2007). The test is performed on DCT specimen 150 mm wide, 145 high, and 50 mm thick. The initial fracture ligament length was 82.5mm. Tensile loading was applied at the holes through a constant CMOD rate of 0.017 mm/s.

4.3. Test results of laboratory compacted samples

The IDT strength results are reported Figure 39. The figure presents the mean strength values calculated from three test replicates. The strength of the mixtures decreases as the temperature drops, however, SBS and PPA+Elvaloy modified mixture with 7% air void content appear to be less sensitive to the change in temperature. As expected, mixtures with less void content have higher strengths than the mixture with higher void content. With regard to the effect of modification, several observations can be drawn: SBS and PPA +SBS modified mixtures have higher strength values at all air void and test temperature levels; PPA+Elvaloy modified mixture has about the same strength of PPA modified mixture.

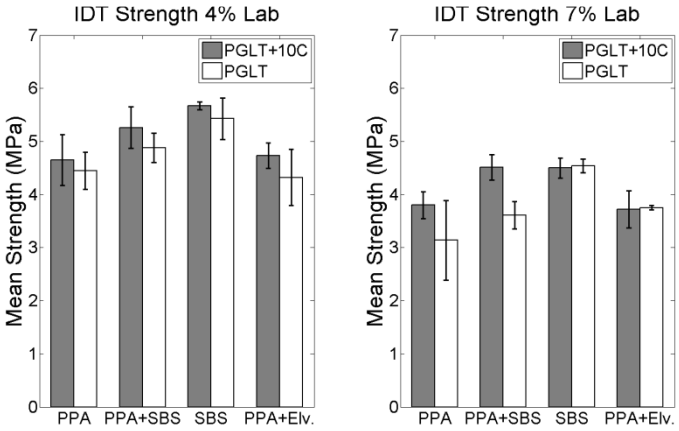

Figure 39. IDT Strength test results

Figure 39 summarizes the IDT stiffness at 60 and 500 seconds results. It can be seen that, for all considered mixtures, stiffness increases dramatically when temperature drops. Similarly, the stiffness is much higher in the 4% void content mixtures. Overall, the highest increase in stiffness, due to temperature change, is observed in the

PPA+Elvaloy modified mixture. PPA modified mixture is relatively less responsive to change in temperature at 4% void content. On the contrary, at 7% void content, the PPA modified mixture has the second highest increase in stiffness. With regard to the effect of modification, overall SBS alone and PPA+SBS modified mixtures have higher stiffness values compared to PPA modified mixture. However, when only the highest test temperature is considered, the difference between the mixtures is reduced.

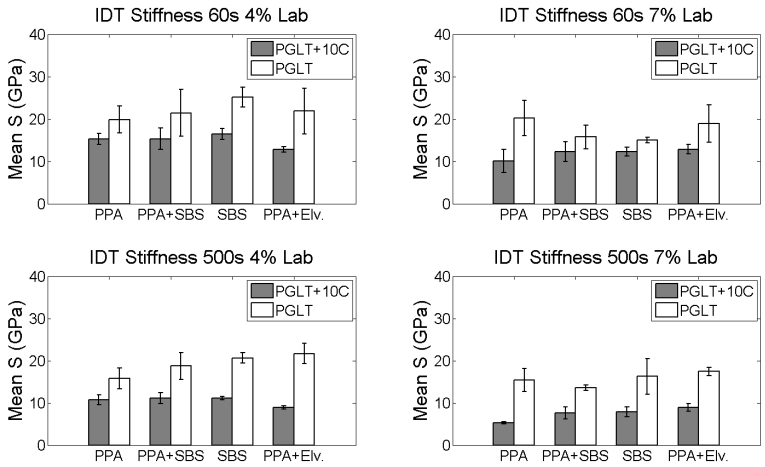

Figure 40. IDT creep stiffness results

The SCB fracture test results are summarized in Figure 41. The highest fracture toughness values are observed in SBS and PPA+SBS modified mixtures, regardless of the air void content level. From Figure 41, it can also be inferred that PPA and PPA + Elvaloy mixtures are basically equivalent with respect to their K_{IC} values. With respect to SCB fracture energy, SBS and PPA+SBS modified mixtures, tested at the highest test temperature, have higher values than the rest. For all the mixtures, G_F decreases with temperature and with increase of void content. Interestingly, the rate of decrease in G_F,

due to decrease in temperature, is similar for PPA and PPA+SBS modified mixtures. Both fracture parameters, K_{IC} and G_F, are negatively affected by increase in air void content. An exception to this trend is seen in SBS modified mixtures tested at the highest test temperature (PGLT+10 C).

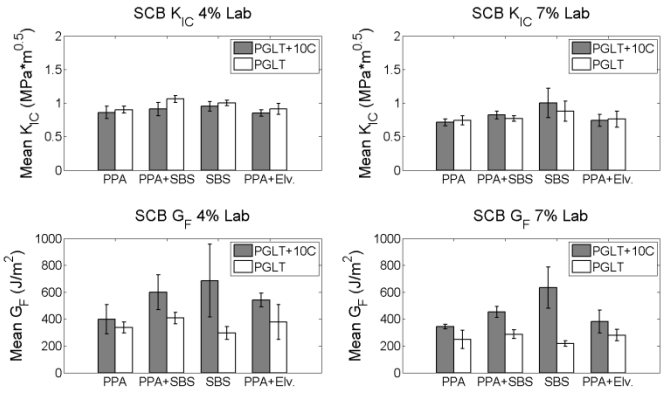

Figure 41. SCB fracture test results

Fracture energy was also computed from DCT test. The results are shown in Figure 42. The DCT fracture energy results are slightly higher than those obtained from the SCB because of the different specimen geometry and the much higher loading rate used in DCT testing. Nevertheless, The DCT results also confirm that SBS and PPA+SBS modified mixtures have higher fracture energy than PPA and PPA+Elvaloy modified mixtures.

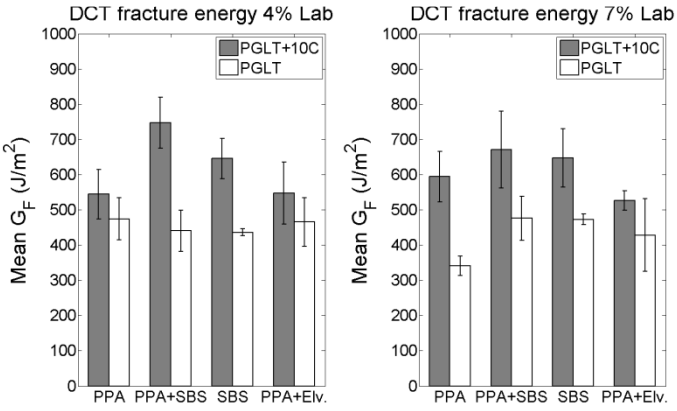

Figure 42. DCT fracture test results

4.3.1. Statistical analysis of results from laboratory compacted samples

MacAnova statistical software package was utilized to perform statistical analysis and a three-way analysis of variance (ANOVA) was used to examine the differences among the mean response values of the different treatment groups. Results for each test parameter were separately analyzed. The experiment factors were: test temperature (two levels), air void content (two levels), and type of asphalt modification (four levels).The significance of the differences was tested at 0.05% level of error. In running the statistical tests, particular attention was paid to some aspect of the ANOVA models. The methods of analysis of experimental results by comparing the average responses of different treatment groups using ANOVA or contrasts and pairwise comparison are based on the assumption that the errors in the data are independent normals with constant variance. If these model assumptions do not hold, the inference may be misleading. Therefore, for each of the ANOVA model used in this study, the nature and degree to which the model-assumption were violated was checked, and corrective measures were taken if needed.

Graphical and numerical tools (provided in MacAnova) such as normal probability plots and residual plots were used to assess the violation of the assumption. The primary tool used to deal with the violation of assumptions was the transformation of the response to a different scale (square root, logarithm etc.). In addition, the occurrence of unbalanced data (not all factor-level combinations have the same amount of replication) necessitated ANOVA models adjusted to type III sum of squares. It is to be noted that, all four treatments are comparable, in that none of them represent a control group (no treatment). Therefore, the statistical analysis is intended to evaluate whether the difference in response among the four differently modified mixtures is significant.

Table 12. Summary of ANOVA analysis

Factor	DCT	SCB	SCB	IDT	IDT	IDT
	G_f	G_f	K_{IC}	strength	S@60sec	S@500sec
mix type	★★	★★	★★	★★	-	-
void content	-	★★	★★	★★	★★	★★
test temperature	★★	★★	-	★★	★★	★★
mix.void	-	-	-	-	-	-
mix.temp	-	★★	-	-	-	-
mix.void.temp	-	-	-	-	-	-

(★★) highly significant; (★) moderately significant; (-) not significant

A summary of the ANOVA results for all test parameters is shown in Table 12. The significant treatment effects are indicated in the table. According to the statistical

analysis, the effects of temperature and air void content observed for all test parameters, and discussed above, are statistically significant. The effect of modifiers, which is the subject of this research work, is found to be statistically significant in the following test parameters: DCT fracture energy, SCB fracture toughness, SCB fracture energy and IDT strength. The change in stiffness due to the effect of modifiers was found to be not significant. This means, the change in mixture stiffness attributed to the four different types of modification is comparable.

In addition, multiple comparisons at 5% level of significance were performed to compare and rank the tested mixtures according to the different test methods. The outcomes are reported in Table 13, in which statistically similar mixtures are grouped together.

Table 13. Statistical grouping and ranking of modified mixtures – lab compacted

	IDT strength [MPa]		SCB K_{IC} [MPa*$m^{0.5}$]		SCB G_F [J/m^2]		DCT G_f [J/m^2]	
Modifier	Group Mean	Rank	Group Mean	Rank	Group Mean	Rank	Group Mean	Rank
SBS	5.1	A	0.96	A	451.57	A	561	A/B
PPA+SBS	4.57	B	0.89	A/B	428.87	A	584	A
PPA+Elv.	4.19	C	0.81	B	390.13	A/B	496	B
PPA	4.01	C	0.80	B	323.67	B	490	B

The letter A is used to indicate the best performing group of mixtures. The letter B refers to the second best performing group of mixtures, and so on. Mixtures which are difficult to distinguish are indicated by two or three group letters. Accordingly, SBS and PPA +SBS modified mixtures have generally higher strength and higher fracture

resistance than the mixtures containing PPA or Elvaloy+PPA. In the case of IDT strength the difference between PPA+SBS and SBS is also considered to be statistically significant; SBS alone provides higher material strength.

4.4. Test results of field cored samples

In Figure 43 and Figure 44, the test results of field and long-term aged laboratory samples are plotted along with their corresponding un-aged laboratory compacted samples. The laboratory samples plotted are all 7 % air void content. Both field samples and aged samples were tested only at PGLT test temperature.

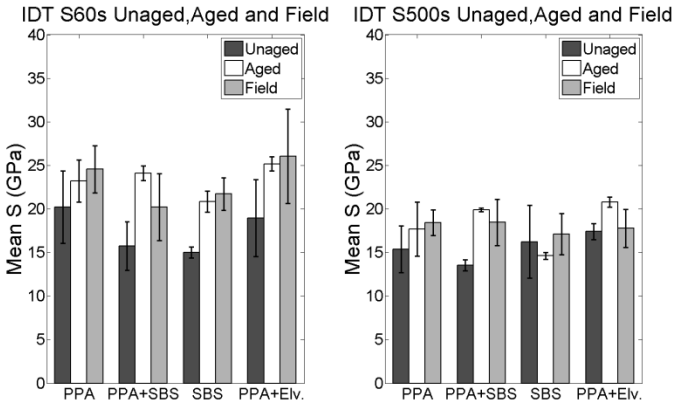

Figure 43. IDT creep stiffness test results for un-aged, aged and field samples

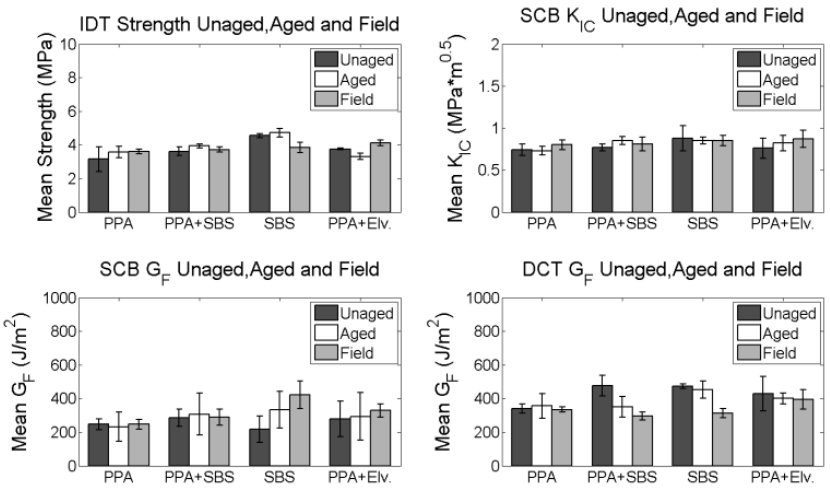

Figure 44. IDT strength, SCB and DCT test results un-aged, aged and field samples

With respect to the stiffness of field cores (see Figure 43), it can be observed that mixtures containing PPA or Elvaloy+PPA have higher stiffness at 60 sec than mixtures containing SBS or SBS+PPA. However, when stiffness is measured at 500 sec, the difference diminishes. Based on strength and the fracture parameters results, it appears that, generally, SBS or PPA +SBS modified mixtures performs better. This finding is similar to what was observed for the laboratory compacted mixtures.

4.4.1.Statistical analysis of results from field cored samples

Statistical analysis of the results was also performed. The analysis of variance was used to test whether the differences, observed in the responses of the four field mixtures, were statistically significant. It was found that the field mixtures were similar with respect to their IDT stiffness, IDT strength, SCB K_{IC}, and DCT G_F. The differences in

SCB fracture energy results are small but statically significant. In Table 14, the mixtures are ranked with respect to their SCB fracture energy value.

Table 14. Statistical grouping and ranking of modified field mixtures SCB

Modifier	Mean [J/m^2]	Rank
SBS	421.29	A
PPA+Elvaloy	301.46	A/B
PPA+SBS	288.36	A/B
PPA	246.34	B

4.5. Test results of long-term aged laboratory compacted samples

Finally, the effect of long-term laboratory aging on the modified mixtures was investigated. The test results are summarized in Figure 43 and Figure 44. Long-term aging increases the stiffness of all mixtures, except the SBS modified at 500 sec. In the IDT strength plot, an increase of about 9% in strength is observed, due to the aging, for all mixtures, except for the PPA+Elvaloy modified one. In the SCB fracture toughness plot, the effect of long-term aging is almost inexistent in PPA and SBS modified mixtures. On the contrary, PPA+polymer modified mixtures exhibit almost a double-digit percent increase due to the long term aging. The SCB fracture energy always increases due the long term aging to which the mixtures were subjected. The highest increase is observed in PPA and SBS modified mixtures. Finally, the DCT fracture energy results show no difference between the long term aged and un-aged mixtures. PPA+SBS modified mixture has a steep decrease in DCT G_F due to long-term aging.

Based on ANOVA the effect of long term aging on IDT, SCB and DCT results was found not to be statistically significant. The results appear to suggest that the current long term aging procedure needs to be further investigated to understand if this method is appropriate for simulating field aging with respect to low temperature properties.

4.6. Test section field performance

After 4 years in service,, MnROAD cells 33, 34, and 35 show no thermal cracking. The only test section with transverse cracking is Cell 77 (Elvaloy+PPA), which has two cracks in 350 feet. There are several construction-related reasons why this section may have some cracking, so there is little concern that the low temperature cracking is excessive. Overall, the performance of each of the PPA modified binders has been very good.

4.6. Summary of findings

The low temperature properties of asphalt mixture modified with PPA and PPA in combination with traditional polymer modifiers were investigated using traditional and newly developed test methods. All mixtures had the same mix design except for the type and amount of modifiers used to upgrade the base binder to PG 58-34. The type of modification considered were: PPA, SBS, PPA+SBS, and PPA+Elvaloy. Test were performed on both laboratory compacted and field cored test specimens.

Based on the analyses performed on the experimental results the following conclusions were drawn:

- The differences in IDT stiffness due to the type of modification were not statistically significant. Therefore, the four types of modifications considered in the present work had a similar effect on mixture stiffness.
- For IDT strength, PPA+SBS and SBS modified mixtures are significantly stronger than PPA alone and PPA+Elvaloy modified mixtures.
- Comparison of the mixtures with regard to SCB and DCT fracture parameters confirmed that PPA+SBS and SBS modified mixtures have better resistance to cracking than PPA and PPA+Elvaloy modified mixtures.
- For the field cored samples, the mixtures were found statistically different only for SCB fracture energy. The mixtures containing PPA alone had worse fracture properties than the others.
- The long term aging method did not produce statistically significant differences among the mixtures. This result brings into question the validity of using this method to simulate field aging on low temperature properties.
- Field performance of the cells investigated has been very good, including all PPA modified mixtures.

Overall, it can be concluded that the low temperature fracture properties of mixtures modified with 0.7% PPA are reasonably good. The SBS and PPA+SBS modified mixtures have the highest resistance to low temperature cracking of all mixtures

investigated. The results suggest that using PPA+SBS modified mixtures, in which the amount of SBS is half of the amount used in typical SBS modified mixtures, may provide a cost effective alternative for improving the cracking resistance of asphalt pavements. These results are confirmed by the field performance of the MnROAD test sections that have not thermally cracked.

Chapter 5. Determination of Creep Compliance from Semi-Circular Bend Test

In this chapter, the feasibility of determining both viscoelastic deformation properties and fracture parameters from a single SCB test configuration was investigated. As a result, a test methodology consisting of an initial creep test followed by a standard SCB fracture test is proposed. Finite element (FE) analyses were performed to understand the stress state in the SCB, and an optimal load range producing appreciable displacement measurements while preserving the linear viscoelastic conditions was identified. Expressions that relate displacement measurements, from particular regions of the SCB specimen, to creep function were derived. The validity of the proposed SCB creep method was tested both by numerical simulations and experimental testing. Good agreement was found between the creep function obtained from SCB and those obtained from three-point bending beam and IDT creep test. This would significantly reduce the cost in material, time, and testing equipment needed for asphalt concrete. The research works, as well as the findings are discussed next.

5.1. Determining creep compliance from SCB test

The test methodology proposed in this paper consists in using a standard notched SCB specimen to obtain both creep compliance and fracture parameters. In addition to the LLD and CMOD gauges used for fracture testing, a third gauge is employed for creep

displacement measurement from a particular region of the specimen. The testing involves a mixed load and CMOD control approach. The specimen is conditioned at the desired test temperature for 2 hours and then subjected to a constant load for 1000 sec. At the completion of the creep test, the loading control is switched to a constant CMOD control to perform standard SCB fracture test. For the entire duration of creep and fracture testing, the specimen is kept in the environmental chamber. Determination of the best location for creep displacement measurement, as well as the optimal creep load, small enough to maintain the material in the linear viscoelastic region and yet produce appreciable displacements, are critical in this research investigation.

5.1. Linear viscoelastic conditions

The composition and mechanical behavior of asphalt concrete are widely discussed in the literature review section. For the purpose of this chapter, it is worthwhile reiterating that at low temperatures asphalt concrete behaves as a linear viscoelastic material (Lytton, et al., 1993; Buttlar, et al., 1994). The linear viscoelastic constitutive equations (2.1.a and 2.1.b.) describe such behavior using the relaxation modulus $E(t)$ or the creep compliance $D(t)$. Due to its simplicity, creep test is most commonly used to characterize asphalt concrete. Nevertheless, $D(t)$ and $E(t)$ are related through a Voltera integral presented in as in equation 2.2.

The estimation of a material parameter from stress and strain data involves an inverse problem solution. In theory, stresses and strains corresponding to sufficiently

small loads and measured at a point far from the SCB specimen crack tip can be used to determine the material's elastic parameters. For creep loading, the viscoelastic parameters are then easily derived through the elastic-viscoelastic correspondence principle. However, asphalt concrete is a non-homogeneous material composed of aggregate, asphalt and air, and each component has different material properties. Thus material parameters derived from point measurements may not be accurate. To overcome this problem, the stress and strain are averaged along a sufficiently long segment. It is therefore important to identify and quantify accurately the regions of high stress concentration. By isolating the crack and boundary governed regions, the SCB elastic region is used for the determination of the elastic and viscoelastic parameters.

5.1. Analysis of stress state in SCB specimen

Due to the complex geometry, the stress state of notched SCB specimen in three-point bending was investigated through FE analyses. For this purpose the commercially available software ABAQUS was employed.

Numerical simulations were performed using the standard dimensions and loading configuration of a SCB specimen. A two dimensional plane stress model was developed using second-order quadrilateral elements. The material was assumed to be isotropic, homogeneous and linear elastic. Thus, the bulk of the model was described through the Young Modulus E and the Poisson's ratio υ. The initial crack notch was modeled using a seam-crack, which is a crack modeling tool provided in ABAQUS. The crack tip was

meshed using rings, centered at the crack tip, of collapsed quadratic quadrilateral elements. A "single node" degeneracy method was used for the elements in the first contour so that one edge of each element collapses to zero length allowing the nodes to locate at the crack tip. This type of settings allows the introduction of square root singularity for stress near the crack tip. Very fine meshes were used near singular points where high stress concentrations are expected to occur. For the rest of the specimen, relatively coarse mesh was applied.

The SCB finite element model was first used to compute the normalized stress intensity factor Y_I for varying initial notch lengths. The results were found to be in good agreement with the well established normalized stress intensity factor equation for SCB specimen provided by Lim et al., (1993), as shown in Figure 45. This implies that the stress state, especially near the crack tip, is accurately captured by the adopted SCB finite element model. Hence, it can be used to isolate the regions of SCB specimen in which the stresses change rapidly over short distances.

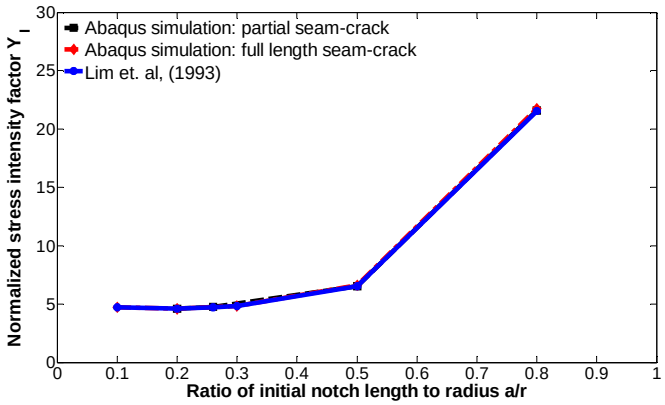

Figure 45. Calibration and verification of the FE model

The stress state displayed in a SCB specimen under three-point loading is a very complex one. Figure 46 shows the Von Mises stresses in a SCB specimen under a compressive load of 2 kN. The contour scale has been adjusted in order to identify the areas in the analysis that exceeded typical strength of asphalt mixtures. The strength value was set equal to 3 MPa, very conservatively. The dark areas (colored in gray in color print) represent high stress concentration, above the material strength. These areas correspond to the region near the crack tip, loading point, and in the vicinity of the support rollers. The sizes of these areas increase drastically with load as depicted in Figure 47.

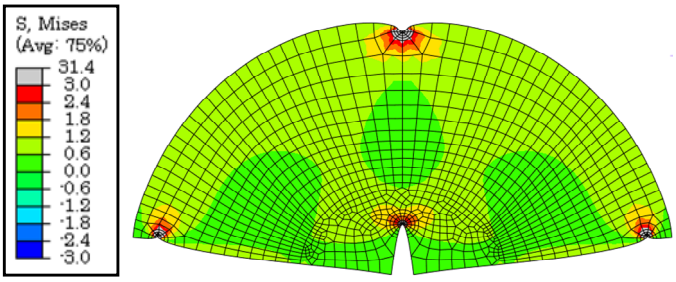

Figure 46. SCB stress state for a load of 1 kN

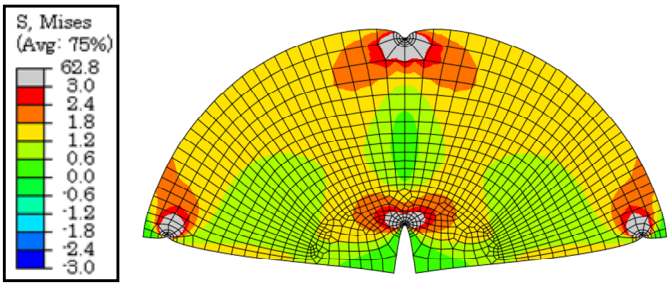

Figure 47. SCB stress state for a load of 2 kN

The analysis of the principal stresses (see Figure 48) indicated that large tensile stresses are generated at the bottom of the specimen. The principal directions, of elements in the bottom region, are parallel to the longitudinal axis-x, hence the shear stress are practically close to null. While, in the upper region a compressive arch is developed. The inclined principal stresses, in the upper region, indicate the existence of shear stress.

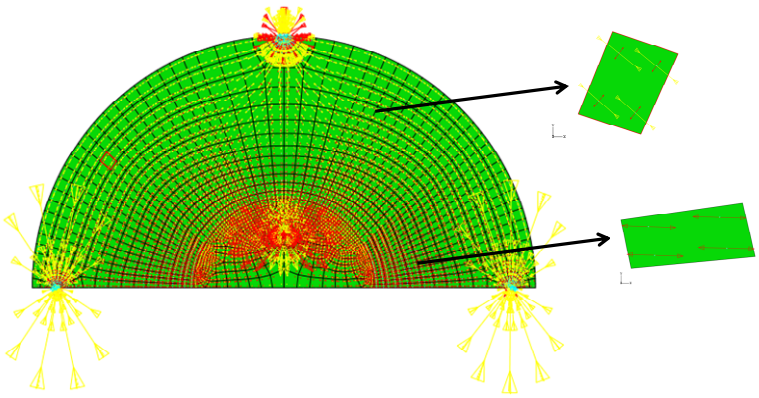

Figure 48. SCB stress state – plot of principal stress

Parametric analytical studies conducted by varying the material constants, E and υ, indicated that the stress state in a SCB specimen subjected to three-point loading is independent of the material constants. Thus, the stresses developed in an elastic SCB specimen subjected to a three-point bend test are similar to those in a viscoelastic SCB specimen tested at the same condition. This behavior is analogous to that observed in testing IDT specimens, in which the equations for the stresses along the central x and y axes are independent of material constants and remain unchanged when subjected to

Laplace transforms (Zhang, et al., 1997). Another necessary requirement in order to apply the Laplace transforms in the viscoelastic analysis is that the stresses are constant in time. The variation of stresses in time in a three point bending tests of a standard SCB specimen was analyzed through a viscoelastic FE model, and discussed in the next section.

The SCB elastic finite element model, with a notch of 15 mm, was used to analyze the stress distribution along several horizontal paths, on the SCB specimen surface, that could be used for displacement measurements. The transverse σ_x and the vertical σ_y stresses along the considered paths are shown in Figure 49. For the purpose of finding an approximated creep compliance equation, the shear stresses in the upper region of the SCB specimen were neglected. Thus, strains computed from displacement measurement of two points along the indicated horizontal trajectories can be considered normal strains and used to compute the creep function. The stresses in the plot are normalized by the nominal stress $\sigma = P/bD$, where P, b and d represent, respectively, the applied load, the thickness and diameter of the specimen.

The trajectories that provide a sufficiently long segment in which the stresses have the same sign (tension or compression) and are almost uniform are favored. For y=10 mm (10 mm from the x-axis) the stresses are almost uniform in the middle region but exhibit an abrupt change near the crack tip and the support rollers. It might be difficult to accurately identify a segment not affected by the boundary induced stresses.

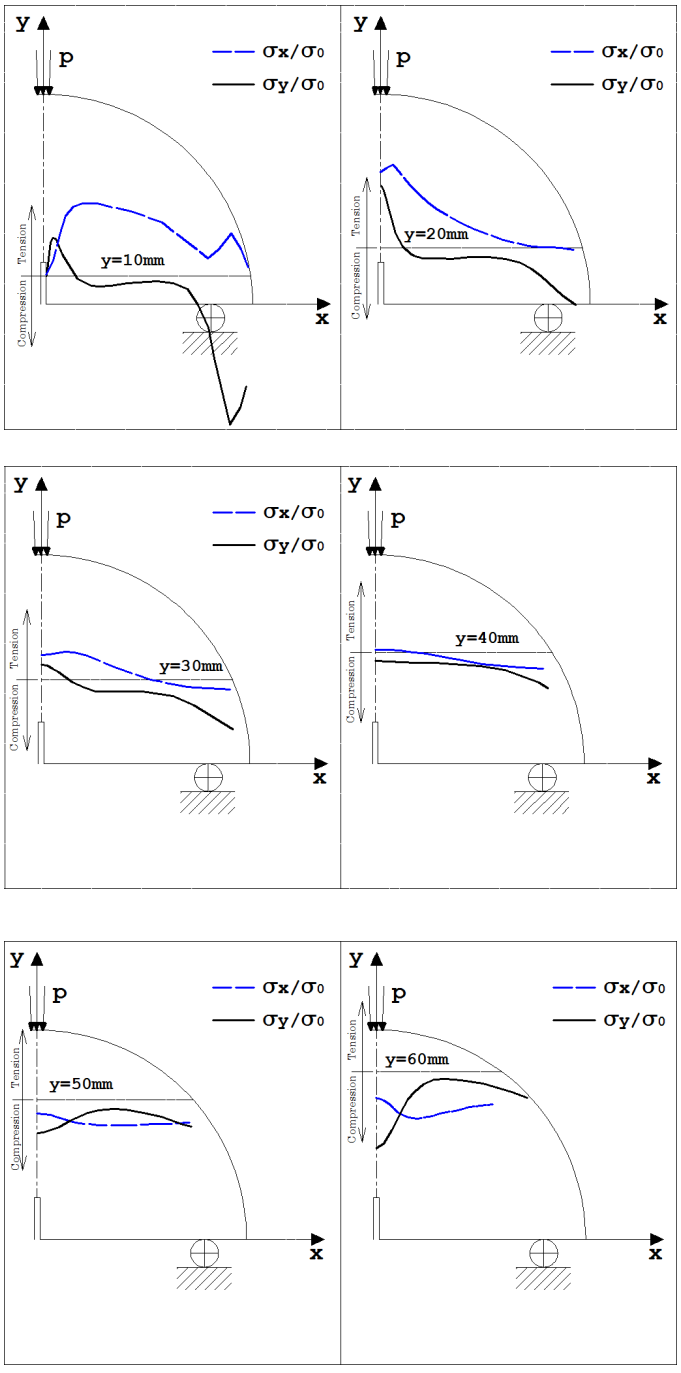

Figure 49. Stress distribution along several horizontal trajectories in SCB specimen

The stress distribution in the y = 20, y = 30, y = 40 and y = 60 trajectories exhibit one or all of the following: rapid change of slope, lack of sufficiently long segment with same sign of stresses. In contrast, a significant portion of the trajectory identified as y=50 mm exhibits uniform distribution of the considered stresses. In addition, the stresses do not change drastically at both ends of this line.

Based on the analyses of stress distributions, two strips (see Figure 56) having the central axis located, respectively, at 10 mm and 50 mm from the base of the specimen were selected for further investigation. The thickness of the strips was set to 5 mm in order to reflect the diameter of button gauges used in experiments for measuring displacement.

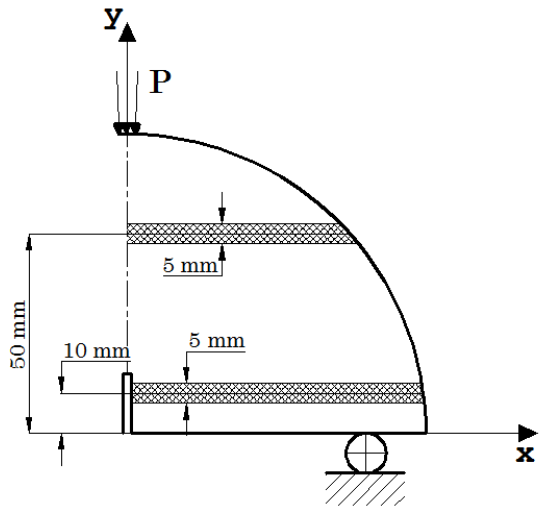

Figure 50. Potential strips for displacement measurements

5.1.1. Variation of stresses along the y-axis

The variations of the stresses along the thickness of the displacement measurement strips indicated in Figure 50 were analyzed. The stresses along the lower and upper segments of the strips were obtained from FE analysis and the percent relative differences were computed through:

$$var = \frac{\sigma_{upper} - \sigma_{lower}}{|max\ (\sigma_{upper}, \sigma_{lower})|} \qquad [5.1]$$

where σ_{upper} and σ_{lower} represent, respectively, the stresses along the upper and lower end segments of the two strips (at the top and bottom region of the SCB specimen) selected for displacement measurements. The results are plotted in Figure 51 and Figure 52.

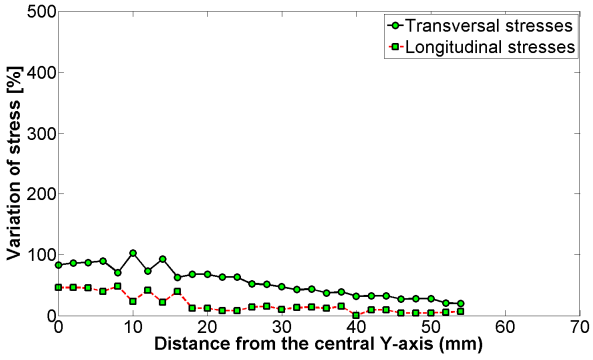

Figure 51. Variation of stresses in y-direction in the top strip

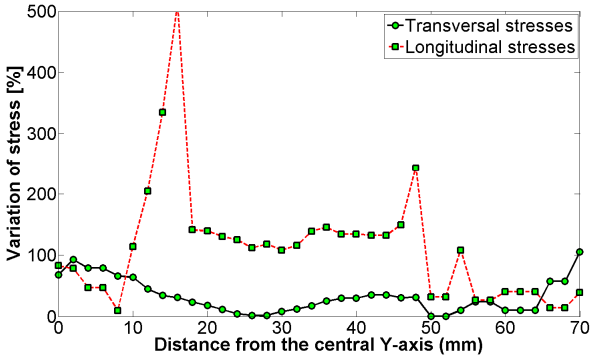

Figure 52. Variation of stresses in y-direction in the bottom strip

The variations of both transverse and longitudinal stresses in the top strip are moderate and far from the central y-axis they remain almost constant. These facts support the idea of approximation of the stresses by integration and averaging, as discussed in the next section. On the contrary, the variations of stresses, specially the transverse ones, in the lower strip are stronger. This means that the stresses along horizontal segments in the lower strip are significantly different from each other.

5.1.2. Variation of stresses in time

In order to investigate the variation of the stresses with time in a SCB specimen subjected to a three-point bend creep test, a 2D finite element viscoelastic model was developed. Asphalt concrete at low temperatures was modeled as homogeneous and linear viscoelastic material using the Generalized Maxwell Model (GMM) which is a built-in material model in ABAQUS. The viscoelastic model, presented in Figure 53, consisted of a single spring element representing instantaneous elasticity, and three spring-dashpot Maxwell elements to account for the relaxation that occurs in time.

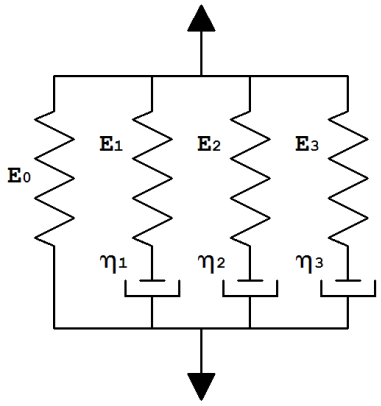

Figure 53. Generalized Maxwell Model (GMM)

The relaxation modulus for the GMM is written as:

The relaxation modulus for the GMM is written as:

$$E(t) = E_0 + \sum_0^n E_i \, e^{-\frac{\tau}{\rho_i}} \qquad [5.2]$$

where E_i and ρ_i represent, respectively, the modulus and the relaxation time for the i-th spring-dashpot element. The relaxation time is the ratio of viscosity and modulus:

$$\rho_i = \frac{\eta_i}{E_i} \qquad [5.3]$$

The GMM model parameters can be determined from experimental creep data. The creep data is fitted in 3 term Prony series model through linear and non-linear optimization methods. The resulting creep model is then converted to a relaxation function through Laplace transform. ABAQUS requests that the modulus input parameters, for the spring-dashpot elements, are given in the form of normalized shear

g_i and bulk k_i modulus. The work of obtaining these GMM parameters from experimental data was performed in a previous work by Zofka (2007). Accordingly, the instantaneous modulus and Poisson's ration for the model were set equal to 8.44 GPa and 0.13, respectively. The normalized shear and bulk modulus, as well as the relaxation time values are reported in Table 15.

Table 15. Input parameters for GMM model in ABAQUS

g_i [-]	k_i [-]	ρ_i [sec]
0.3542	*0.3542*	*2.8889*
0.2114	*0.2114*	*33.0071*
0.2417	*0.2417*	*334.0924*

Using the viscoelastic model, the stresses along the axis y=10 mm and y = 50 mm, respectively, the central axis of the bottom and the top displacement measurement strips, were measured at 0.5 sec and 1000 sec. The variations of the stresses in time computed using equation [5.1] are reported in Figure 54 and. In this case, σ_{upper} and σ_{lower} were substituted, respectively, by the initial stresses (corresponding to time 0.5 sec) and final stresses (corresponding to time 1000 sec). It can be observed that in the middle region of both top and bottom strips, the variations are negligible. However, in the bottom strip the longitudinal stresses exhibit a relatively strong fluctuation. This may violate the assumption of constant stresses required for the application of Laplace transforms.

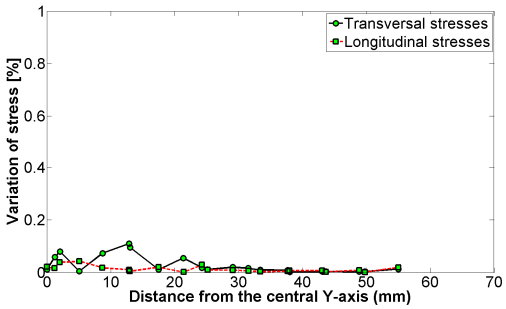

Figure 54. Variation of stresses in time in the top strip

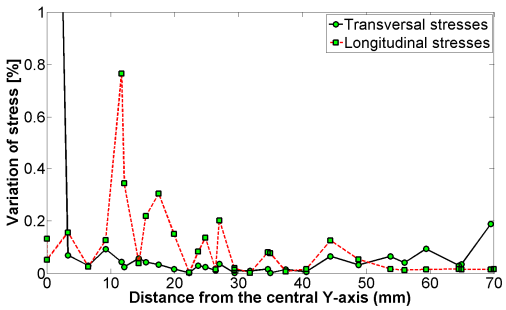

Figure 55. Variation of stresses in time in the bottom strip

5.2. Equations for computing stresses in the SCB strips

Based on the considerations discussed in the previous section, two segments, within the y=10 and y=50 axis, shown in Figure 56, were selected for experimental investigation. The length of these segments was set to reflect the length of typical strain gauge l. The segment located at the bottom strip displays transverse tensile and vertical compressive stresses. In the second both stresses are compressive ones. As mentioned above, the extent by which the stresses in y=10 are influenced by the boundary effects (crack tip and support) is difficult to accurately assess. This might cause certain degree of errors in experimental testing of materials.

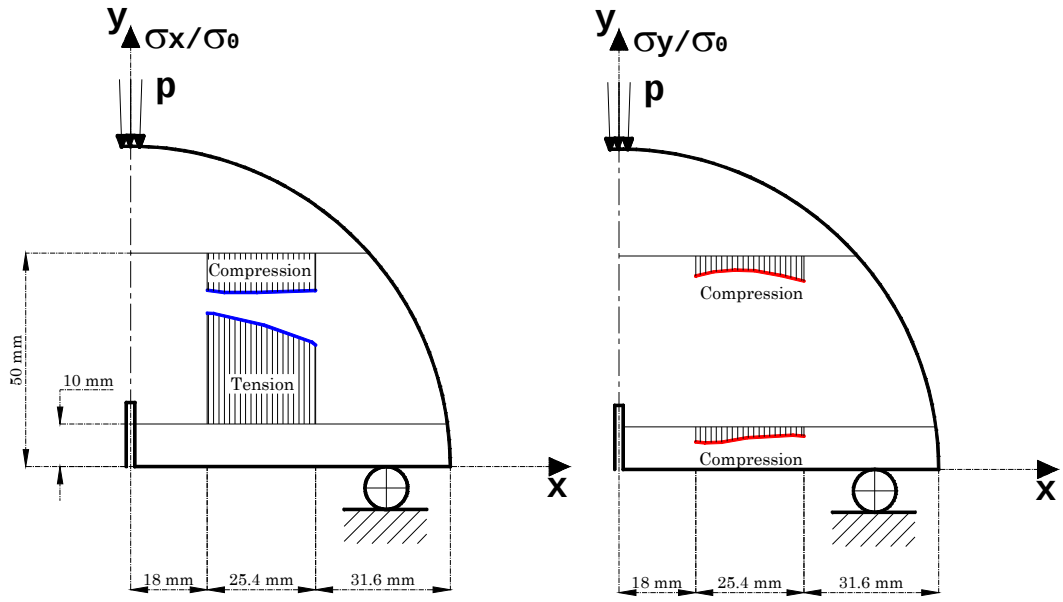

Figure 56. Stresses along the segments selected for displacement measurements

The strain values for the calculation of the creep function are to be obtained from displacement measurements in these segments. Whilst, the stress functions were determined numerically from the SCB finite element model and fitted into polynomial functions thorough the least square error (LSE) method, as shown in equations [5.4]:

$$\sigma_x = \frac{P}{BD}\left(a_x\, x^3 + b_x\, x^2 + c_x\, x + d_x\right) = \frac{P}{BD} \cdot m(x) \qquad [5.4.a]$$

$$\sigma_y = \frac{P}{BD}\left(a_y\, x^3 + b_y\, x^2 + c_y\, x + d_y\right) = \frac{P}{BD} \cdot n(x) \qquad [5.4.b]$$

The values for the fitting coefficients are reported in Table 16.

Table 16. Stress function fitting coefficients

Coeff.	segment in Y= 10 mm		segment in Y= 50 mm	
	x	y	x	y
a	-0.00002	-0.00005	-0.00003	0.00004
b	0.00011	0.00189	0.00171	-0.00384
c	-0.02081	-0.00719	-0.02292	0.06122
d	2.69094	-0.37243	-1.78151	-0.98555

5.3. Equations for computing the creep compliance

An extensometer of length l is used to measure the change in length, corresponding to load P, between two points located in the selected segments. Equation [5.5] provides an average strain over the measurement length:

$$\varepsilon_{x,ave} = \frac{1}{l}\int_0^l \varepsilon_x \, dx \qquad [5.5]$$

Equations in [5.6] are used to compute the average stress values through:

$$\sigma_{x,ave} = \frac{P}{bD}\int_0^l m(x) \, dx \qquad [5.6.a]$$

$$\sigma_{y,ave} = \frac{P}{bD}\int_0^l n(x) \, dx \qquad [5.6.b]$$

In a creep test loading, the load P can be described using the Heaviside step function $H(t)$ as:

$$P = P(t) = P_0 H(t) \qquad [5.7]$$

Noting that the change in time of the stresses is negligible (specially for the stresses in the top strip), equation [5.7] can be substituted in equations in [5.6] and taking the Laplace Transform the average stress values in the s variable are obtained:

$$\hat{\sigma}_{x,ave}(s) = \frac{\sigma_{x,0}}{s} \qquad [5.8.a]$$

$$\hat{\sigma}_{y,ave}(s) = \frac{\sigma_{y,0}}{s} \qquad [5.8.b]$$

where $\sigma_{x,0}$ and $\sigma_{y,0}$ represent

$$\hat{\sigma}_{x,0} = \frac{P_0}{bD} \cdot \frac{1}{l} \int_0^l m(x)\, dx \qquad [5.9.a]$$

$$\hat{\sigma}_{y,0} = \frac{P_0}{bD} \cdot \frac{1}{l} \int_0^l n(x)\, dx \qquad [5.9.b]$$

Equation [5.10] introduces Hooke's law for a linear elastic material in plane stress condition:

$$\varepsilon_x = \frac{1}{E}\left(\sigma_x - \upsilon\sigma_y\right) = D\left(\sigma_x - \upsilon\sigma_y\right) \qquad [5.10]$$

At this point, the elastic-viscoelastic correspondence principle can be used to determine the viscoelastic solution. Assuming the Poisson ratio to be time and frequency independent, the plane stress constitutive equation for viscoelastic material is given by [5.11]:

$$\hat{\varepsilon}_x(s) = s\,\widehat{D}(s)\left(\hat{\sigma}_x(s) - \upsilon\hat{\sigma}_y(s)\right) \qquad [5.11]$$

Note that the stress functions were found to be independent of material constants, hence they are not altered by either Laplace or Inverse Laplace Transforms. Then the creep compliance is determined by:

$$\widehat{D}(s) = \frac{1}{s}\frac{\hat{\varepsilon}_x(s)}{\left(\hat{\sigma}_x(s) - \upsilon\hat{\sigma}_y(s)\right)} \qquad [5.12]$$

Substituting the average stress values [5.9] into equations [5.12] yields:

$$\widehat{D}(s) = \frac{\hat{\varepsilon}_x(s)}{\left(\sigma_{x,0} - \upsilon\sigma_{y,0}\right)} \qquad [5.13]$$

The Inverse Laplace Transform of equation [5.13] yields the creep compliance function in time:

$$D(t) = \frac{\varepsilon_x(t)}{\left(\sigma_{x,0} - \upsilon\sigma_{y,0}\right)} \qquad [5.14]$$

5.4. Model verification

The validity of the creep compliance equation proposed in this research work was checked through numerical simulation and experimental testing. The scheme outlined in Figure 57 summarizes the verification approach adopted. The verification strategy consisted in comparing creep functions obtained from well established traditional creep test methodologies to that measured from SCB creep test as outlined in this paper. If the SCB procedure is reasonable, the different tests should yield similar creep functions.

Both numerical simulations and experimental testing were adopted. In the numerical simulation the SCB was compared to the Three-Point Bending Beam test.

Whereas, in the experimental testing standard IDT test were first performed. The IDT specimens were then used to prepare notched SCB specimens on which SCB creep tests were performed. This way it was ensured that same specimens were tested by two different methods.

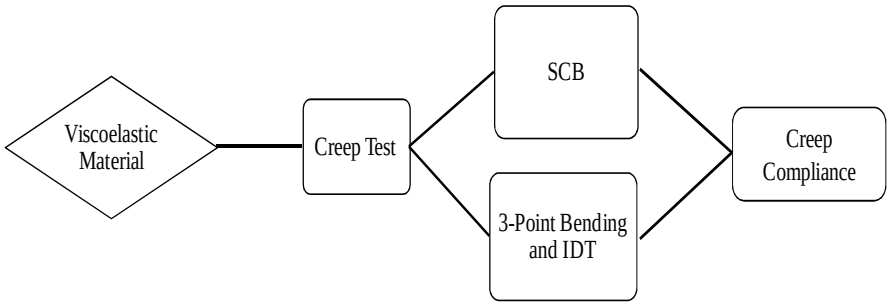

Figure 57. Strategy for verification of the of SCB creep model

5.4.1. Numerical validation

Numerical simulations of SCB and 3-Point Bending creep tests were performed in ABAQUS. The GMM model parameters in Table 15 were used to define the material in both tests. Both models were modeled in 3D as simply supported structures without overhanging parts beyond the supports. The height, thickness, and length of the beam dimensions were set, respectively, 6.35 mm, 12.7 mm, and 101.6 mm. While the SCB specimen had 150 mm, 25 mm, and 15, respectively for, diameter, thickness, and length of initial notch. The FE models are presented in Figure 58.

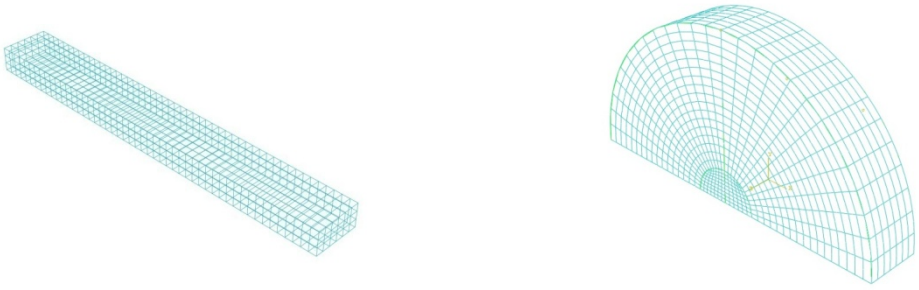

Figure 58. 3D finite element models subjected to creep test

Concentrated vertical compressive forces were applied in creep mode, in the middle of the beams top surface. Therefore, an instantaneous force was applied at time =0 sec and hold for 10sec.

Different meshes were tried until convergence of results was achieved. For the BBR model convergence was obtained with a mesh of 6584 brick elements C3D20R. The SCB model required 7018 wedge elements of C3D20R.

The bending beam theory states that in the 3-point bending beam, depicted in Figure 59, the maximum deflection δ_{max} occurs at the midpoint of the span and can be computed using equation [5.15].

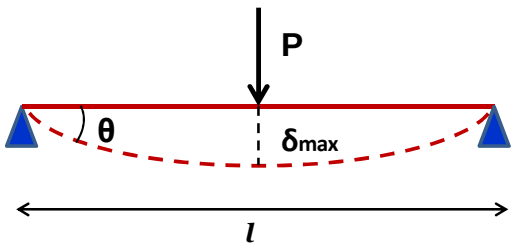

Figure 59. Schematization of 3-point bending beam

$$\delta_{max} = \frac{P\, l^3}{48\, EI} \qquad [5.15]$$

where l is the length of the span, P applied load, and I moment of inertia. The equation can be modified using the elastic-viscoelastic correspondence principle and applied using creep displacement history to determine the creep compliance $D(t)$:

$$D(t) = \frac{48\, I\, \delta(t)}{Pl^3} \qquad [5.16]$$

Equation [5.16] was used to calibrate and check the accuracy of the 3-point bending beam creep model. The initial elastic deflection should equal δ_{max}. The FE model used met this requirement as it is shown in Figure 60.

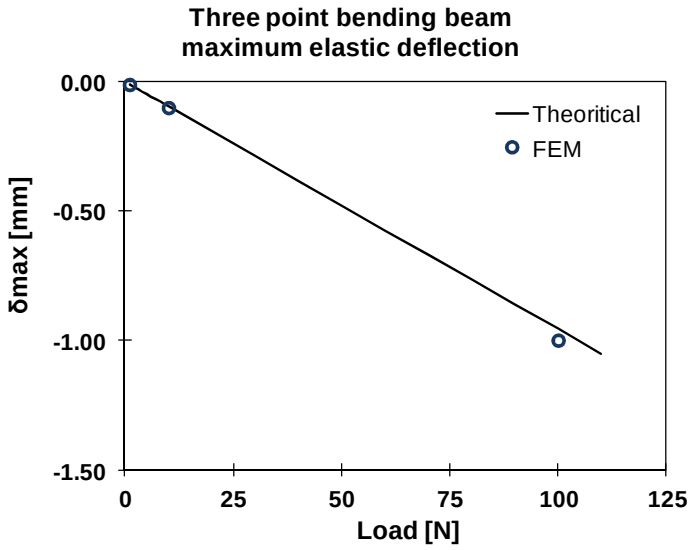

Figure 60. Calibration of the 3-point bending beam FE model

In the case of SCB creep simulation, the change in length between two model nodal points, located in the end points of the segments indicated in Figure 56 were used to determine the average strain values. Then using the stress equations proposed in equations [5.4] and the creep function in equation [5.14] the SCB creep functions were computed.

5.4.2. Experimental validation

A single reference asphalt concrete mixture was used to investigate the low temperature creep function through two different test procedures: IDT and SCB. The selected mixture is part of an ongoing research project at the University Minnesota and is identified as MIF 58-34 19mm Virgin. The nominal maximum aggregate size of the mixture is 19 mm and a plain PG58-34 asphalt binder was used for its mixing.

The loose mixture was gyratory compacted into cylindrical specimens with diameter 150 mm, height 171 mm and target air void content of 7%. Three cylinders were obtained as a result of this operation. The upper and lower 10 mm layers were cut and discarded. From each cylinder a standard notched SCB specimen was obtained for preliminary tests, from which the optimal creep load was determined. This process consisted in cyclic creep loading and unloading with increasing load to determine the load magnitude that produces appreciable displacement measurements without damaging the specimen. In addition, the peak fracture load was determined to verify that the

selected creep load remains within fraction of the peak load. The optimal creep load was found to be 0.8 kN.

Three IDT specimens were obtained from each gyratory cylinder and subjected to IDT creep test according to AASHTO T-322 (2007). A constant load of 1.6 kN, double of that required for SCB, was found to be in agreement with the standard's specification.

After IDT testing, the IDT plates were cut into SCB slices with a notch of 15mm. The SCB slices were then creep tested. The testing setups for both test procedure are presented in Figure 61.

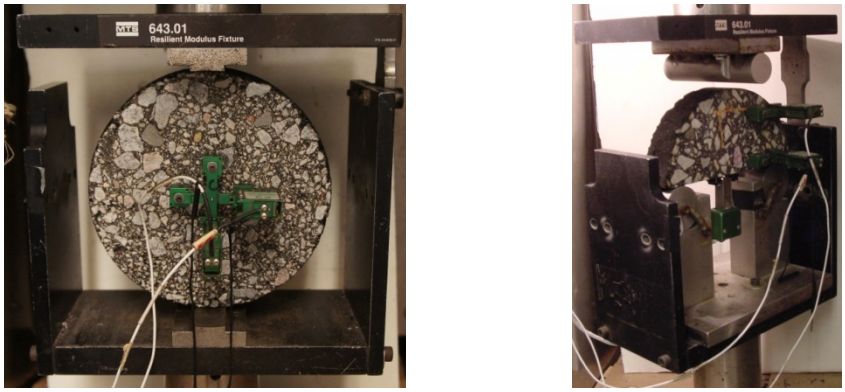

Figure 61. IDT and SCB experimental testing setup

All tests were performed in closed environmental chamber at -12°C. Prior to testing the specimens were conditioned for 2 hours at the testing temperature. The load was kept constant for 1000 sec.

The displacement and load measured from IDT creep test were used to compute the creep compliance of the asphalt mixture according to AASHTO T 322-07. The expression for D(t) is given as:

$$D(t) = \frac{\Delta X \cdot D_{avg} \cdot b_{avg}}{P_{avg} \cdot GL} \cdot C_{CMPL} \qquad [5.17]$$

where D, b, P, and GL indicate, respectively, diameter, thickness, load, and gauge length. ΔX is the trimmed horizontal deformation and $CCMPL$ creep compliance parameter computed as:

$$C_{CMPL} = 0.6354 \cdot \left(\frac{X}{Y}\right)^{-1} - 0.332 \qquad [5.18]$$

where X and Y represent, respectively the measured horizontal and vertical deformations.

The SCB creep compliance was determined according to the procedure proposed in this paper.

5.5. Results

The creep compliance $D(t)$ functions obtained from different test set-ups, using both finite element numerical simulations and experimental laboratory tests are presented next. Additionally, the creep stiffness $S(t)$ parameter can be easily computed as the inverse of $D(t)$. The results are reported in Figure 62 and Figure 63.

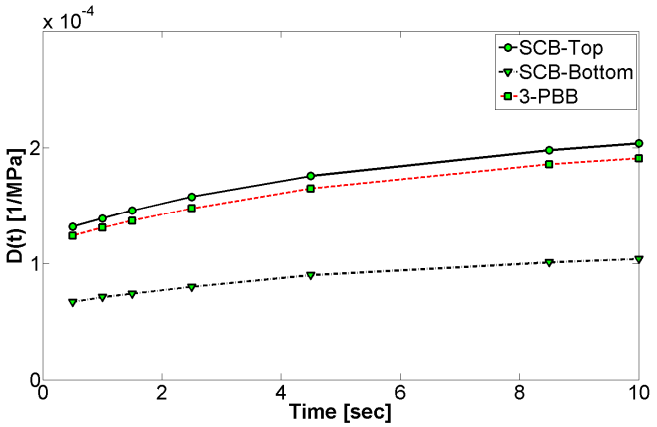

Figure 62. Results from numerical simulation

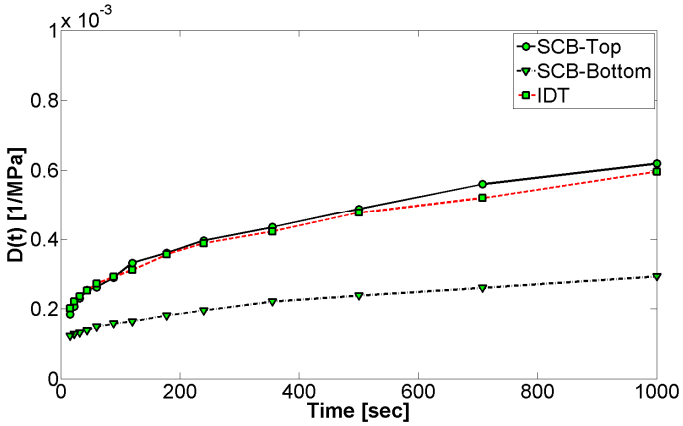

Figure 63. Results from experimental testing

The creep functions obtained from the SCB and the other two reference test configurations appear to have similar trends. However the creep compliance computed from the bottom region of the SCB is always smaller than the others. The vicinity to the crack tip and the support roller, as well as the relatively high variation of stress both in time and space observed in the bottom strip of the SCB specimen can be indicated as plausible reasons for this discrepancy. For these reasons, the average stress values used in

the approximated SCB creep model described in equation [5.14] may not be suited for the determination of the creep function from the bottom segment.

On the other hand, good agreement are obtained between the creep functions from the top segment of SCB specimen and those obtained from 3-point bending beam and IDT creep tests.

5.6. Summary of findings

In this chapter, the idea of determining asphalt concrete's creep compliance from the existing SCB fracture test was discussed. As a result, expressions that relate displacement measurement from particular region of the notched SCB specimen to the creep function of the asphalt concrete were derived. In particular two segments, one on the upper and another on the lower region of the SCB specimen, were identified for displacement measurement from which strains are to be computed.

The creep function computed from displacement measured at the upper segment of SCB specimen is in good agreement with creep functions from 3-point bending beam and IDT creep tests.

The findings of this research work indicate that the low temperature characterization of asphalt concrete can be entirely achieved from a single SCB test configuration. By eliminating the need for IDT creep testing, significant saving in material, time, and cost are achieved.

Chapter 6. Conclusions

6.1. Summary

In the first part of this study, laboratory experiments and numerical simulations were conducted in order to evaluate the fracture behavior of asphalt concrete tested in the SCB at low temperatures. In this study taconite asphalt concrete with a nominal maximum aggregate size (NMAS) of 4.75 mm and PG 64-34 was used. Notchless, shallow-notched, and deep-notched SCB specimens of different sizes were tested at -24°C, equivalent to the low service temperature limit of the PG 64-34 binder plus 10°C.

The size effect on the nominal strength of the tested mixture was reasonably well described by the energetic size effect theory. The data obtained from notchless specimens revealed the Type I size effect; the results from the shallow notch specimens indicated a size effect whose small-size asymptote is close to the Type I size effect and large-size asymptote is close to Type II size effect; and the data from the deep notch specimens demonstrated the Type II size effect.

The energetic size effect theory was also used to estimate the length of the FPZ of the tested asphalt concrete mixture and to determine size independent fracture properties. It was conclude that the standard SCB specimen can provided accurate fracture parameters of small size aggregate mixtures tested at very low temperature.

Building on the above findings, the ability of the standard SCB test protocol to characterize and differentiate relatively small aggregate size mixtures with respect to

their resistance to low temperature cracking was investigated. In specific, SCB, IDT, and DCT test methods were used to investigate if acid modifiers (PPA) can partially or completely substitute traditional polymer modifiers (SBS and Elvaloy) without adversely affecting the mixture's resistance to thermal cracking. Laboratory compacted and field cored specimens were tested and the results were statistically analyzed to generate performance rankings. Remarkably close agreement was found between the results from the two different fracture tests (SCB and DCT). In addition, the ability of both SCB and DCT to capture the effects of temperature, air void content and type of modifiers was visibly higher than that of IDT.

In the last part of the present work, the idea of determining asphalt concrete's creep compliance from the existing SCB fracture test was investigated. As a result, expressions that relate displacement measurement from particular region of the notched SCB specimen to the creep function of the asphalt concrete were derived. In particular two segments, one on the upper and another on the lower region of the SCB specimen were identified for displacement measurement from which strains are to be computed. The creep function computed from displacement measured at the upper segment of SCB specimen were in good agreement with creep functions from 3-point bending beam and IDT creep tests.

6.2. Conclusions

The main findings of this dissertation can be summarized as follow:

- The fracture behavior of asphalt concrete mixtures tested in the SCB test configuration at temperatures close to the glass transition of the component asphalt binder can be described very well by the energetic size effect theory of quasi-brittle materials.
- The size effect exhibited in testing deep-notched SCB specimens of asphalt concrete indicate that the material fails in a fairly brittle manner. By comparing the type II strength scaling law and the straight line asymptote for LEFM, it can be noticed that the deviation from LEFM is minimal and can be reduces to less than 2% for SCB specimens sizes larger than 80 mm, equivalent to approximately 16 times the NMAS of the tested asphalt concrete mixture.
- The above findings suggests that for asphalt concrete mixtures, with relatively small NMAS, tested in the standard SCB test configuration at very low temperature, the concepts of LEFM are applicable.
- Another important application of the energetic size effect theory of quasi brittle materials is that it can be used to determine the length of the effective fracture process zone (FPZ) of the investigated material. For the taconite asphalt concrete considered in this study, the lengths of the effective FPZ computed from the type I and type II size effect laws were 23.75 mm and 17 mm respectively. These FPZ length values are approximately 3 to 5 times the NMAS. It is worth mentioning that Li *et al.,* (2010) computed the size of FPZ

in asphalt concretes using AE technique, and found that the length of the FPZ was approximately 30 mm. Note that in this previous research, the asphalt concrete mixtures used had a NMAS of about 12 mm.

- An application of the type II size effect law to determine non-linear fracture parameters of the asphalt concrete was demonstrated. As a result, size independent fracture parameters for the tested material were determined. These size and shape-independent parameters are defined as LEFM parameters for infinitely large specimens.
- The SCB fracture test can be effectively used to select new paving materials with higher resistance to thermal cracking and to improve existing mix design. The case study conducted as part of the thesis research showed that acid modified (PPA) mixtures had relatively poor fracture resistance when compared to polymer modified (SBS and Elavloy) mixtures. However, when acid (PPA) is used to substitute part of the polymer (SBS), a mixture with comparable fracture resistance to the SBS-only modified mixture is obtained. This technology provides a cost effective alternative for improving the cracking resistance of asphalt pavements. The results of this investigation were confirmed by the field performance of the MnROAD test sections that have not thermally cracked.

- The low temperature characterization of asphalt concrete can be entirely achieved from a single SCB test configuration. By eliminating the need for IDT creep testing, significant saving in material, time, and cost are achieved.

References

AASHTO T 322-07, “Determining the creep compliance and strength of hot-mix asphalt (HMA) using the indirect tensile test device”, *American Association of State Highway and Transportation Officials*, 2007.

Anderson T.L., “Fracture mechanics, fundamentals and applications”, *London CRC Press, Inc*., 1995.

Arnold T.S., Needham S.P. and Youtcheff J.S., “Use of Phosphoric Acid as a modifier for Hot-Mix Asphalt”, *Journal Transportation Research Board 88th Annual Meeting*, 2009, pp. 40.

ASTM D7313- 07a, “Standard test method for determining fracture energy of asphalt-aggregate mixtures using the disk-shaped compact tension geometry”, *American Society for Tesing and Materials*, 2007.

Bahia H., Anderson D.A. and Christensen D., “The bending beam rheometer: a simple device for measuring low-temperature rheology of asphalt binders”, *Journal of Association of Asphalt Paving Technologists*, Vol. 61, 1992, pp. 117-153.

Barenblatt G.I., “The mathematical theory of equilibrium of cracks in brittle fracture”, *Advanced Apllied Mechanics*,Vol. 7, .1962, pp. 55-129.

Bažant Z.P. and Le J.L., “Size effect on strength and lifetime distributions of quasi-brittle structures”, *Proc. ASME*, 2009- pp. 1-9.

Bažant Z.P. and Yu Q., “Universal size effect law and effect of crack depth on quasi-brittle structure strength”, *Journal of Engineering Mechanics*, Vol. 135 (2), 2009, pp. 78-84.

Bažant Z.P., “Scaling of structural strength”, *Butterworth-Heinemann*, 2005.

Bažant Z.P., “Size effect on structural strength: a review”, *Archive of Applied Mechanics, Springer-Verlag*, Vol. 69, 1999,- pp. 703-725.

Bažant Z.P. and Planas J. “Fracture and size effect in concrete and other quasibrittle materials”, *Washington, D.C., CRC Press LLC*, 1998.

Bishara S.W., Mahoney D., McReynolds R.L., and King G.N., “Modification of binder with acid: advantages and disadvantages”, *Presented at the 80th Annual Meeting of the Transportation Research Board*, Washington, D.C., 2001.

Buttlar W.G. and Roque R., “Development and evaluation of the strategic highway research program measurements and analysis for indirect tensile testing at low temperature”, *Transportation Research Record*, No. 1454, 1994, pp. 163-171.

Chong K.P. and Kuruppu M.D., “New specimen for fracture toughness determination for rock and other materials”, *International Journal of Fracture*, No. 26, 1984, pp. 59-62.

Chong K.P. and Kurupu M.D., “New specimens for mixed mode fracture investigations of geomaterials”, *Engineering Fracture Mechanics*, Vol. 30, No, 5, 1988, pp. 701-712.

Christensen R.M., “Theory of Viscoelasticity, an introduction”, *Academic Press*, 1982.

Clyne T.R., Johnson E.N.,Worel B., McGraw J., and Reinke G., “Field Investigation of Polyphosphoric Acid Modified Binder at MnROAD” *Report: Workshop on Polyphosphoric Acid (PPA) Modification of Asphalt Binders*; April 7-8, Minneapolis, MN, 2009.

Clyne T., Johnson E. and Worel B., “Use of taconite aggreagtes in pavement applications”, *Report MN/RC-2010-24, 2010 MnDOT*, 2010.

Dickinson E.J., “Constitution and quality of paving grade asphalts produced by air blowing distillation residues of Kuwait and Light Arabian crude oil”, *Conf. Proc. Association of Asphalt Paving Technologists (AAPT)*, Vol. 43, 1974, pp. 132.

Dugdale D.S., “Yielding of steel sheets containing slits”, *Journal of Mechanics and Physics of Solids*, Vol. 8, 1960, pp. 100-108.

Fee D., Maldonado R., Reinke G., and Romagosa H, “Polyphosphoric Acid modification of asphalt”, *Transportation Research Record: Journal of the Transportation Research Board*, Vol. 2179, 2010, pp. 49-57.

Findley W.N., Lai J.S. and Kasif O., “Creep and relaxation of nonlinear viscoelastic materials”, *New York: Dover Publications*, 1989.

Frocht M., “Photoelasticity”, Vol. 2, *New York: John Wiley & Sons INC*., 1948.

Gere J.M. and Timoshenko S.P., "Mechanics of materials", *Boston, PWS-KENT Publishing Company*, 1990.

Giavarini C., Mastrofini D. and Scarsella M. "Macrostructure and rheological properties of chemically modified residue and bitumens", *Journal of Energy & Fuel*, Vol. 14, 2000, pp. 495-502.

Griffith A.A., "The phenomena of rupture and flows in solids", *Philosophical Transactions*, Series A, Vol. 221, 1920, pp. 163-198.

Alexander S.H. "Method of treating asphat", US Patent: 3,751,278, August 7, 1973.

Hillerborg A., "The theoretical basis of a method to determine the fracture energy G_F of concrete", *Material Structures*, 1985, pp. 291-296.

Hillerborg, A.; Modeer, M.; Peterson , P.E., "Analysis of crack formation and crack growth in concrete by means of fracture mechanics and finete element", *Cement Concrete Res*., Vol. 6, 1976, pp. 773-782.

Ho S., Zanzotto L. and MacLeod D., "Impact of chemical modification on composition and properties of asphalt binders", *Proc., Canadian Technical Asphalt Association*, Vol. 46, 2001, pp. 153-170.

Hondros G., "The evaluation of Poisson's ratio and the modulus of materials of a low tensile resistance by the Brazilian Test with particular reference to concrete", *Australian Journal of Applied Science* No.10, 1959, pp. 243-268.

Hopkins I.L. and Hamming R.W., "On Creep and Relaxation", *Applied Physics*, Vol. 28, 1957, pp. 906-909.

Inglis C.E., "Stresses in a plate due to the presence of cracks and sharp corners", *T. Inst. Naval Architects*, Vol. 55, 1913, pp. 219-241.

Kodrat I., Dave S., and Hesp S.A.M., "Comparison of Polyphosphoric acid-modified asphalt binders with straight and polymer-modified materials", *Transportation Research Record: Journal of the Transportation Reasearch Board*, Vol. 1998, 2007, pp. 47-55.

Irwin G.R., "Analysis of stresses and strains near the end of a crack traversing a plate", *Applied Mechanics*, Vol.24, 1957, pp. 361-364.

Irwin G.R., “Fracture.Handbuck der Physik”, *Berlin, Fluge,ed., Springer-Verlag*, Vol. 6, 1958, pp. 551-590.

Irwin G.R., “Onset of fat crack propagation in high strength steel and aluminum alloys”, *Sagamore Research Conference Proceeding*, Vol.2, 1956, pp. 289-305.

Irwin G.R., “Plastic zone near a crack and fracture toughness”, *Sagamore Research Conference Proceeding*, Vol.4, 1961.

Jenq Y.S. and Shah S.P., “A two paramter fracture model for concrete”, *Journal of Engineering Fracture Mechanics, Elsevier*, 1985, pp. 1055-1069.

Jung D.H. and Vinson T.S., “SHRP-A-399 - Low-temperature cracking binder validation”, *Washington, D.C., Strategic Highway Research Program, National Research Council*, 1994.

Kesler C.E., Naus D.J. and Lott J.L., “Fracture mechanics - Its applicability to concrete”, *Proc. Int. Conf. Mechanical Behaviour of Materials*, Vol. IV , 1972, pp. 113-124.

Labuz J.F. and Dai S., “Cracking of asphalt concrete at low temperatures”, *Report-Minneapolis MN: Center for Transportation Studies, University of Minnesota*, 1994.

Le J.L. and Bazant Z.P., “Unified nano-mechanics based probabilistic theory of quasibrittle and brittle structures: I. Strength, static crack growth, lifetime and scaling”, *Journal of the Mechanics and Physics of Solids*, 2011.

Leaderman H., “Elastic and creep properties of filamentuous materials and other high polymers”, *Textile Foundation*, 1955, pp. 183-190.

Leicester R.H., “The size effect of notches”, *Proc., 2nd Australian Conf. Mech. Strut. Mater*., 1969, pp. 4.1-4.20.

Li X. and Marasteanu M.O., “Evaluation of the low temperature fracture resistance of asphalt mixtures using the semi-circular bend test”, *Journal of the Association of Asphalt Paving Technologist*, Vol.73, 2004, pp. 401-426.

Li X. and Marasteanu M.O., “The fracture process zone in asphalt mixture at low temperature”, *Journal of Engineering Fracture Mechanics*, Vol. 77- 7, 2010, pp. 1175-1190.

Li X.-J. and Marasteanu M.O., “Using semi circular bending test to evaluate low temperature fracture resitance for asphalt concrete”, *Experimental Mechanics,* 2009, Published online.

Lim I.L. and Johnston I.W., “Stress intensity factors for semi-circular specimens under Three-Point Bending”, *Engineering Fracture Mechanics*, Vol.44, No.3, 1993, pp. 363-382.

Lytton R.L. et al., “SHRP-A-357 - Developement and validation of prediction models and specifications for asphalt binder and paving mixes”, *Strategic Highway Research Program. National Research Council, Washington DC, National Academy of Science*, 1993.

Maldonado R., Falkiewicz M., Bazi G., and Grzybowski K, “Asphalt modification with Polyphosphoric acid”, *Proc., Canadian Technical Asphalt Association*, Vol. 51, 2006, pp. 163-178.

Marasteanu M.O. et al., “Determining the low-temperature fracture toughness of asphalt mixtures”,*Transportation Research Record 1789, TRB, National Research Council, Washington D.C.*, 2002, pp. 191-199.

Marasteanu Mihai et al., “Low temperature cracking of asphalt concrete pavements”, *MN/RC -2004-23, Minnesota Department of Transportation*, 2004.

Mobasher B., Mamlouk M. and Lin H., “Evaluation of crack propagtion properties of asphalt mixtures”, *Journal of Transportation Engineering*, Vol. 123(5), 1997, pp. 405-413.

Mobasher Barzin, Mamlouk Michael S. and Lin How-Ming, “Evaluation of crack propagation properties of asphalt mixtures”, *Journal of Transportation Engineering*, 1997, pp. 405-413.

Molenaar J.M.M and Molenaar A.A.A., “Fracture toughness of asphalt in the semi-circular bend test”, *Proc. 2nd Euroasphalt & Eurobitume Congress Barcelona,* 2000.

Monsmith C.L. and Secor K.E., “Viscoelastic behaviour of asphalt concrete pavements”, *Journal of the Association of Asphalt Paving Technologist*, Vol.34, 1962, pp. 248-285.

Nallathambi P. and Karihaloo B.L., “Determination of specimen-size indipendent fracture toughnessof plain concrete”, *Mag. Concrete Res*., Vol. 38, 1986 (a). pp. 67-76.

Nallathambi P. and Karihaloo B.L., “Stress intensity factor and energy release rate for three-point bend specimen”, *Eng. Fract. Mech.*, Vol. 25 -3, 1986 (b), pp. 315-321.

RILEM TC-50 FMC, “Determination of the fracture energy of mortar and concrete by means of the Three-Point Bend Test on notched beams”, *Material Structures*, No. 18, 1985, pp. 287-290 (endorsed May 1993).

Roque R. and Buttlar W.G., “The development of a measurement and analysis system to accurately determine asphalt concrete properties using the Indirect Tensile mode”, *Association of Asphalt Paving Technologist*, Vol. 61, 1992, pp. 304-328.

Roque R., Zhang Z. and Sankar B., “Determination of crack growth rate parameters of asphalt mixtures using the Superpave”, *Journal of the Association of Asphalt Paving Technologists,* Vol. 65, 1999, pp. 404–433.

Schwarzl F. and Staverman A. J., “Time-temperature dependence of linear viscoelastic behaviour”, *Journal of Applied Physics*,. Vol. 23 – 8, 1952, pp. 838-843.

Secor K.E. and Monsmith C.L., “Analysis and interrelation of stress-strain-time data for asphalt concrete”, *Transaction of the Society of Rheology,* Vol. 8, 1964, pp. 19-32.

Swartz S.E., Hu K.K. and Jones G.L., “Compliance monitoring of crack growth in concrete”, *J. Eng. Mech. Div.- ASCE*, Vol. 104, 1979, pp. 789-800.

Wagoner M., Buttlar W. and Paulino G., “Developement of a single-edge notched beam test for asphalt concrete mixtures”, *Journal of Testing and Evaluation*, Vol. 33-6, 2005, pp. 452-460.

Wagoner M., Buttlar W. and Paulino G., “Disk-shaped compact tension test for asphalt concrete fracture”, *Journal of Experimental Mechanics*, Vol. 45-3, 2005, pp. 270-277.

Wagoner M.P. and Buttlar W.G., “Influence of specimen size on fracture energy of asphalt concrete”, *Journal of the Association of Asphalt Paving Technologists*, 2007, pp. 391-418.

Walsh P.F., “Crack initiation in plain concrete”, *Magazine of Concrete Research,* Vol. 28, 1976, pp. 37-41.

Walsh P.F., “Fracture of plain concrete”, *Indian Concrete J.*, Vol 46 - 11, 1972

Williams M.L., Landel R.F. and Ferry J.D., “The temperature dependence of relaxation mechanism in amorphous polymers and other glass-forming liquids”, *Journal of the American Chemical Society*, Vol. 77 – 14, 1955, pp. 3701-3707.

Zhang W., Drescher A. and Newcomb D.E., “Viscoelastic analysis of diametral compression of asphalt concrete”, *Journal of Engineering Mechanics*, 1997, pp. 596-603.

Zhang Z., Roque R. and Birgisson B., “Evaluation of laboratory measured crack growth rate of asphalt Mixtures”, *Transportation Research Record*, Vol. 1767, 2001, pp. 67-75.

Zofka A. [et al.], “Comparison of data interpretation procedures for Indirect Tensile (IDT) creep test for linear viscoelastic materials”, *Road Materials and Pavements Design*, Vol. X, No. X.- 2010.

Zofka A.,”Investigation of asphalt concrete creep behaviour using 3-Point Bending test”, *PhD Disseration Thesis*, 2007.